



UNIVERSITÀ  
DI PAVIA

PhD IN BIOMEDICAL SCIENCES  
DEPARTMENT OF BIOLOGY AND BIOTECHNOLOGY  
"L. SPALLANZANI"

# **Characterization of mycobacterial enzymes as targets for potential antitubercular compounds.**

PhD Tutor  
Laurent R. Chiarelli

PhD dissertation of  
Giovanni Stelitano

**XXXIV Cycle - Academic Year 2020/2021**

# Index

<b>Introduction .....</b>	<b>3</b>
Tuberculosis: general features and historical overview. ....	3
Epidemiology .....	6
Drug treatment against TB .....	8
Drug-resistance in <i>M. tuberculosis</i> .....	11
Host-pathogen interaction of <i>M. tuberculosis</i> .....	12
Metabolic features. ....	12
Host-pathogen interaction. ....	12
Virulence factors. ....	13
Iron metabolism control: siderophores. ....	14
Mycobactins biosynthesis in <i>M. tuberculosis</i> .....	15
<b>Chapter 1. MbtI, a novel potential therapeutic target .....</b>	<b>18</b>
MbtI general features.....	18
Aim of the work.....	21
Materials and methods.....	23
Materials .....	23
Methods.....	23
Results and discussion .....	28
Expression, purification and characterization of the recombinant MbtI .....	28
Inhibition assays of the compounds from virtual screening on MbtI activity .....	30
Structure-activity relationship (SAR) studies.....	32
Optimization of the lead compound MM40.....	41
SAR of the furan moiety.....	48
Optimization of the new MM-83 lead compound .....	51
<b>Chapter 2. Virulence factor PtpB as potential therapeutic targets .....</b>	<b>56</b>
PtpA and PtpB general features.....	56
Aim of the work.....	59
Materials and methods.....	61
Materials .....	61

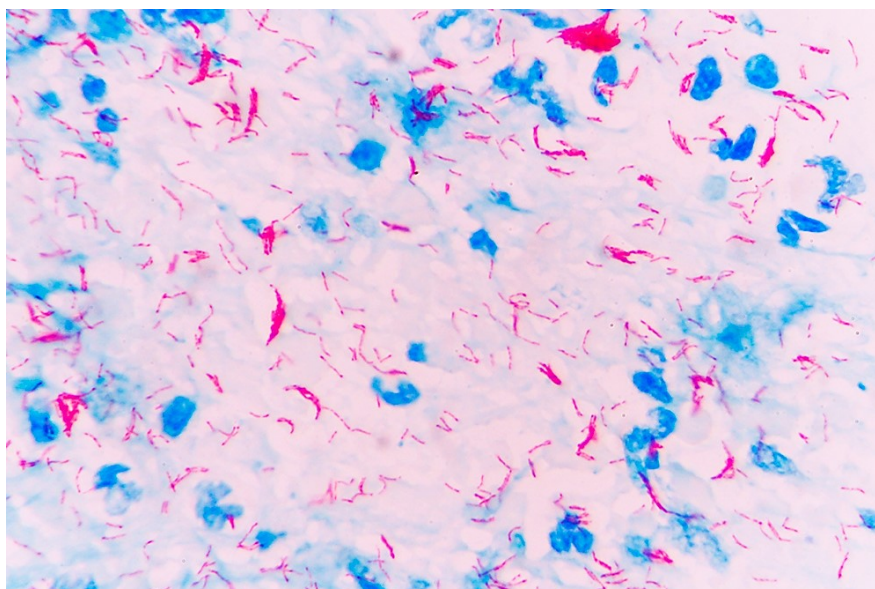
Results and discussion .....	64
Expression, purification and characterization of the recombinant PtpB.....	64
Inhibition assays of a selection of MbtI compounds on PtpB activity .....	66
Inhibition assays of the compounds from virtual screening on PtpB activity .....	68
Structure-activity relationship (SAR) studies.....	73
PtpB selectivity study.....	77
<b>Conclusion .....</b>	<b>79</b>
<b>Bibliography .....</b>	<b>81</b>

# Introduction

## Tuberculosis: general features and historical overview.

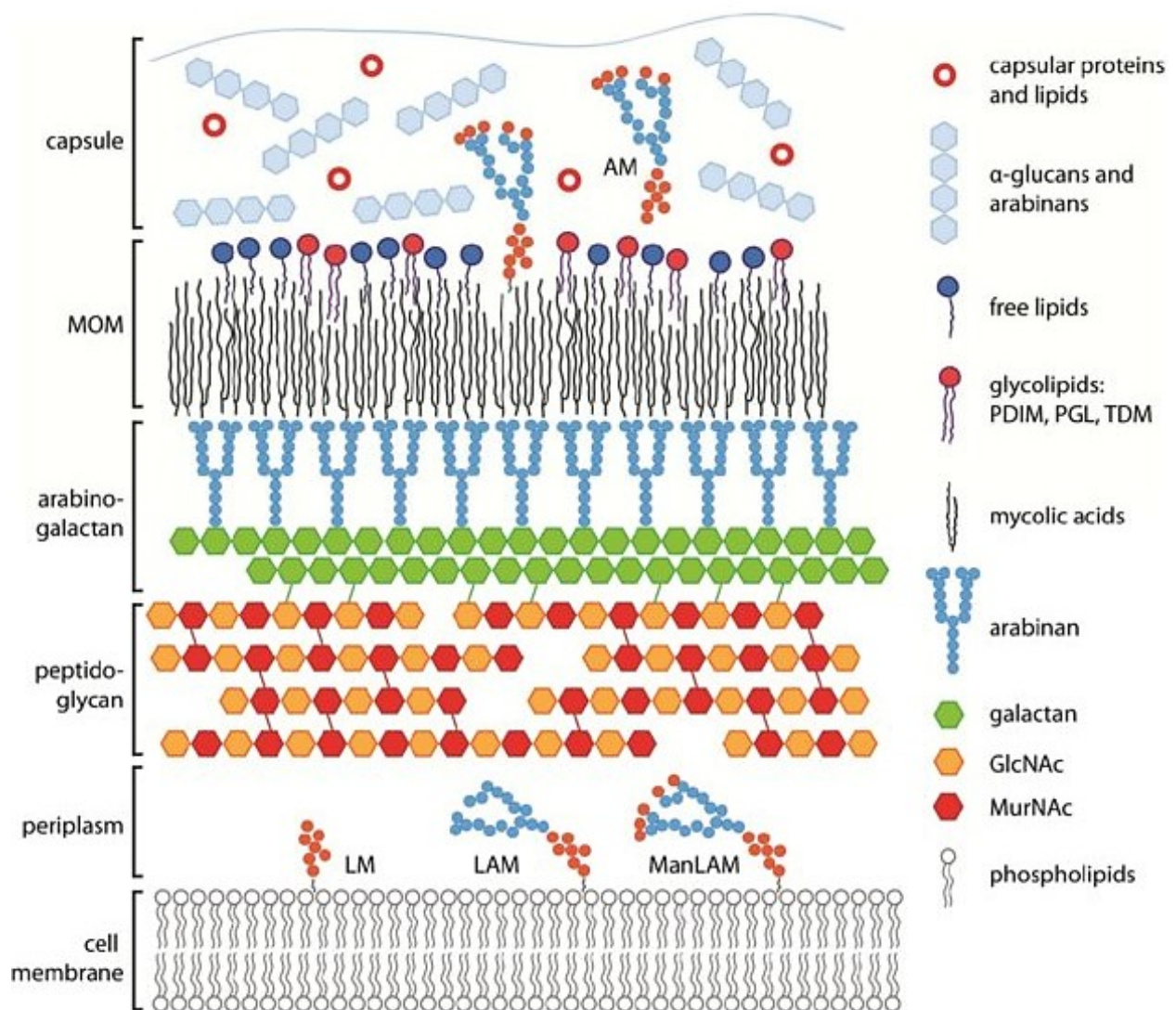
Tuberculosis (TB) is an ancient infectious disease caused by *Mycobacterium tuberculosis*, an aerobic pathogen that establishes infection mainly in lungs. In 25% of cases, *M. tuberculosis* may reach the bloodstream, targeting the lymphatic system, the urogenital tract, bones, joints and meninx (Rivers and Mancera, 2008). *M. tuberculosis* is pathogenic in its active form, but it mostly hides inside the host in a latent non-pathogenic form, the so-called inactive, to avoid to the immunity system response. The inactive form is associated to the development of granulomas and the switch to active is related to the weakening of the host immunity defenses (Ducati *et al.*, 2006). It has been evaluated that 1/3 of world population is infected by inactive TB (Bhardwaj *et al.*, 2015).

*M. tuberculosis* (Figure 1) is a bacterium belonging to the family of *Mycobacteriaceae*. It is an acid-alcohol-resistant bacteria, consequently can't be classified neither as Gram-positive or Gram-negative. Anyway, genome-based analysis revealed that it is a closely-related Gram-negative bacteria (Fu and Fu-Liu, 2002). *M. tuberculosis* is a small bacillus 1-4  $\mu\text{m}$  long and 0.3-0.6  $\mu\text{m}$  large (Cole *et al.*, 1998) that replicates every 24 hours at 37°C (Bloom and Murray, 1992), showing light-yellow colonies on agar-based media Petri dish after 3-4 weeks. It is typically visualized by Ziehl-Neelsen (acid-fast) staining appearing as a rod-shaped red bacillus (Gengenbacher and Kaufmann, 2012). *M. tuberculosis* does not sporulate, produce toxins or possess a flagellum, therefore it is not motile. It is transmitted by air, through cough, sputum and sneezes.



**Figure 1.** *M. tuberculosis* visualized in microscopy through Ziehl-Neelsen stain. (<https://www.rockefeller.edu/news/24686-study-identifies-genetic-mutation-responsible-tuberculosis-vulnerability/>)

One important feature of *M. tuberculosis* is its thick cell wall (Figure 2). It is organized in a complex structure, disposed on different layers and composed by peptidoglycans covalently linked to an arabinogalactan-peptidoglycan matrix and associated to lipids, polysaccharides, lipoglycans and proteins that are not covalently attached to the matrix (Daffé *et al.*, 2014). This wall is responsible of antibiotic resistance, low permeability and hydrophobicity of the bacterium (Alderwick *et al.*, 2007). It is also involved in mycobacterial longevity and pathogenesis since it may trigger inflammatory host reactions (Cole *et al.*, 1998).



**Figure 2.** Schematic representation of mycobacterial cell wall. MOM = mycobacterial outer membrane, LM = lipomannan, AM = arabinomannan, LAM = lipoarabinomannan, ManLAM = mannose-capped LAM, GlcNAc = N-acetyl-glucosamine, MurNAc = N-acetyl-muramic acid (Raffetseder, 2016).

*M. tuberculosis* H37Rv strain genome was completely sequenced in 1998 and it is composed by 4 411 529 base pairs, with high content of guanines and cytosines (around 65% of total). It is organized in a circular chromosome presenting 4173 genes, mostly involved in lipolysis and lipogenesis, indeed around 250 enzymes are involved in fatty acids metabolism (Cole *et al.*, 1998). The genome of different mycobacteria is quite conserved, with a genetic variation among mycobacteria species between ~0.01 and 0.03%, even if differences in phenotypes are present (Homolka *et al.*, 2009).

Mycobacteria are often found in complex with other bacteria of the same species or closely-related different species. In fact, *M. tuberculosis* is also commonly found in association with *M. bovis* and *M. africanum* (Jarlier and Nikaido, 1994).

For research, two non-pathogenic species are used, *M. bovis* Bacillus Calmette–Guerin (BCG), attenuated form of *M. bovis*, and *Mycobacterium smegmatis*. BCG is also used as vaccine with partial success.

Historically, it was estimated by genome sequencing and phylogenetic reconstruction techniques that mycobacteria originated around 70 thousand years ago. It was also predicted that the common ancestor of modern *M. tuberculosis* infected hominids around 20-15000 years ago (Kapur *et al.*, 1994). It coevolved and spread outside the African continent following human migration (Comas *et al.*, 2013). Paleontological studies, indeed, proved its presence on the skeletons of a woman and a child lived 9 thousand years ago in the Oriental Mediterranean Sea (Hershkovitz *et al.*, 2008), and only more recently in Saxony (Nicklisch *et al.*, 2012) and East Europe (Skepper *et al.*, 2012). It's curious to underline that this disease was never described in Egyptian papyrus, while its first written documentation is dated back to 1300-300 BC in Indian and Chinese documents (Barberis *et al.*, 2017).

In Western Europe, Hippocrates, known as the “father of Medicine”, described the tuberculosis as “φθισις”, that means consumption or deterioration, to underline the effect of the disease on human body (Ducati *et al.*, 2006). He was the first to accurately illustrate the symptoms and the classical tuberculosis lung lesions in his texts.

This illness was known as "king's evil" in England and France in XIII century, and it was believed that affected people could recover after a royal touch (Murray *et al.*, 2016). This practice continued until XIX century. In 1679, Francis Sylvius illustrates for the first time the exact physiological and pathological description in his Opera Medica (Saeed, 2006).

A new pandemic in XVIII century killed 900 people every 100 000, with an increased rate among young. For this reason, it was called “the robber of youth”.

It spread again between the late XIX and the beginning of XX century, and again it was one of the main causes of death in these centuries. In this period, it was called “great white plague” for the extreme anemic pallor of the skin of people affected.

TB reaped many notorious victims as, for example, Frédéric Chopin, Niccolò Paganini, Saint Francis of Assisi, Charlotte Brontë, John Keats, Byron, George Orwell and many others.

Its memory survived the time and lasted until us in literature and art, as in Thomas Mann's "The Magic Mountain", in Van Morrison's song "T.B. Sheets", in Puccini's "La Traviata" or in Monet's painting "Camille Monet on her deathbed".

On 1882 Robert Koch identified in *M. tuberculosis* the etiological agent of the disease (Koch, 1882). He was able to isolate and cultivate *M. tuberculosis*, proving the bacterial pathogenicity, and he received the Nobel prize for Medicine in 1905 thanks to his studies (Daniel, 2006). Koch's discovery was an important step in development of more efficient medical treatments for patients affected by TB (Ducati *et al.*, 2006). Today, Clemens von Pirquet's tuberculin skin test, developed in 1907 (Ducati *et al.*, 2006), is still used to prove latent infection among the population.

## Epidemiology

Tuberculosis has been considered for a very long period a disease of the past, but contrary to popular belief, it is still nowadays a global emergency (Riccardi and Pasca, 2014). According to the last WHO TB report (WHO, 2021) indeed, tuberculosis is one of the top 10 causes of death worldwide, the first caused by an infectious agent.

In the same report is estimated that arose 10 million new TB cases in 2020. In the same year around 1.3 million people died of this disease, plus other 214 000 cases of death were reported in association with HIV.

Geographically, most of the new cases were reported in the South-East Asia region (43%), Africa (25%) and Western Pacific area (18%), with smaller outbreak in Easter Mediterranean region (8.3%), America (3.0%) and Europe (2.3%). India reported most of the cases, the 26% of globality. The large diffusion of this disease is strictly linked to different factors like emigration from poor countries, premature interruption of treatments and coinfection with other diseases that compromise immune system (Ducati *et al.*, 2006).

The discovery of antibiotics such as streptomycin used from 1947, isoniazid, which was synthesized in 1912 but used only 40 years later, and p-aminosalicylic acid, had an important impact on TB treatment, reducing the mortality rate of patients (Bloom and Murray, 1992; Daniel, 2006). An important contribution is also due to the introduction of rifampicin since 1971, the most used first-class drug in treatments today.

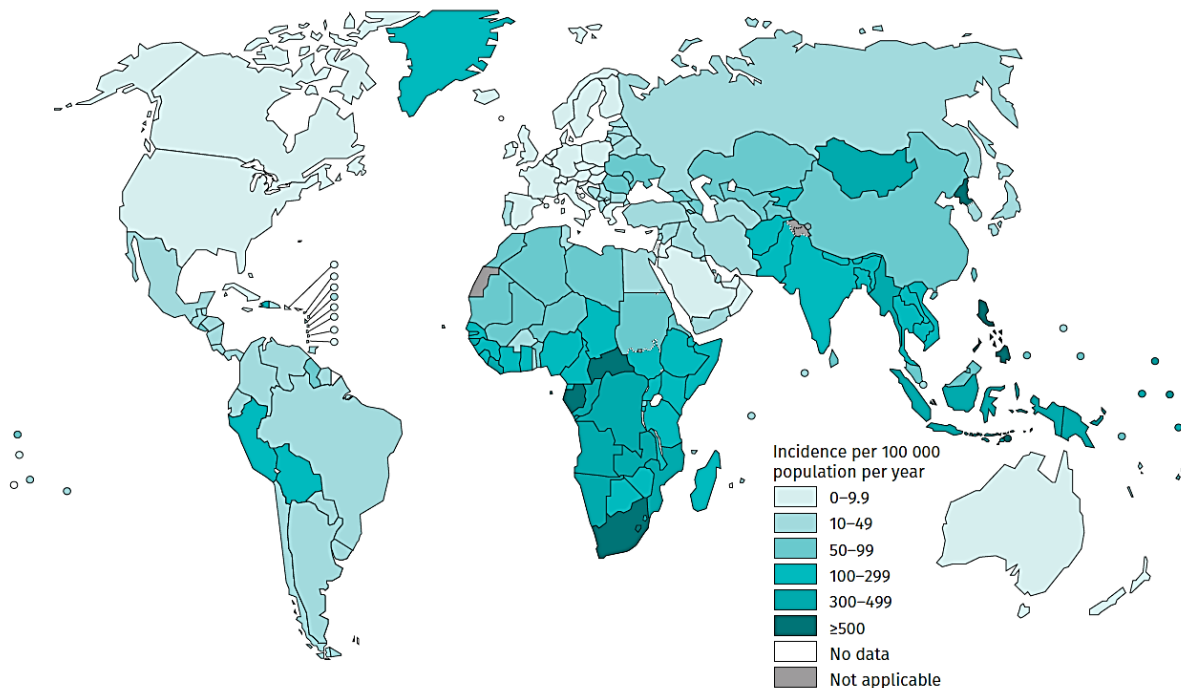
According to WHO, in 2020 TB incidence fell of 20% compared to 2015, but this progress was compromised in 2021 by the disruptions to diagnosis and treatments caused by the COVID-19 pandemic (WHO, 2021).

Anyway, a more concerning problem is rising cause of the often-incomplete treatments in poor Countries, that is the insurgence of multidrug-resistant strains (MDR). These strains are resistant to

two or more first-class drugs used in treatments. Moreover, extensively drug-resistant strains (XDR) can survive also to at least one second-class drug.

In 2020, 71% of diagnosed cases (2.1/3.0 million people) were rifampicin-resistant TB, of which 132 222 were MDR-TB plus other 25 681 XDR-TB (WHO, 2021). These strains were reported mostly in India (27%), China (14%) and the Russian Federation (8%). It is noteworthy that in the last 10 years the 3-4% of new TB cases were MDR-strains and 18-21% were previously treated cases of rifampicin-resistant or MDR-TB. The highest proportions (>50% in previously treated cases) were in countries of the former Soviet Union.

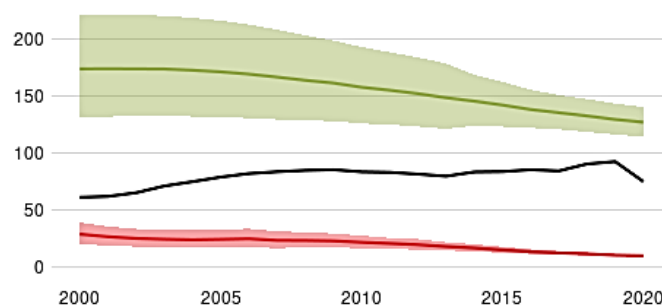
**Estimated TB incidence rates, 2020**



**Figure 3.** Estimated TB incidence rate in 2020 (WHO, 2021).

**Incidence, New and relapse TB cases notified, HIV-positive TB incidence**

(Rate per 100 000 population per year)



**Figure 4.** Incidence of total TB cases (green), new cases (black) and HIV associated cases (red) from 2000 to 2020. The rate is evaluated per 100 000 population (WHO, 2021).



## Drug treatment against TB

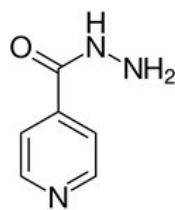
Nowadays, more than 20 new drugs are undergoing clinical trials in Phase I, II, or III. Three drugs are already in trial for market approval, two have received accelerated or conditional regulatory approval based on Phase IIb results. Nine drugs are repurposed. Various new combination regimens are in Phase II or Phase III trials, based on the combination of different drugs (Working Group on New TB Drugs, <https://www.newtbdrugs.org/>).

There are also 12 vaccine candidates in clinical trials, three in Phase I, and nine in Phase II or Phase III since the available vaccine is not always effective. New diagnostics, drugs and vaccines are anyway necessary to achieve the ambitious targets set in the End TB Strategy.

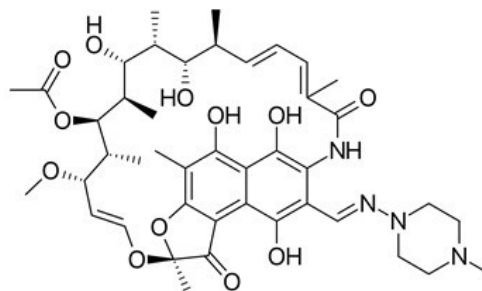
The actual regimen for drug sensitive TB strains was established forty years ago and it includes an initial 2-months intensive phase of four combined first-line drugs, continued by the dual therapy of isoniazid and rifampicin for the last 4 months (Tiberi *et al.*, 2018). For the MDR strains, the regimen includes 20-28 months of treatment with at least four second-class drugs, depending on previous MDR-TB treatments that have been administered (Zumla *et al.*, 2013).

The first-class drugs (Figure 5) are mainly bactericidal, with a moderate toxicity and high efficacy. They are often used in cocktails for actual regimen. Main examples are:

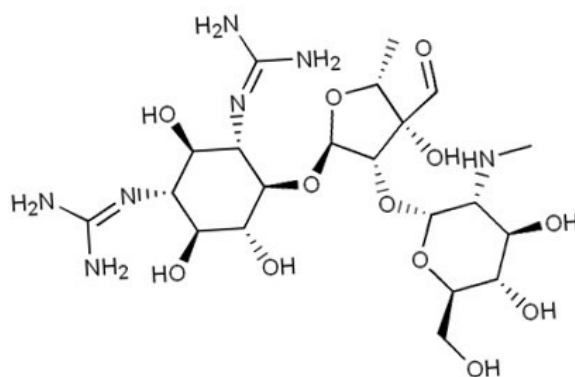
- **Isoniazid** (isonicotinyl hydrazide, INH). It is a prodrug that becomes active thanks to *M. tuberculosis* catalase-peroxidase KatG enzyme. It binds NAD<sup>+</sup> creating an adduct that stops the NADH-dependent enoyl-ACP reductase, a fatty acid synthase involved in mycolic acids biosynthesis (Vilcheze and Jacobs, 2007).
- **Rifampicin** (RIF). It targets the  $\beta$  subunit of RNA polymerase encoded by *rpoB* gene, interfering with the mRNA elongation. Thanks to its action, it is active on both replicating and non-replicating strains (Campbell *et al.*, 2001). However, a big problem of this compound and its derivatives is that they are metabolized by cytochrome P450 in liver, becoming reactive with other TB drugs and antiretrovirals compounds (Zumla *et al.*, 2013).
- **Streptomycin** (SM). It binds the ribosomal 30S subunit, causing the misreading of the bacterial mRNA and stopping the protein synthesis (Davies *et al.*, 1965).
- **Ethambutol** (EMB). It blocks cell wall biosynthesis by inhibiting the enzyme arabinosyl transferase. Indeed, this enzyme transfers a mycolic acid on the 5'-hydroxyl groups of the D-arabinose residues of an arabinogalactan, forming a mycolyl-arabinogalactan-peptidoglycan complex that is essential for the cell wall (Takayama *et al.*, 1979).



Isoniazid



Rifampicin



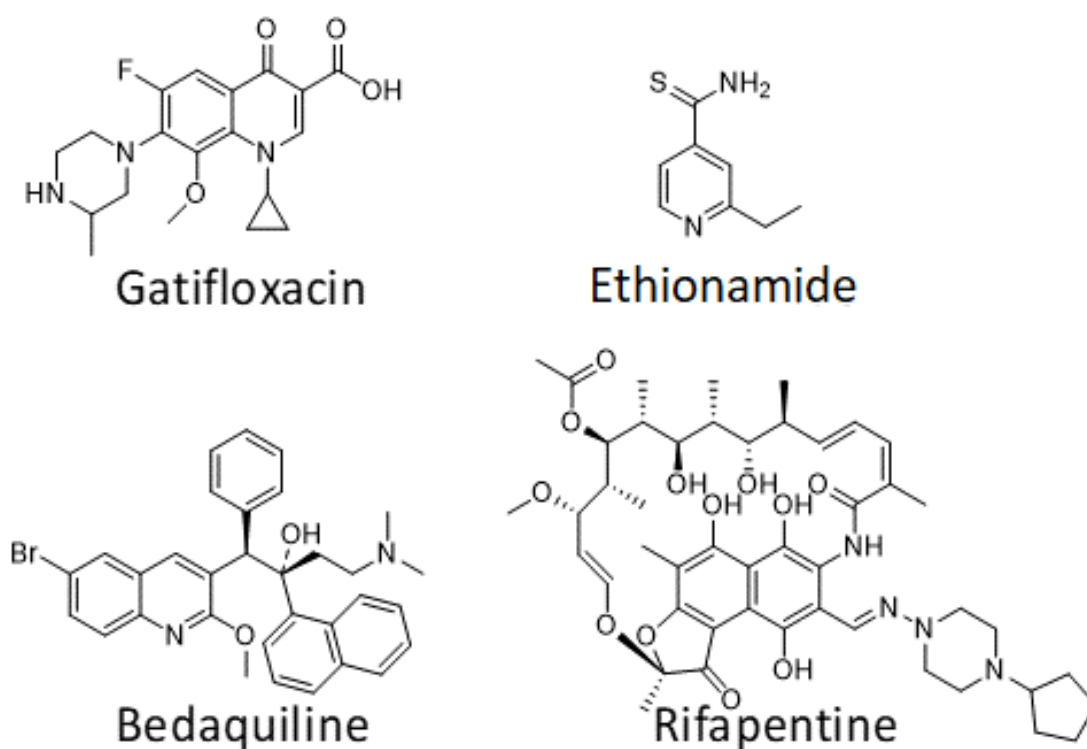
Streptomycin

**Figure 5.** Principal first-class antitubercular drugs.

The second-class drugs (Figure 6) may be both bactericidal or bacteriostatic, often with higher toxicity and less efficacy. Examples are:

- **Fluoroquinolones** family. These drugs target the topoisomerase II, also known as DNA gyrase, an heterotetrameric enzyme that catalyzes the DNA supercoiling through a transient double strand break. Fluoroquinolones act during the enzyme catalysis, inducing a covalent enzyme-DNA stable adduct, the so called “cleaved complex” (Chiarelli *et al.*, 2016). They have been proposed as first-class drugs when their potential to reduce actual regimen was clear. Gatifloxacin and moxifloxacin are two molecules of this family in phase III clinical trials (Zumla *et al.*, 2013).
- **Etionamide** (ETH). Structurally similar to isoniazid, it is one of the most commonly administered second-class drugs. ETH is a prodrug that has the same molecular mechanism of INH, except that it is activated by EthA monooxygenase (Baulard *et al.*, 2000; DeBarber *et al.*, 2000).

- **Rifamycins.** Derived from rifampicin, they work with the same molecular inhibition mechanism. Rifapentine, one of these compounds that has a longer half-life than RIF, is already in phase II clinical trials and it appears to be more tolerate by the host. For this reason, it can be administered more than once per week, reducing the actual regimen period (Zumla *et al.*, 2013).
- **Bedaquiline.** It targets the c-subunit transmembrane region of *M. tuberculosis* ATP synthase, completely blocking its activity (Andries *et al.*, 2005). This drug is effective on both replicating and latent TB, and currently in phase 3 clinical trial, have been approved by U.S. Food and Drug Administration for the treatment of multidrug-resistant TB.



**Figure 6.** Principal second-class antitubercular drugs.

## Drug-resistance in *M. tuberculosis*

*M. tuberculosis* drug-resistance mechanisms follow the Darwinian model of natural selection, based on casual mutations that are picked by environmental factors and then, spread in the population. Some of these mutations, mostly associated to single nuclear polymorphism (SNPs), may occur on specific genes, changing the interaction between a drug and its target, altering the metabolism of the same drug or activating efflux pumps (Wilson and Tsukayama, 2016). For example, a mutation in an enzyme active site may deeply modify its interaction with the drug, lowering the affinity and the inhibiting power of the compound. Also, a drug can undergo inactivating modification cause of the pathogen detoxifying enzymes, such as the monooxygenases, that turn the compound more hydrosoluble changing its toxic properties. Finally, the efflux pumps are multiprotein complexes that export a drug outside the cell before it reaches its target, avoiding the cytotoxic effect.

*M. tuberculosis* is naturally resistant to many antibiotics and other chemotherapeutic agents, such as the  $\beta$ -lactams, thanks to the presence of specific hydrolytic enzymes, as the  $\beta$ -lactamase, that target the  $\beta$ -lactam ring and inactivate the inhibitor (Ducati *et al.*, 2006). Anyway, a combination of  $\beta$ -lactamase inhibitors with carbapenems showed an interesting inhibitory effect *in vitro* against *M. tuberculosis* (Horita *et al.*, 2014), and this cocktail is actually in phase 2 clinical trial.

Recently, efflux pumps were well characterized and associate to specific drug resistances. Rv1258c, for example, is a major facilitator superfamily (MFS) efflux pump associated to the export of gentamicin and spectinomycin outside the bacterium though the cell wall (Balganesh *et al.*, 2012).

Historically, streptomycin was introduced in regimen around 80 years ago. Soon resistant strains were selected leading to the synthesis of second-class drugs (Crofton and Mitchison, 1948). Those new compounds allowed the establishment of more effective strategies based on combined administration of different antibiotics. These cocktails are still valid today, but new multi-resistant *M. tuberculosis* strains are emerging (Wilson and Tsukayama, 2016). Moreover, it's important to remember also the extensively drug-resistant (XDR) strains, less common but more deadly, such as the fluoroquinolones-resistant *M. tuberculosis*. They appeared in 2005 in South Africa during an epidemic that had a mortality rate close to 100% (Gandhi *et al.*, 2006), then they were also isolated in East Europe (WHO global report, 2017). Actual therapies have only a moderate efficacy on XDR strains, so identification of new therapeutic targets and development of novel drugs is mandatory.

## Host-pathogen interaction of *M. tuberculosis*

To discover new possible therapeutic targets and to develop innovative antimicrobial drugs, it is essential to study the pathogen metabolic pathways, its virulence factors and the host-pathogen interaction mechanisms. All these features have been largely studied also in *M. tuberculosis*, but still not every molecular process is already being discovered.

### Metabolic features.

According to evidence, *M. tuberculosis* evolved peculiar mechanisms of growth and regulation. One example is the carbon metabolism. Usually, bacteria have repressors for carbon catabolism, called carbon catabolism repressors (CCRs), that are important to achieve the maximum growth using the carbon substrates at the best of their possibilities (Görke and Stülke, 2008). Instead, *M. tuberculosis* lacks CCRs. It co-catabolizes different carbon substrates in a compartmented manner, for example glucose and acetate, simultaneously through glycolysis and gluconeogenesis (de Carvalho *et al.*, 2010). This is probably due to the biochemical stringent niches in which it nuzzles *in vivo*. These niches, indeed, do not possess a balanced supply of glucose and fatty acids. Therefore, *M. tuberculosis* peculiar mechanism of carbon metabolism allows a faster more extensively growth.

In addition to the optimization of extracellular nutrient, the bacterium may also recycle most of its metabolites depending on the necessity. For example, the trehalose released from the glycolipid trehalose monomycolate present on its cell wall, can be re-internalized to establish infection in mouse model (Kalscheuer *et al.*, 2010). In case of hypoxia, anyway, when the nutrient uptake is decreased, the trehalose can be used again for peptidoglycan biosynthesis (Eoh *et al.*, 2017).

### Host-pathogen interaction.

The interaction between *M. tuberculosis* and its host is modulated by host-imposed environmental stimuli. The host cell, indeed, may trigger specific event on bacterial cell wall. This wall is the key to mycobacteria pathogenicity thanks to the peculiar lipid composition. During persistent infection, for example, it can induce an inflammatory response that can cause liquefactive tissue necrosis which can remain asymptomatic for decades, if not the lifetime of the host (Stamm *et al.*, 2015). To set up a persistent infection, it can also induce the granulomas formation through interaction with alveolar macrophages (Ishikawa *et al.*, 2009). The composition and quantity of immune stimulatory molecules of the cell wall depend, again, on environmental stimuli. For example, during hypoxia, the envelop composition reduce the immunoregulation impact of the bacteria (Galagan *et al.*, 2013).

## Virulence factors.

The full virulence of *M. tuberculosis* depends not only on the cell wall, but also on at least three different secretion systems of five that have been characterized.

Among all, the type VII secretion system (ESX-1) is one of its most important. ESX-1 is involved mainly in two processes: to avoid the fusion between phagosome and lysosome, and for the phagosomal rupture (Gröschel *et al.*, 2016). ESX-1, indeed, seems to mediate the protein EsxA secretion that, working in concert with the lipid phthiocerol dimycocerosates present on *M. tuberculosis* cell wall, results in the vacuoles lipid bilayer disruption (Augenreich *et al.*, 2017; Smith *et al.*, 2008). Once the bacterium escapes the phagosome, it is released in macrophagic cytosol, one of its replicative niches. The vaccine strain *M. bovis* lacks a portion of the gene *esx-1* encoding one subunit of the system, resulting into the loss of function of the whole ESX-1 (Mahairas *et al.*, 1996). ESX-3 is important for mycobactins secretion and iron and zinc homeostasis (Serafini *et al.*, 2013). Mycobactins are siderophores that sequester the host's iron and bring it back to the pathogen, since iron is essential for the activity of a plethora of *M. tuberculosis* metabolic enzymes. ESX-5 is involved in fatty acid uptake (Ates *et al.*, 2015) and secretion of mycobacteria specific proteins such as Pro-Glu and Pro-Pro-Glu proteins. The role of these proteins is still unclear, and more studies are ongoing. The role of ESX-2 and ESX-4 is still unclear.

*M. tuberculosis* secretes different phosphatases and other enzymes in the external environment that are known as virulence factors. SapM, for example, is a phosphatase with a large substrate spectrum. It is active against phosphoenolpyruvate, glycerophosphate, GTP, NADPH, phosphotyrosine, trehalose-6-phosphate and phospho-inositol-3-phosphate (PI3P) (Saleh and Belisle, 2000). Phagosomal maturation is arrested when PI3P is removed from its lipid bilayer, impairing its fusion with the late endosome (Vergne *et al.*, 2005).

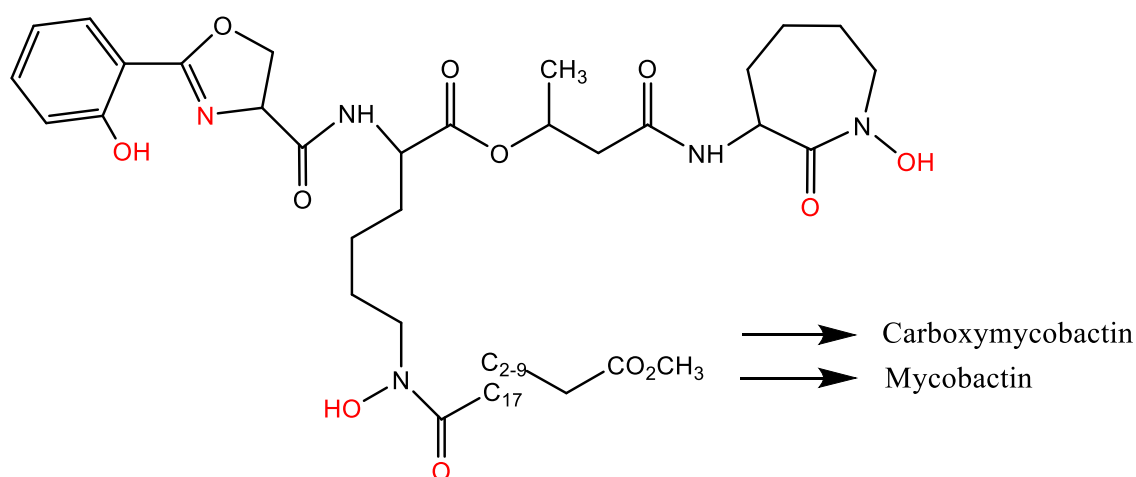
MptpA and MptpB are other two secreted proteins of the phosphatase family still not well characterized. MptpA, or more simply PtpA, probably interferes with the phagosomal maturation. According to the proposed model, it acts in two ways: it disrupts specific key components of the endocytic pathway like the 33B (VPS33B) human vacuolar protein sorting (Bach *et al.*, 2008), and it excludes the vacuolar ATPase, preventing acidification and fusion with lysosomes (Wong *et al.*, 2011).

Finally, MptpB, also known as PtpB, negatively regulates the macrophages processes of inflammation and apoptosis induced by *M. tuberculosis*. This phosphatase, indeed, inhibits the expression of proinflammatory IL-6 and IL1- $\beta$  in addition to NF $\kappa$ B and MAPK signaling pathways but its molecular targets are still not well known. Anyway, the decreased inflammatory response and the apoptosis impairment caused by this virulence factor result into mycobacteria survival in macrophages (Fan *et al.*, 2018).

## Iron metabolism control: siderophores.

Iron is an indispensable nutrient for all the organisms, with only few exceptions. It is required in essential metabolic pathways for the activity of many enzymes, from respiration to DNA replication. Since in neutral pH it is not soluble in presence of oxygen, its uptake is a challenge for all bacteria. Moreover, pathogenic species do not find free iron in hosts, but only in association with specific high affinity iron-binding proteins (Weinberg, 1999). Also, an excess of iron inside the cells reacts with normal aerobic metabolism products catalyzing the formation of cytotoxic oxygen radicals (Imlay *et al.*, 1988). For this reason, iron metabolism must be tightly controlled, starting from sensing the presence and concentration of the metal in the environment, to its uptake and efflux. These processes depend on different factors, like stress response, cellular metabolism, iron availability and virulence properties of the bacteria (Litwin and Calderwood, 1993).

Many bacteria are able to catch the iron in extracellular environment through siderophores, high affinity iron chelator proteins that selectively bind ferric iron ( $\text{Fe}^{3+}$ ). Even mycobacteria possess typical siderophores, the so called mycobactins, that are hexadentate ligands with a tripodal architecture (Figure 7) synthesized starting from a molecule of salicylate as core brick. Their basic structure is composed by a *o*-hydroxyphenyloxazoline moiety bound to an acylated hydroxylysine residue that is esterified with a 3-hydroxybutyric acid and finally linked to a terminal cyclized hydroxylysine forming a seven-membered lactam ring unit.



**Figure 7.** Mycobactin core structure. The groups in red are involved in binding of Fe(III) (adapted from Rodriguez., 2006).

Mycobactins are produced in two different forms: the more soluble carboxymycobactin and the lipophilic mycobactin. The carboxymycobactin possesses a carboxy(alkyl) side chain and it is secreted to chelate the host iron (Gobin and Horwitz, 1996), while the lipophilic mycobactin is less polar and it is anchored to the cell membrane thanks to a long alkyl or alkenyl side-chain ( $\text{C}_{18}\text{-C}_{20}$ )

that confers lipid-like properties to the molecule (Ratledge, 2004). Both types of mycobactins are encoded by the *mbt* genes clusters exclusively at stringent iron concentration (Rodriguez *et al.*, 2002).

Carboxymycobactins are synthesized by a specific pathway then secreted in the host (dendritic cells, macrophages or monocytes) through ESX-3 system (Jones *et al.*, 2014). Once a carboxymycobactin catches an iron atom from proteins like, for example, transferrin or lactoferrin, it is reinternalized in the mycobacterium cytoplasm. The reinternalization of this iron-carboxymycobactin complex is a two-step process that requires 1) a porin system in which the complex migrate into the periplasmic space by passive diffusion and 2) by specialized membrane receptors that are part of the ATP-binding cassette (ABC) transporters family for the passage to the cytoplasm (Braun and Killmann, 1999; Shyam *et al.*, 2021). Here, the iron is finally released probably by reduction from  $Fe^{3+}$  to  $Fe^{2+}$ , while the carboxymycobactin is recycled (Jones *et al.*, 2014).

Data also suggest a second iron import mechanism: in iron excess condition the carboxymycobactins may also temporarily donate the captured iron to the lipophilic mycobactins that are anchored on the cell membrane. This iron may be internalized in the cytoplasm upon reduction from  $Fe^{3+}$  to  $Fe^{2+}$  by a specific ferri-reductase enzyme present on the cell membrane (Shyam *et al.*, 2021). According to Gobin and Horwitz (1996), the lipophilic mycobactins may also work both as iron acceptor and ionophore, that is, an ion transporter able to cross itself the cell membrane. Once in cytoplasm, these mycobactins may assume the third role of temporary iron storage (Ratledge, 1999). Mutagenesis studies show that the lack of mycobactins decreases the replication capability of mycobacteria in low-iron conditions inside the macrophages (De Voss *et al.*, 2000), while mutations on ABC transporters genes do not impair the bacterium metabolism (Rodriguez and Smith, 2006). These results suggest that other transporters may be involved in the uptake of the complex iron-carboxymycobactins.

According to these observations, one current research-line is addressed to stop the biosynthetic pathway of mycobactins as possible therapeutic cure against *M. tuberculosis*.

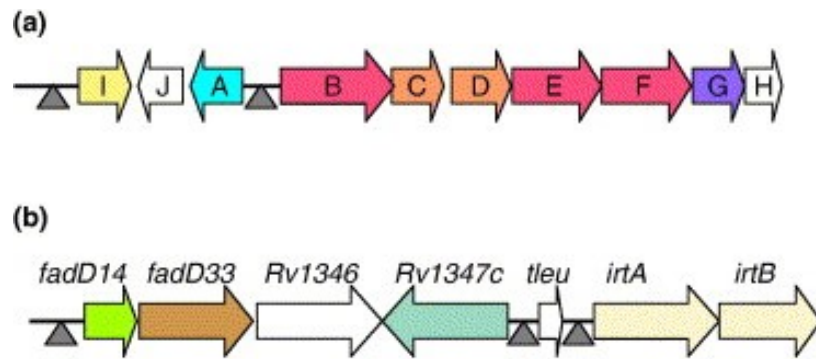
## **Mycobactins biosynthesis in *M. tuberculosis*.**

Two operons of *Mycobacterium tuberculosis* clusters all the genes involved in the mycobactins biosynthetic pathway. Mbt operon includes the genes *mbtA-J* that are involved in the siderophore core formation while *mbt-2* operon encodes the enzymes that add the acyl substitution to the core (Figure 8).

More in specific, genes located in the *mbt* operon are: *mbtB*, *mbtE* and *mbtF* that codify for three non-ribosomal peptide synthases, *mbtD* and *mbtC* for two polyketide synthases, *mbtA* for an adenylating and salicyl-AMP ligase, *MbtI* for an isochorismate synthetase and *mbtG* for a hydroxylase (Rodriguez, 2006).



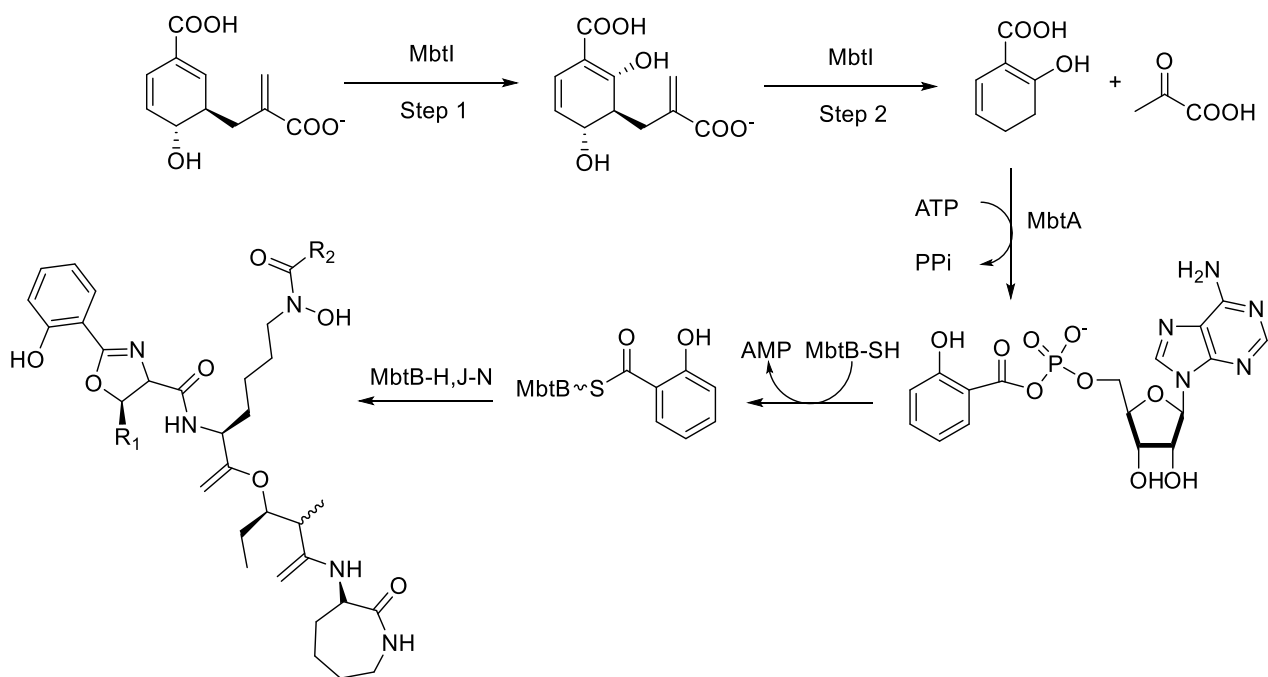
Genes located on *mbt-2* operon are: *fadD33* encoding for a fatty acyl-AMP ligase, *fadD14* for an acyl carrier protein, *rv1346* and *rv1347c* for two different acyl transferases. This locus possesses other two genes, *irtA* and *irtB* that encode for iron-regulated transporters (Rodriguez, 2006).



**Figure 8.** Mbt (a) and *mbt-2* (b) operons. Triangles are the regulative binding sites of IdeR (Rodriguez, 2006). Colors are related on enzyme class: on operon a, red is for nonribosomal peptide synthetases, orange for polyketide synthetases, yellow for isochorismate synthetase, blue for adenylating and salicyl-AMP ligase and purple for hydroxylase. On operon b, brown is for fatty acyl-AMP ligase, bright green for acyl carrier protein, blue-green for acyl transferase.

Both operons, in presence of high intracellular iron concentration are repressed by IdeR, an iron-dependent regulator (Schmitt *et al.*, 1995) that binds specific regulative regions as shown in figure 8. When the iron concentration drops, the complex IdeR-Fe<sup>3+</sup> cannot form and the two operons are expressed.

Mycobactins biosynthesis starts when one molecule of chorismic acid is processed by MbtI into salicylic acid (mycobactin core) via isochorismate. The multi-enzyme complex composed by MbtA-N enzymes catalyzes the subsequent reactions that ends with the formation of the mature mycobactin (scheme 1) (Meneghetti *et al.*, 2016).



**Scheme 1.** Structures of MBTs/cMBTs and their biosynthesis. (Adapted from Meneghetti *et al.*, 2016)

# Chapter 1. MbtI, a novel potential therapeutic target

## MbtI general features

MbtI is the first enzyme involved in mycobactin biosynthesis and its structure has been solved for the first time in 2006 by Zwahlen J. and colleges. It is a monomeric protein of the length of 450 amino acids and a mass of 49 643 Da. It is organized in one large single domain, with two  $\alpha/\beta$  subdomains, each with a large antiparallel  $\beta$ -sheet with helices packed against it on the protein surface (Figure 9). The active site is located in a deep cleft, at the interface of the two  $\beta$ -sheets subdomains (Harrison *et al.*, 2006). Co-crystallization of the enzyme with different inhibitors confirmed this model (Manos-Turvey *et al.*, 2010).

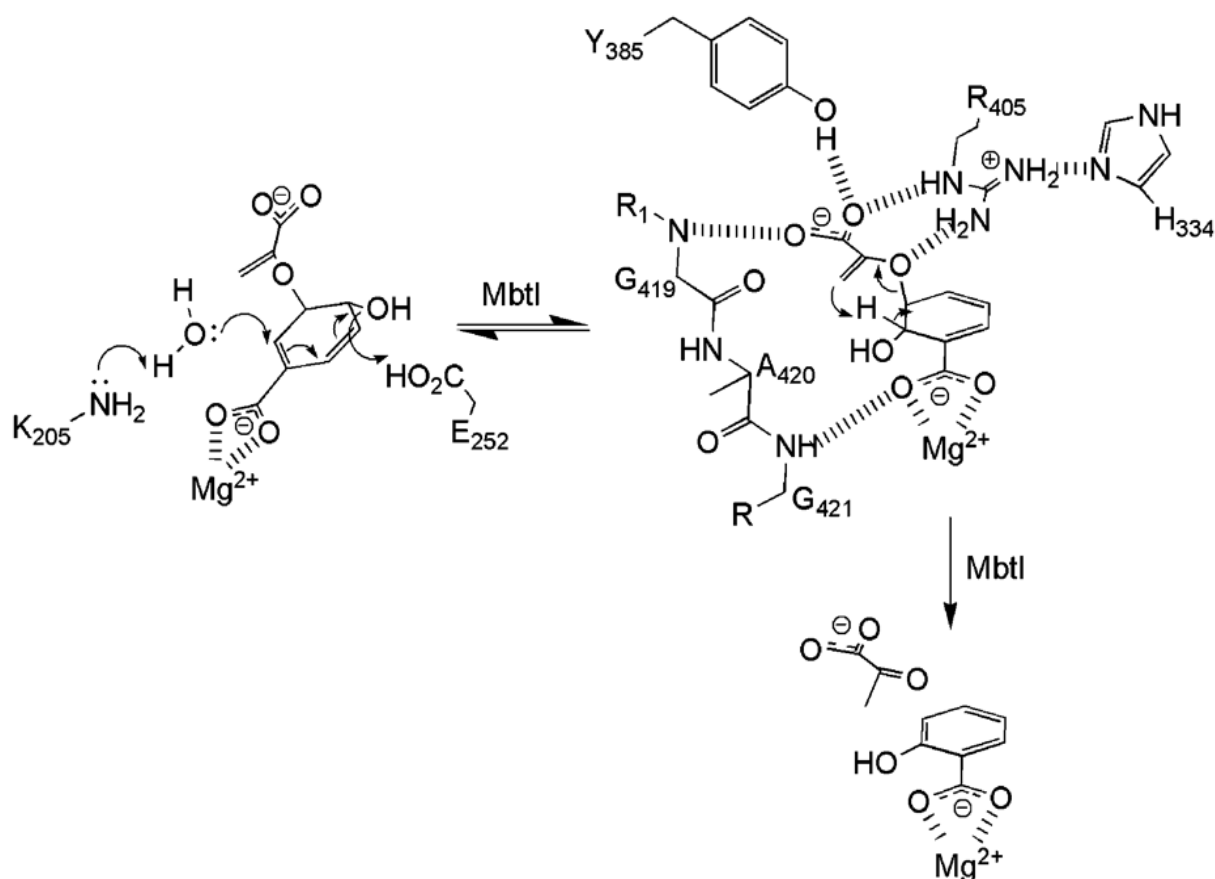


**Figure 9.** Structure of MbtI. (<http://www.rcsb.org/structure/2I6Y>)

The enzyme possesses both isochorismate synthase and isochorismate-pyruvate lyase activities. In presence of  $Mg^{2+}$  it catalyzes two partial reactions within the same active site (Zwahlen *et al.*, 2007). According to the proposed model, Lys205 binds one molecule of water and uses it to attach the chorismite C2 carbon atom for the isomerization reaction, then the two acidic amino acids, Glu297

and Glu434, mediates the acid catalysis for the elimination of the hydroxyl group from the C4 carbon (Zwahlen *et al.*, 2007), as shown in scheme 2. The following intramolecular [3,3]-sigmatropic rearrangement allows the release of pyruvic acid and salicylic acid (Zwahlen *et al.*, 2007).

Salicylic acid has other fates than mycobactins biosynthesis. In fact, it is also converted in prephenate and anthranilate that are precursors of the aromatic amino acids, in *p*-aminobenzoic acid (PABA) for the folate biosynthesis and in *p*-hydroxybenzoate for the ubiquinone and menaquinone biosynthesis (Harrison *et al.*, 2006).

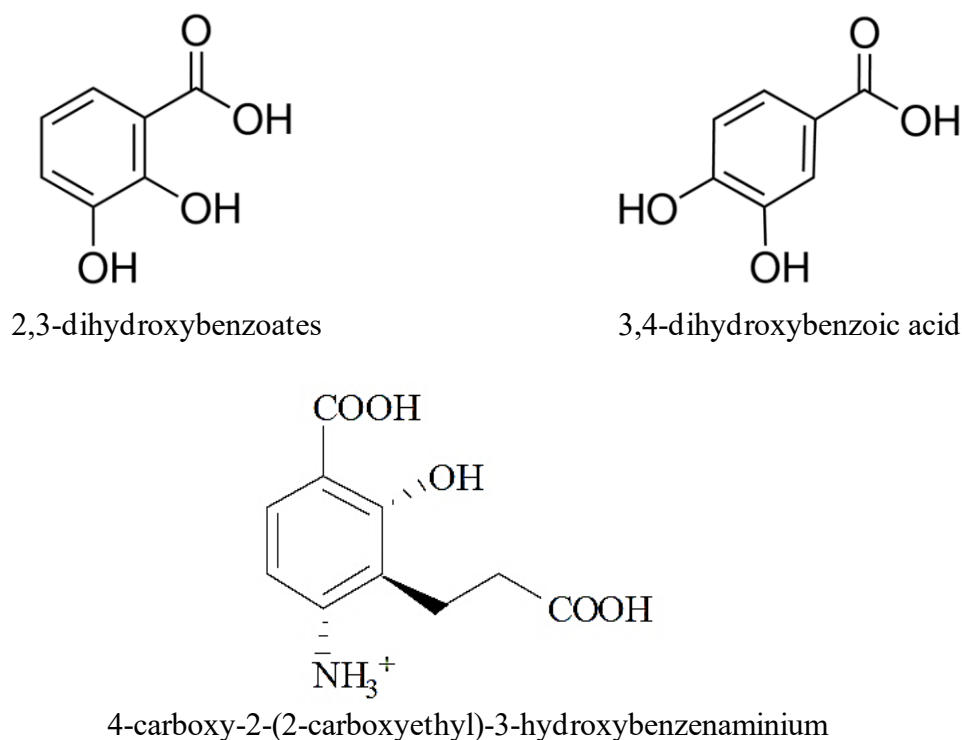


**Scheme 2.** Mechanism of action of MbtI (Zwahlen *et al.*, 2007).

Considering the importance of this molecule in mycobacteria and according to literature, different ongoing researches focus on stopping the salicylate biosynthesis, inhibiting MbtI enzyme activity, to develop new effective therapeutic strategies against *M. tuberculosis*. One important point to underline is that only bacteria, fungi and plants have MbtI homologous enzymes and there is not a corresponding protein in animals nor human. Thanks to its peculiarity, targeting MbtI may avoid the toxicity problem in putative regimens.

In literature are already reported some MbtI inhibitors, classified as chorismate analogues, isochorismate analogues and other inhibitors (Meneghetti *et al.*, 2016) (Figure 10).

The chorismate analogues are derivatives of the 3,4-dihydroxybenzoic acid. They have a  $K_i$  (dissociation constant) in a range of 190-1300  $\mu\text{M}$  and, because of this, they're considered as poor or moderate inhibitors.



**Figure 10.** Structures of MbtI known inhibitors.

The isochorismate analogues, derivatives of the 2,3-dihydroxybenzoates, are on the contrary strong inhibitors, with a  $K_i$  in the order of few  $\mu\text{M}$ . They were co-crystallized with MbtI, showing a structural rearrangement of the binding pocket that allowed to discover few information about the active site flexibility, important for the following docking studies. The derivatives of this family that showed the strongest inhibition have a dimethyl ester substituent.

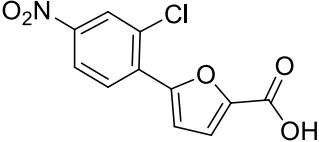
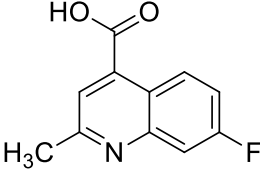
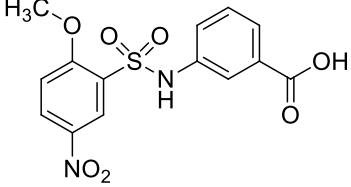
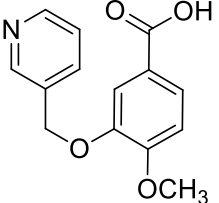
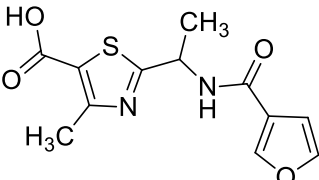
About the other inhibitors, they were chemically synthesized *ad hoc*, for example to mimic the transition state during the salicylic acid biosynthesis or have been identified by virtual docking screenings. In the first case, has been demonstrated that these inhibitors have high  $K_i$  (Liu *et al.*, 2015). In the second case, for example for benzisothiazolones, they are very powerful inhibitors with an  $\text{IC}_{50}$  close to the protein concentration, but they were also demonstrated to be PAINs (pan-assay interference compounds).

Finally, the benzimidazole-2-thiones are a family of reversible noncompetitive inhibitors that provided new information on inhibition studies.

## Aim of the work

Considering the literature and the previous studies about *M. tuberculosis*, we focused on identification and evaluation of new MbtI inhibitors as putative drugs to reduce the actual therapeutic regimens or as alternative drugs against MDR/XDR strains.

The medicinal chemists group lead by Prof. Stefania Villa (Dipartimento di Scienze Farmaceutiche DISFARM, Università degli Studi di Milano), following the strategy “target-to-drug”, performed a first virtual screening of Enamine database against MbtI using the software Ligandscout. The analysis set up was based on the protein crystal 3D structure. Starting from 1 500 000 available commercial compounds, they identified 5 candidates as potential good MbtI inhibitors.

Code	Chemical structure
I	
II	
III	
IV	
V	

**Table 1.** MbtI inhibitors identified by virtual screening (Chiarelli *et al.*, 2018).

To assess if the identified compounds are indeed effective MbtI inhibitors, the *mbtI* gene from *M. tuberculosis* was cloned in an expression vector. The recombinant enzyme was produced in *E. coli* and purified. Finally, to evaluate the effects of the different compounds was set up the appropriate inhibition enzymatic assay.

Moreover, together with the team of Prof. Villa, that chemically tailors the molecules, we analyzed all the derivates to understand the effect of the modifications on different substituents in different positions of the core molecule, focusing on building up a stronger and stable inhibitor.

## Materials and methods

### Materials

#### *Chemicals*

Tryptone, Yeast extract, SOB medium, agar were from Becton-Dickinson; K<sub>2</sub>HPO<sub>4</sub>, KH<sub>2</sub>PO<sub>4</sub>, KCl, NaCl, MgCl<sub>2</sub>, MgSO<sub>4</sub>, CuSO<sub>4</sub>, Tris(hydroxymethyl)aminomethane (Tris), Na<sub>2</sub>CO<sub>3</sub>, were from Nova Chimica.

Glucose, Na-K tartrate, sodium dodecyl sulfate (SDS), ammonium persulfate, isopropyl β-D-1-thiogalactopyranoside (IPTG), phenylmethylsulfonylfluoride (PMSF), kanamycin sulfate, Folin-Ciocalteu reagent, bovine serum albumine, acrylamide/methylen-bis-acrylamide solution, TEMED, dialysis tubes were from Sigma-Aldrich.

PageRuler Prestained Protein Ladder was from ThermoFisher Scientific.

HisTrap column were from GE-Healthcare.

Recombinant TEV protease was produced and purified in-house.

Chorismic acid was produced in *E. coli* KA12 cells according to Grisostomi *et al.* (1997), then purified by Prof. Villa.

All compounds present in this study were supplied by Prof. Villa.

### Methods

#### *MbtI expression and purification.*

The pET28b-MbtI vector encoding for the *M. tuberculosis* MbtI was provided by Dr. M. Bellinzoni (Institut Pasteur Paris, France). The gene was cloned in order to express a protein with a N-terminal 6xHis-tag, separated by the recognition cleavage site for the TEV protease for its removal.

BL21(DE3) *E. coli* cells transformed with pET28b-MbtI were cultured in LB growth medium in presence of 50 mg/ml of kanamycin in a New Brunswick™ Innova® 43 orbital shaker, at 37°C, until the cell culture reached an optical density at 600 nm of 0.6-0.8. IPTG, at final concentration of 0.5 mM, was added to the culture to induce MbtI expression, and cells were incubated at 25°C overnight. Cells were finally recovered from the medium by centrifugation using Avanti JXN-26 high speed centrifuge (Beckman Coulter) at 4 500 g for 20 minutes at 4°C. Cell aliquots were split by weight of ~10 grams and stored at -20°C until use.

A cell aliquot (~10 grams) was resuspended in 100 ml of 50 mM potassium phosphate pH 8.0, 500 mM KCl (buffer A), containing 1 mM PMSF. The cell rupture was performed by sonication using a 80 W sonicator (Felisari). 6 cycles of 30 seconds were alternated with 2 minutes of pause to avoid overheating. The extract was centrifuged at 50 000 g for 20 minutes at 4°C to remove cellular debris,



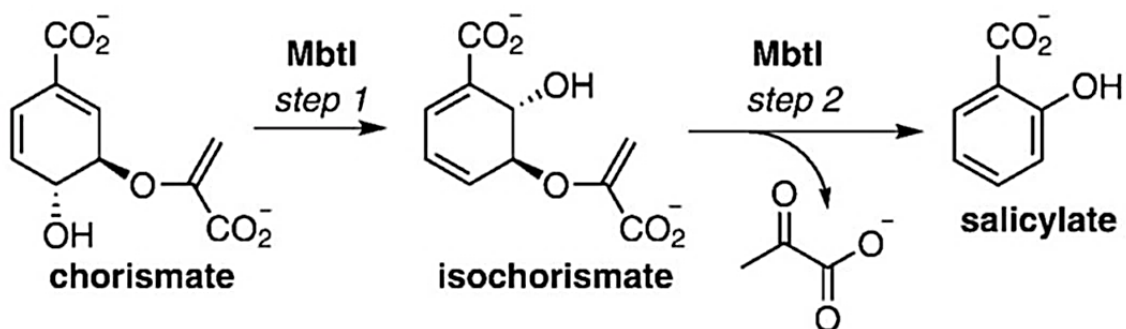
and the clarified cell free extract was purified by Immobilized Metal Affinity Chromatography (IMAC), in a HisTrap HP column (1 ml) equilibrated in buffer A. The column was washed with 50 mM of imidazole in buffer A to remove all the crude components bound, then MbtI was eluted using 500 mM of imidazole in Buffer A, dialyzed overnight in buffer C (50 mM potassium phosphate pH 8.0, 150 mM KCl, 0.5 mM DTT) in the presence of TEV protease.

The digested protein was further purified by a second IMAC in buffer C. Since the protein lacks its histidine tail, it was eluted within the flowthrough while the tag and the protease still bind to the column.

The purity of the enzyme preparation was assessed by 12% SDS-PAGE, and protein concentration determined according to Lowry *et al.* (1951).

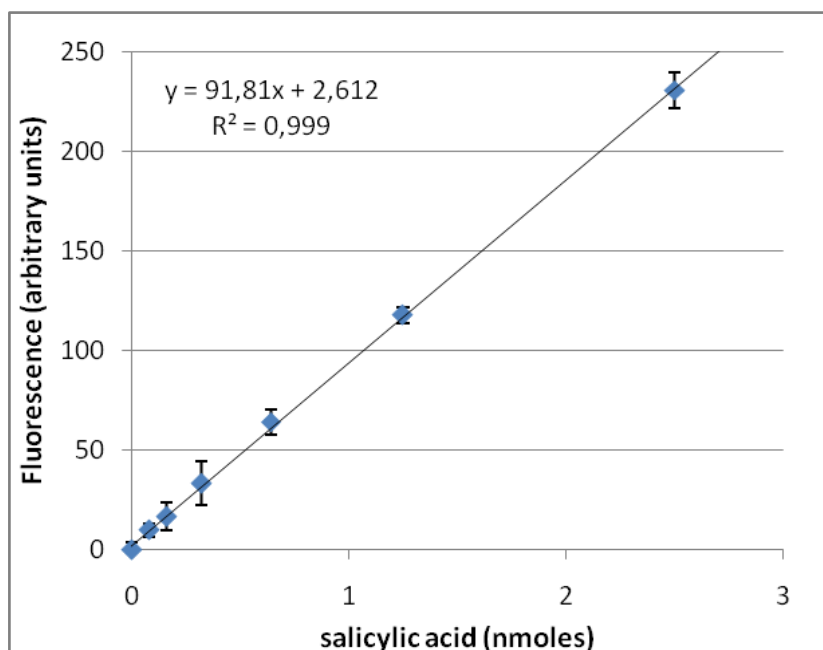
### Enzyme activity assay

MbtI enzyme activity was determined by measuring the production of salicylic acid (Figure 12), by a continuous fluorimetric assay, slightly modified from Vasan and colleagues (Vasan *et al.*, 2010), as this compound emits fluorescence at 410 nm upon excitation at 305 nm.



**Scheme 3.** Conversion of chorismate into salicylate by MbtI.

The assays were performed at 37°C in a final volume of 400  $\mu$ L, using a Perkin-Elmer LS3 fluorimeter. Typically, the reaction mixture contained: 50 mM potassium phosphate pH 8.0, 5 mM  $MgCl_2$ , 1-2  $\mu$ M MbtI, and the reactions were started by the addition of the substrate chorismic acid. Fluorescence signals were converted in product concentrations, by a titration curve built using different amounts of salicylic acid (Figure 11).



**Figure 11.** Titration curve of salicylic acid. In abscissa is reported the fluorescent value, in ordinate the nanomoles of salicylic acid.

Steady-state kinetic parameters were determined by assaying the enzyme activity at 8 different substrate concentrations and fitting the data to the Michaelis-Menten equation. All assays were performed in triplicate, and results analyzed using the Origin 8.0 software.

### *Inhibition assays*

The evaluation of the inhibition activity of different compounds was evaluated using the above reported fluorometric assay.

For a first screen, the assays were performed at subsaturating concentrations of chorismic acid (50  $\mu\text{M}$ ), in presence of putative inhibitors (stock dissolved 20 mM in DMSO) analyzed at final concentration of 100  $\mu\text{M}$ . Blank control was performed by adding DMSO. The assays were performed in triplicate, and the percentage of inhibition was evaluated.

For molecules inhibiting >70% of the enzymatic activity at this concentration the  $\text{IC}_{50}$ , (the inhibitor concentration that halves the enzyme activity), was evaluated.

To this purpose, the enzyme activity was measured in the presence of the compounds and values were estimated according to the following equation:

$$A_{[I]} = A_{[0]} \times \left( 1 - \frac{[I]}{[I] + \text{IC}_{50}} \right)$$

where  $A_{[I]}$  is the enzyme activity at inhibitor concentration  $[I]$  and  $A_{[0]}$  is the enzyme activity without inhibitor.

Finally, for the lead compounds the inhibition constant ( $K_i$ ) value was determined by assaying the MbtI enzymatic activity at different substrate and compound concentrations, using an adapted equation for competitive inhibition.

$$v = \frac{V_{\max} [S]}{[S] + K_m \left( 1 + \frac{[I]}{K_i} \right)}$$

All analyses were performed using the Origin 8 software.

#### *Pan Assay Interference Compounds (PAINS) analysis.*

Pan-assay interference compounds (PAINS) are chemical compounds that are often false positives in high-throughput screens, as they tend to nonspecifically react with numerous biological targets rather than specifically affecting one desired target (Dahlin *et al.* 2015). To exclude that the inhibiting compounds are indeed PAINS, a series of assays were performed.

Firstly, to verify the possible formation of aggregates, the ability of compound to inhibit MbtI activity was also tested in the presence of 0.1 mg/ml of bovine serum albumin (BSA) or in the presence of 0.01% (v/v) Triton X-100 as detergent (Shoichet, 2006; Baell and Holloway, 2010).

Moreover, to exclude a promiscuous enzyme inhibition due to covalent reaction with cysteines, MbtI inhibition activity of compound was also tested in the presence of 100  $\mu$ M of 1,4-dithio-DL-threitol (DTT).

#### *Minimal inhibitory concentration determinations and siderophore production assay*

The MIC<sup>99</sup> of active compounds against *M. bovis* BCG were determined in low-iron Chelated Sauton's medium (Siegrist *et al.*, 2009), using the resazurin reduction assay (REMA). (Palomino *et al.*, 2002). Siderophore activity present in the culture was tested in *M. bovis* BCG using the Universal CAS liquid assay (Schwyn and Neilands, 1987).

To this purpose, *M. bovis* grown in 7H9 medium, subcultured in chelated Sauton's medium, then diluted to an OD<sub>600</sub> of 0.01 in chelated Sauton's containing different concentrations of compound. After 15 days of incubation at 37°C cells were harvested, and supernatants were used to perform CAS assay, and cell pellets for the determination of mycobactins. For CAS assay, a 100  $\mu$ l

of supernatant was mixed with 100  $\mu$ l of CAS assay liquid solution in 96 well plate, incubated 10 min at room temperature, and the absorbance was measured at 630 nm. The siderophore units were calculated using the following equation

$$\frac{A_r - A_s}{A_r} \times 100$$

where  $A_r$  is the absorbance at 630 nm of the blank medium with CAS assay solution and  $A_s$  is the absorbance of the culture supernatants with CAS assay solution.

For mycobactins determination cell pellets were extracted in ethanol overnight, then 0.1 M  $\text{FeCl}_3$  in ethanol was added until no color change was observed. The mixture was incubated at room temperature for 1 h, then mycobactins were extracted in chloroform, washed with water, evaporated and residue dissolved in methanol. The concentration of mycobactins was determined measuring the absorbance at 450 nm (1% solution of mycobactins gives an absorbance of 42.8).

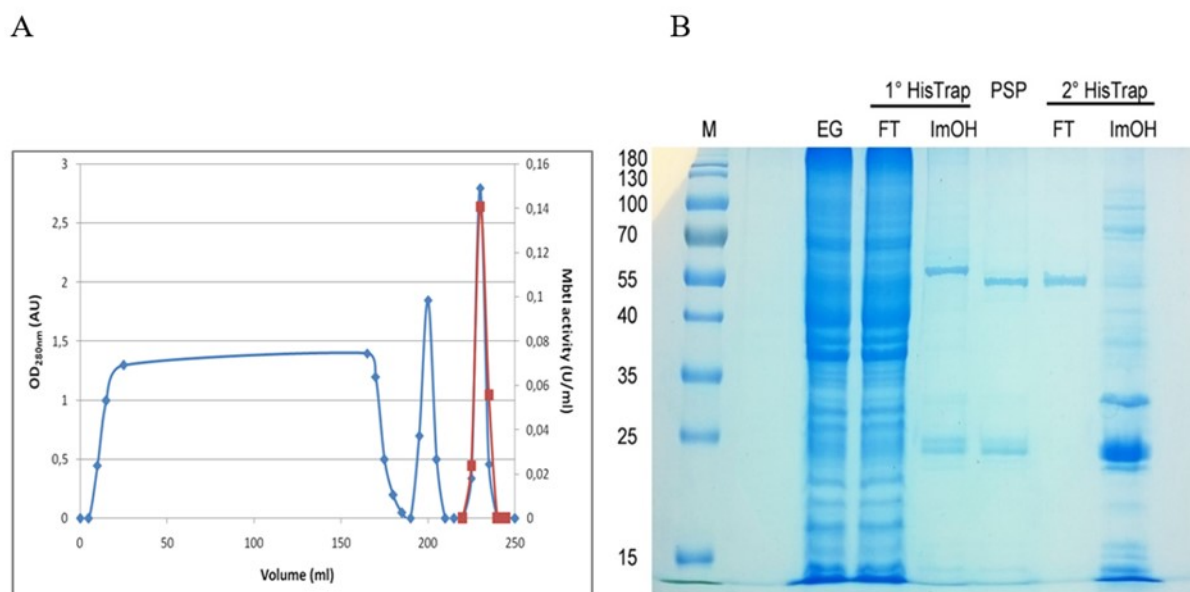
## Results and discussion

As previous studies demonstrated the value of the salicylate synthase MbtI as an antitubercular drug target (De Voss *et al.*, 2000; Manos-Turvey *et al.*, 2010), this study aim to identify new potent inhibitors of this enzyme, as potential lead compounds. In collaboration with the medicinal chemists group lead by Prof. Villa, by virtual screening of Enamine database, five molecules have been identified as putative ligands of MbtI.

These compounds have been evaluated for their activity against MbtI, and for this reason the recombinant enzyme have been produced and purified.

### Expression, purification and characterization of the recombinant MbtI

The recombinant MbtI from *M. tuberculosis* was expressed and purified to homogeneity as reported in material and methods (Figure 12).



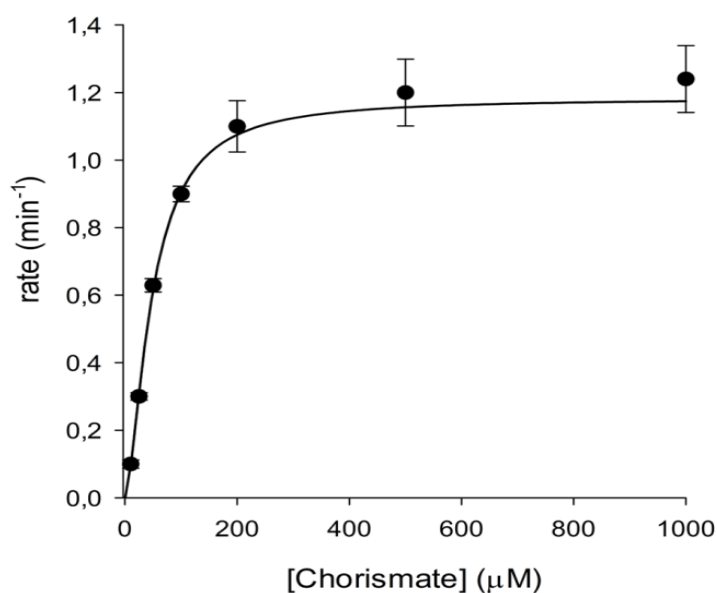
**Figure 12.** Purification of the recombinant *M. tuberculosis* MbtI. A) Elution profile of MbtI from the HisTrap chromatography. Blue line represents the absorbance at 280 nm. Red squares indicate the enzyme activity. B) SDS-Page of different purification steps of MbtI. M: standard marker; EG: free cell extract; FT: elution with 50 mM of Imidazole in Buffer A; ImOH: elution with 500 mM of Imidazole; PSP: MbtI after digestion.

Table 2 summarizes the main results of a typical MbtI purification, showing that the adopted procedure allowed to obtain about 9 mg of purified MbtI, with a yield of 55%, and a specific activity of 0.107 U/mg.

Purification steps	Volume ml	Proteins mg/ml <sup>a</sup>	MbtI activity U/ml	Total proteins mg	Total MbtI activity U	Specific activity U/mg	Yield <sup>b</sup> %	Purification factor
Free cell extract	200	12.0	0.009	2400	1.80	0.001	100	1
1 <sup>st</sup> IMAC	15	3.5	0.075	52.5	1.12	0.021	62,5	28.5
Dialysis and digestion	18	1.2	0.061	21.6	1.10	0.051	61	67.7
2 <sup>nd</sup> IMAC	22	0.42	0.045	9.2	0.99	0.107	55	142.8
<sup>a</sup> Determined according to Lowry								
<sup>b</sup> Calculated on enzymatic units								
<b>Table 2.</b> Example of main results of a typical purification of MbtI.								

To check the catalytic properties of the obtained recombinant MbtI, the main kinetic parameters have been evaluated. To this purpose, activity assays were set up at 37°C on a final volume of 400  $\mu$ l, using a final MbtI concentration of 2  $\mu$ M, in the presence of 7 different concentrations of chorismic acid.

As shown in figure 13, the enzyme showed a hyperbolic response to the substrate, with a  $V_{max}$  of  $1.3 \pm 0.08 \text{ min}^{-1}$  and a  $K_m$  of  $69.6 \pm 8.5 \text{ }\mu\text{M}$ . These values, in agreement with the data previously reported in literature (Zwahlen *et al.*, 2007), confirm the validity of the enzyme preparation, now suitable for our purposes.



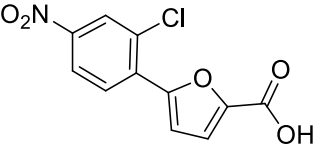
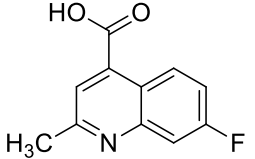
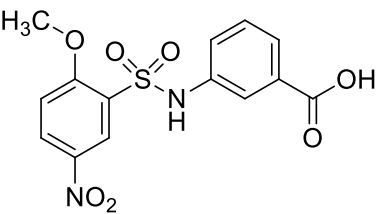
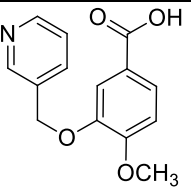
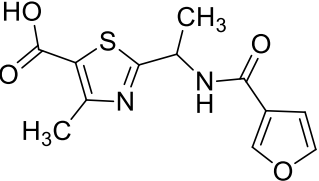
**Figure 13.** Steady state kinetic analysis of MbtI as a function of concentration of chorismic acid. Data are mean  $\pm$  SD of three different replicates.

## Inhibition assays of the compounds from virtual screening on MbtI activity

The obtained recombinant MbtI was used to assess the effects on the enzyme activity of the 5 hit compounds, identified with the virtual screening.

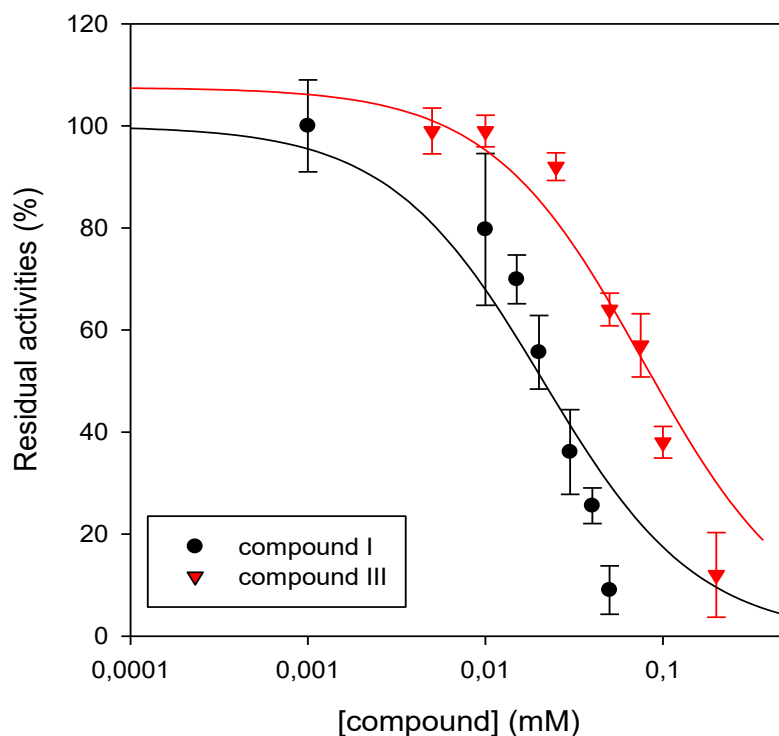
A first inhibition assay evaluates the percentage of inhibition of MbtI enzymatic activity at fixed concentration of 100  $\mu$ M. All assays were performed in triplicate, at a final non-saturating concentration of 50  $\mu$ M chorismic acid, in order to identify also competitive inhibitors. MbtI activity was assayed in presence of 2  $\mu$ l of pure DMSO to exclude solvent interaction with the enzyme.

As shown in Table 3, compound I was found to be provided with a remarkable activity, being able to inhibit more than 80% of MbtI activity at the tested concentration. Compound III displayed a modest activity (residual activity about 40%) while the three other compounds resulted completely inactive.

Compound	Chemical structure	Residual activity at 100 $\mu$ M (%)
I		21.3 $\pm$ 4.3
II		101.3 $\pm$ 3.6
III		38.4 $\pm$ 11.4
IV		104.0 $\pm$ 13.2
V		108.8 $\pm$ 12.0

**Table 3.** Activity of compounds I-V against MbtI.

To confirm these results, the  $IC_{50}$  of the active molecules have been determined. The two active compounds were able to inhibit the enzyme activity in a concentration dependent manner, with  $IC_{50}$  of  $21.1 \pm 4.1 \mu\text{M}$  for I and of  $77.6 \pm 4.1 \mu\text{M}$  for III (Figure 14). Interestingly, compound I showed an activity similar to that of the most potent MbtI inhibitors reported in the literature, belonging to the class of the benzimidazole-2-thiones (Vasan *et al.*, 2010), and to the AMT-series (Manos-Turvey *et al.*, 2010; Manos-Turvey *et al.*, 2012), confirming the validity of the approach and of the virtual screening used for the identification of new hit compounds.

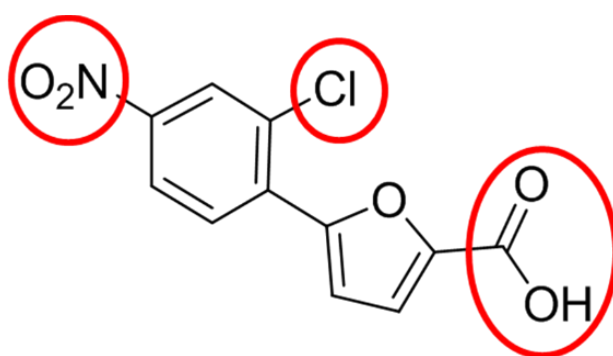


**Figure 14.**  $IC_{50}$  determination of the two active compounds I and III.



## Structure-activity relationship (SAR) studies.

Compound I, which resulted the best inhibitor identified, was the starting point for the development of novel MbtI inhibitors, to obtain new derivatives showing potent *in vitro* inhibition. Firstly, in order to support the importance of each pharmacophoric feature disclosed by the modeling studies, analogs were designed and synthesized to explore the chemical space and to study the structural and functional requirements for the activity against MbtI. Particularly, as shown in Figure 15, two main points, the substituents at the phenyl ring and the carboxylic moiety have been taken into account.



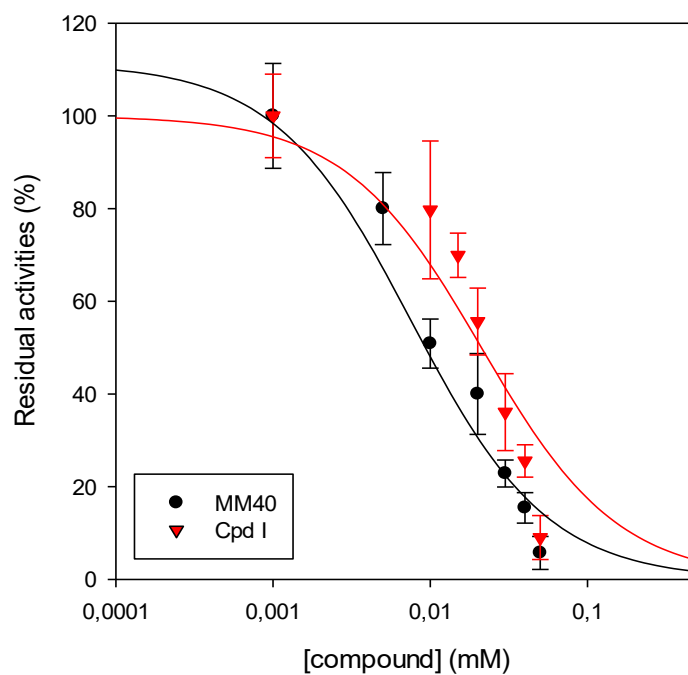
**Figure 15.** Compound I structure in which the moieties considered for SAR studies are highlighted.

To this purpose, the compounds in which *para* nitro group or the chlorine atom have been alternatively (compounds MM-37 and MM-40, respectively), or completely (MM-76) removed from I (Table 4) have been assayed. The removal of the -NO<sub>2</sub> group led to a complete loss of activity of the compound, demonstrating the essentiality of this moiety. By contrast, MM-40, in which the chlorine atom was removed, showed an improved activity, with respect to I, as demonstrated also by an IC<sub>50</sub> 3-fold lower ( $7.6 \pm 1.6 \mu\text{M}$ ) (Figure 18).

Similarly, from experimental data it's clear that the carboxylic group linked to the furan ring it's fundamental for the right molecular interaction with MbtI. Indeed, the esterification of this group significantly lowered the inhibition properties of compound MM-40E.

Molecule	Structure	MbtI residual activity %
I		21.3 ± 4.3
MM-37		92.4 ± 13.8
MM-40		18.2 ± 5.1
MM-76		102.0 ± 8.5
MM-40E		71.1 ± 18.4

**Table 4.** Activity of the compound I analogs synthesized to understand the role of the different moieties.

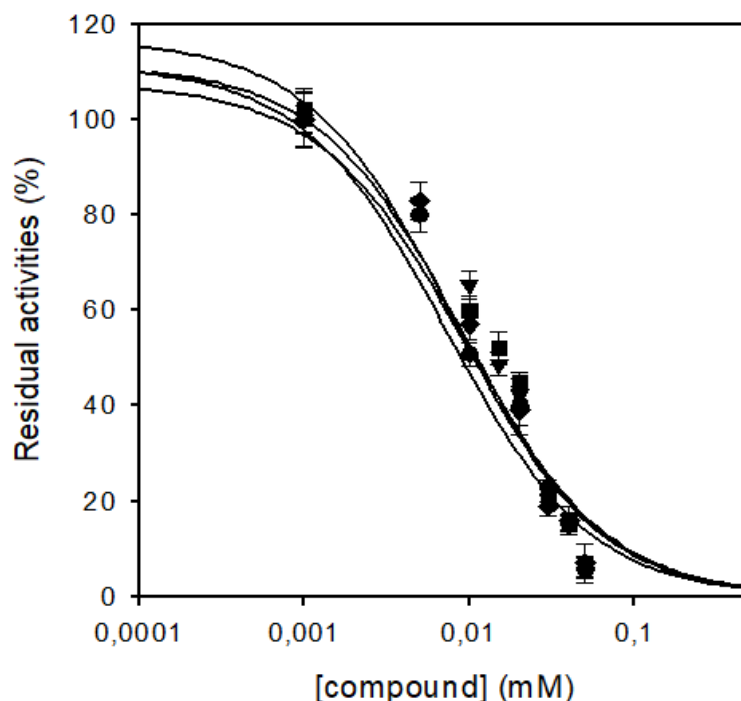


**Figure 16.** Comparison between  $IC_{50}$  of MM-40 and compound I.

A great issue in the drug discovery process is represented by the so-called Pan-Assay Interference Compounds (PAINS). PAINS are chemical compounds that often give false positives in high-throughput screens, that tend to nonspecifically react with several and different biological targets (Dahlin *et al.*, 2015; Dahlin and Walters, 2016). For this reason, it is fundamental to confirm that the identified lead compounds are real and very specific MbtI inhibitors. With this aim, MM-40 was further analyzed to exclude that its effects are due to nonspecific promotion of protein aggregation, or through covalent reactions with the cysteine residues, the two more common mechanism of PAINS.

Firstly, IC<sub>50</sub> values were evaluated in presence of 0.1 mg/ml of BSA or with 0.01% (v/v) of Triton X-100 detergent, to prove that the inhibition is not caused by MbtI aggregation promoted by the presence of the compound. Moreover, the inhibition capacity of the two molecules was also evaluated in presence of DTT, to exclude a promiscuous inhibition due to a covalent reaction of the compounds with MbtI cysteine residues.

As show in figure 17, the IC<sub>50</sub> of the compound is unaltered in the presence of 1 mg/ml of BSA or 0.01% Triton X-100 or 100 μM DTT (diamonds). This data confirms that the inhibitor does not promote MbtI aggregation and is not a thiol reactive agent, proving that MM-40 is real inhibitors of MbtI activity by competition with the chorismic acid for the active site.

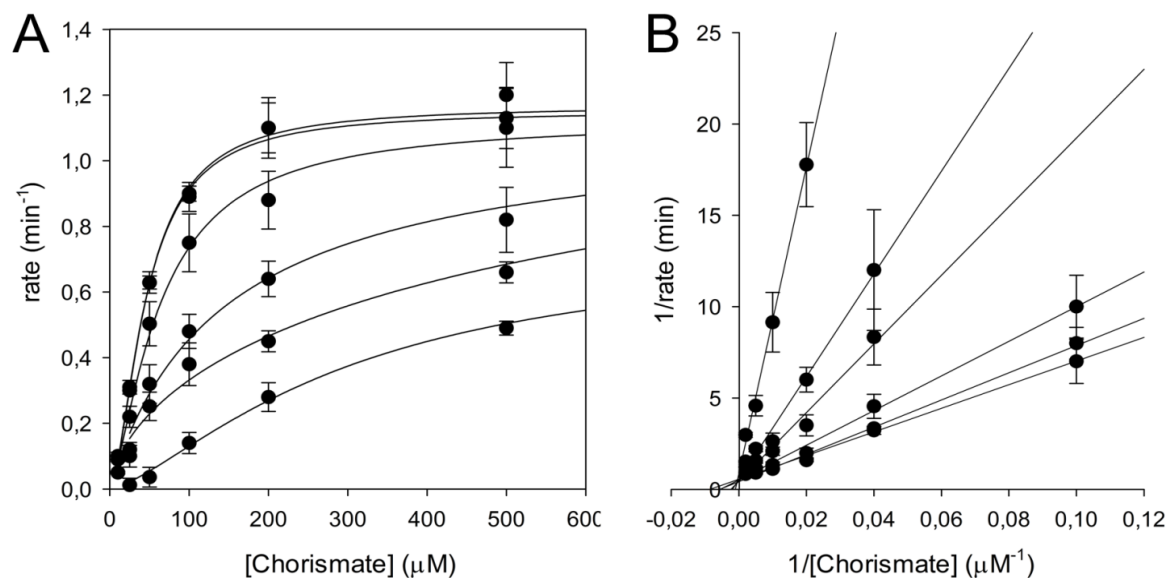


**Figure 17.** IC<sub>50</sub> plot of 1a in the presence of BSA (squares), Triton X-100 (triangles) and DTT (diamonds).

To better investigate the mechanism of inhibition of this new potent MbtI inhibitor, a series of steady-state kinetic analysis towards chorismic acid have been performed in the presence of different concentrations of MM-40 (Figure 19).

The kinetic data clearly demonstrated that the compound behaves as a competitive inhibitor towards the chorismate binding site. Indeed, as shown in the Lineweaver-Burk plot (Figure 18 B), in the presence of the inhibitor the  $V_{max}$  is unchanged, while the  $K_m$  values were increased.

Clearly, this feature is not unexpected, as the initial virtual screening was performed on the active site of the enzyme. The  $K_i$  value of the compound was  $5.3 \pm 0.6 \mu\text{M}$ , confirming that the 5-(4-nitrophenyl)furan-2-carboxylic acid MM-40 compound is the best inhibitor until now reported, thus it was considered as the lead compound, and used to design all other analogs.

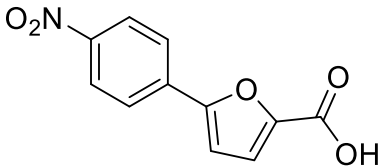
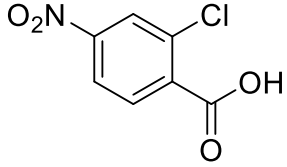
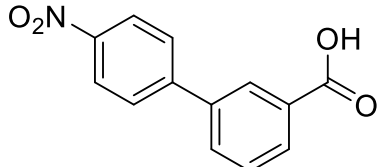


**Figure 18.** Steady state kinetic analyses towards chorismic acid of MbtI in the presence of different concentrations of MM-40 (0, 5, 10, 20, 50 and 100 mM) highlights the competitive behavior of the inhibitor. Global reciprocal plot of data is represented in panel B. Data are mean  $\pm$  SD of three replicates.

In particular, the investigation involved the furan ring, the position of the nitro group, as well as the effects of further substituents on the phenyl ring, and the possibility to replace the  $-\text{NO}_2$  with other functional groups.

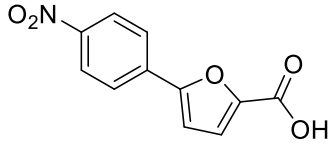
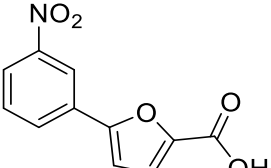
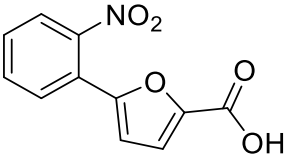
Firstly, to explore the role of the furan ring, two MM-40 derivatives have been tested: MM-43 in which the furan have been removed, and MM-82, bearing instead a phenyl group (Table 5).

The lack of the furan ring abolished almost completely the activity of the compound, while its substitution with a phenyl decreased significantly its potency. From these data it is conceivable that the furan moiety is necessary to maintain the geometry of the carboxylic and nitro group, and their relative distance, in order to bind effectively MbtI.

Molecule	Structure	MbtI residual activity %
MM-40		18.2 ± 5.1
MM-43		89.3 ± 16.1
MM-82		32.2 ± 6.8

**Table 5.** Structures and activities of MM-40 analog compounds with modification of the furanic ring.

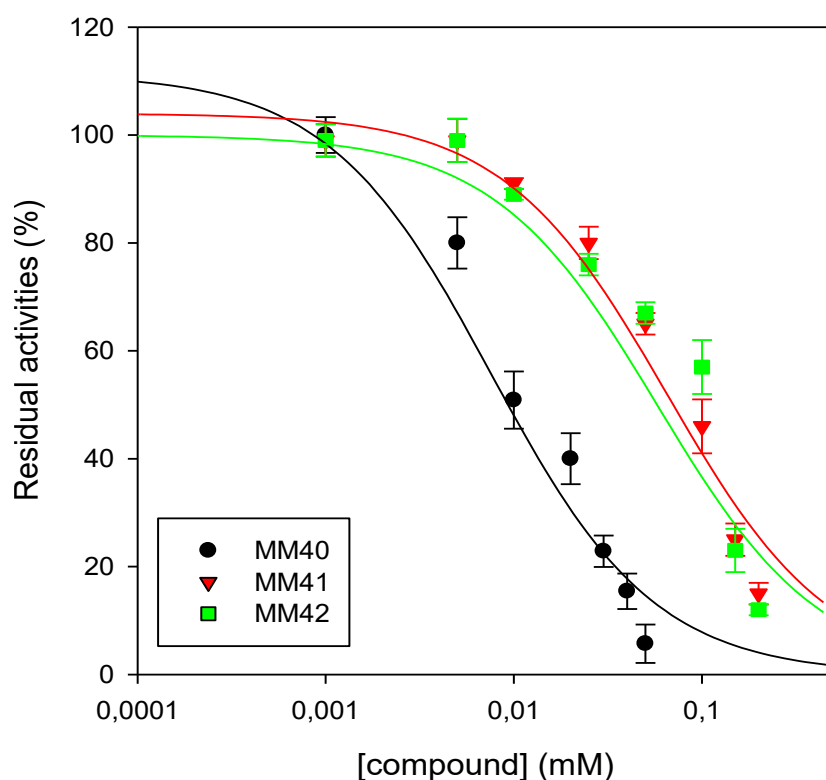
Likewise, to understand if the para position of the nitro group is essential for the inhibitory effects of MM-40, two derivatives with the -NO<sub>2</sub> in meta and in ortho positions (MM-41 and MM-42, respectively) have been assayed (Table 6).

Molecule	Structure	MbtI residual activity %
MM-40		18.2 ± 5.1
MM-41		55.8 ± 5.2
MM-42		55.1 ± 12.7

**Table 6.** Structures of MM-40 analogs, with nitro group in different positions of the phenyl ring.

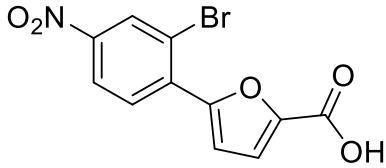
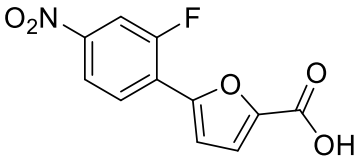
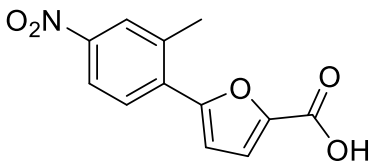
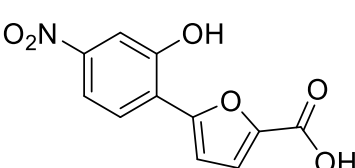

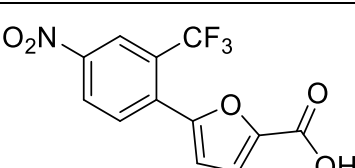
The two compounds were still active against MbtI, but the para-position of the -NO<sub>2</sub> was confirmed to be associated with the best inhibitory properties of the compound. Indeed, the MM-41

and MM-42 were about 10-fold less potent, with  $IC_{50}$  values of  $65.1 \pm 3.2 \mu\text{M}$  and  $57.7 \pm 5.1 \mu\text{M}$ , respectively (Figure 19).



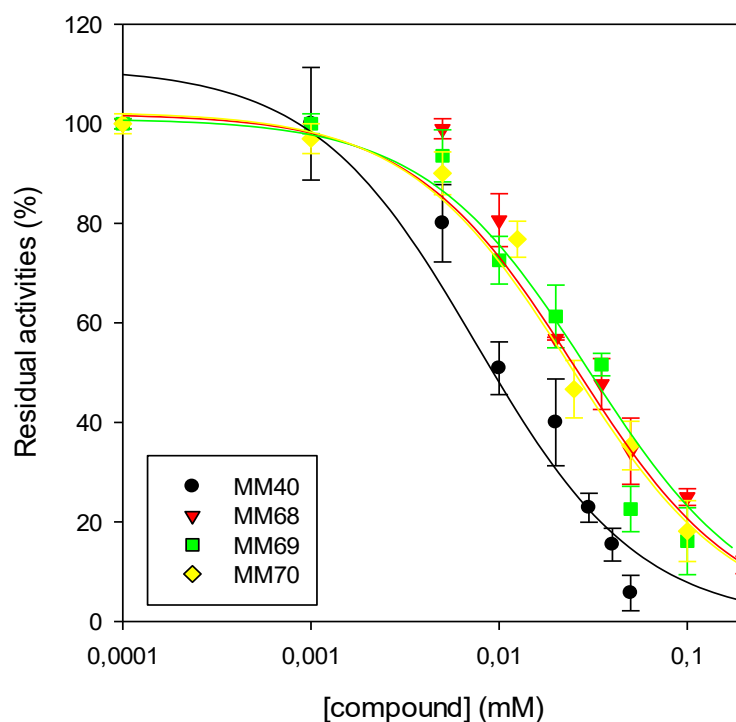
**Figure 19.**  $IC_{50}$  of the three compounds, showing the nitro group in different position of the phenyl ring: MM-40 (in black), MM-41 (in red) and MM-42 (in green).

Compound I and MM-40 differs for the chlorine atom in ortho of the phenyl ring, and the removal of this group improved the inhibitory properties of the compound. Thus, with the aim to further improve the activity, a series of compounds (MM-66 to MM-70 and MM-91) bearing different substituents in ortho position of the phenyl ring have been assayed (Table 7).

Molecule	Structure	MbtI residual activity %
MM-66		32.1 ± 2.4
MM-67		34.9 ± 4.9
MM-68		11.6 ± 4.5
MM-69		13.9 ± 4.0
MM-70		13.5 ± 3.8
MM-91		25.9 ± 3.7

**Table 7.** Structures of MM-40 derivatives compounds with additional substituents in ortho position of the phenyl ring.

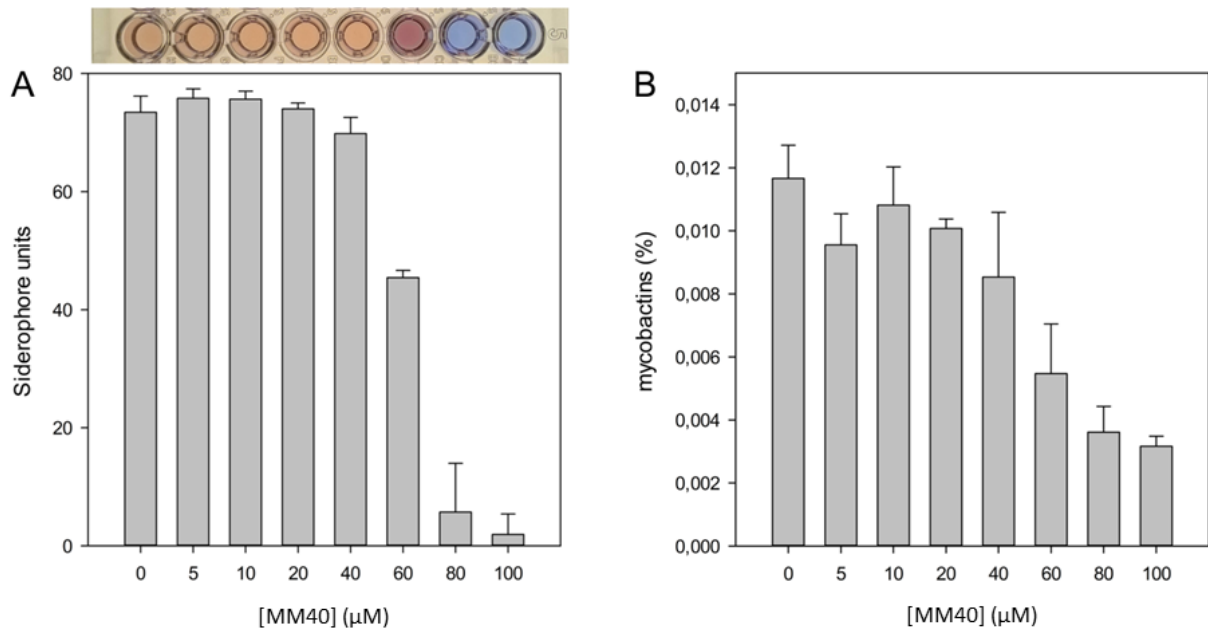
Data showed that all these compounds are strong MbtI inhibitors, at high concentration (100  $\mu$ M), underlining the importance of the electronegative group in para. However, none of them showed a significant improvement in potency respect to MM-40. Indeed, the  $IC_{50}$  of the three best inhibitors of this series have been determined, and as shown in figure 20 there was not a real improvement of the inhibitors ( $IC_{50}$  of  $25.4 \pm 1.9$ ,  $29.8 \pm 4.2$  and  $23.9 \pm 5.2$   $\mu$ M, for MM-68, MM-69 and MM-70, respectively).



**Figure 20.** IC<sub>50</sub> determination of MM-40, MM-68, MM-69 and MM70.

In order to assess its antimycobacterial potential, MM-40 was investigated for its activity against the non-pathogenic *M. bovis* BCG, whose siderophores resemble the structure of *M. tuberculosis* mycobactins, determined in the low iron containing Chelated Sauton's medium. In these conditions, the compound showed a MIC<sup>99</sup> of 80  $\mu$ M. Moreover, the levels of siderophore production were determined using universal CAS liquid assay and through the mycobactins isolation and quantification. As shown in Figure 21, the CAS assay performed on the medium of the cells grown in different MM-40 concentrations, showed a removal of iron inversely related to the concentration of the compound. Similarly, the concentration of mycobactins, determined in the same cells, decreased at higher concentrations of MM-40, confirming that the inhibitory effects are related to mycobactin biosynthesis inhibition.





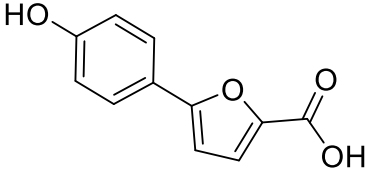
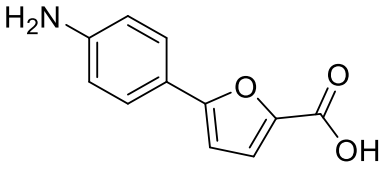
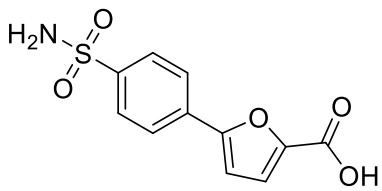
**Figure 21.** A) Universal CAS assay performed on media of *M. bovis* BCG cells grown in the presence of different concentrations of MM-40. B) Determination of the mycobactins in the abovementioned cells. Bars represent mean and standard deviation of three independent experiments.

## Optimization of the lead compound MM40

Despite many antituberculars in use or in clinical trials are characterized by a nitro group, as for example the nitroimidazoles or the benzothiazinones (Chiarelli *et al.*, 2016), this kind of compounds usually are not a preferred choice in medicinal chemistry, mainly due to their potential mutagenic effects. For this reason, several compounds, bearing different substituents in para position of the phenyl ring were assayed. In this series, compounds bearing new substituents with different electronegativity have been explored.

Firstly, the strong electron-acceptor  $-\text{NO}_2$  group have been substituted by electron donor moieties, such hydroxyl or amine groups (Table 8).

These compounds do not show any inhibition properties on MbtI, one more proving the hypothesis that the electronegativity of the group in para position on phenyl ring is important.

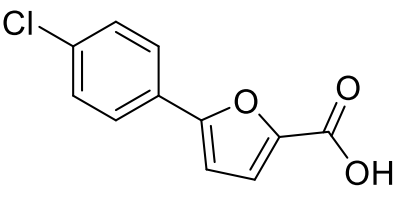
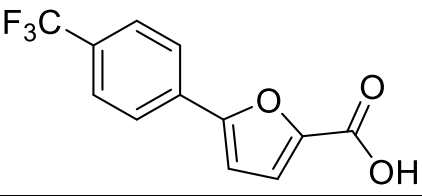
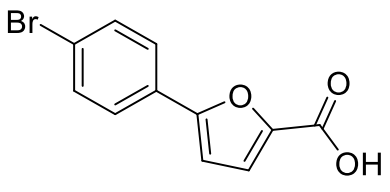
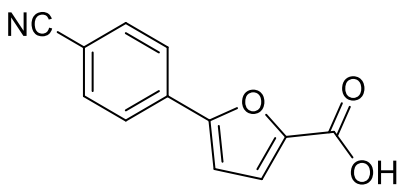
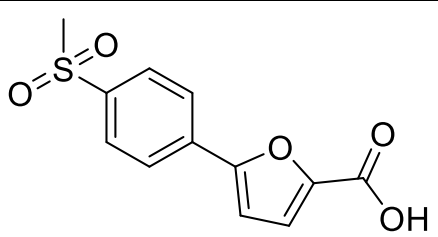
Molecule	Structure	MbtI residual activity %
MM-30		$96.3 \pm 19.2$
MM-45		$100.3 \pm 11.5$
MM-59		$85.1 \pm 16.2$

**Table 8.** Structure of MM-40 analogs with electron donor groups, instead of the  $-\text{NO}_2$ .

Moreover, different electron acceptor groups were substituted to the nitro: weak acceptors (halogen atoms in MM-36, MM-44), intermediate (sulfonyl group of MM-58), or strong (trifluoromethyl or nitrile in MM-38 and MM-55) (Table 9).

As expected, weak and intermediate acceptor substituents led to a complete loss of the compound activity. Moreover, also the substitution with the cyanide ( $-\text{CN}$ ) group abolished the

inhibitory effects, while the presence of a trifluoromethyl (-CF<sub>3</sub>) significantly decreased the potency of the compound.

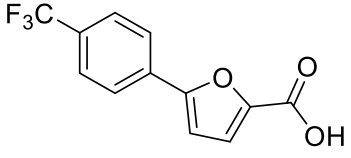
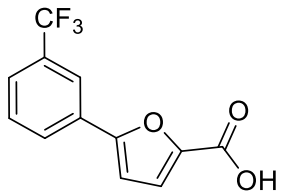
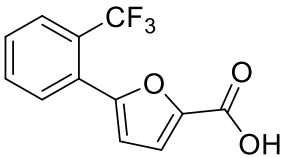
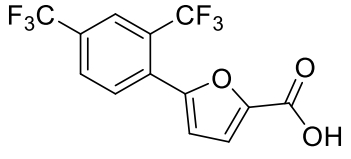
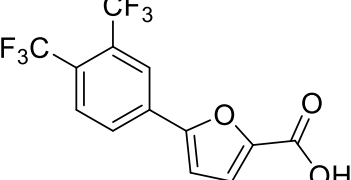
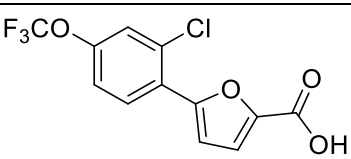
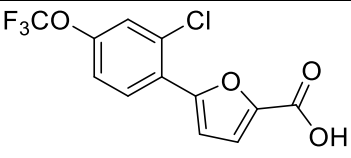
Molecule	Structure	MbtI residual activity %
MM-36		130.3 ± 36.2
MM-38		56.3 ± 9.7
MM-44		88.5 ± 22.4
MM-55		125.6 ± 17.9
MM-58		98.5 ± 14.4

**Table 9.** Structures of MM-40 derivatives with different electron acceptor groups instead of the nitro moiety.

Anyway, since MM-38, at 100 μM, halves the MbtI residual activity and the -CF<sub>3</sub> is potentially less cytotoxic compared to the -NO<sub>2</sub>, compounds with -CF<sub>3</sub> substituents in ortho and para positions have been tested, in the attempt to explore their inhibition power. Also, the effects of the para -CF<sub>3</sub> in combination with other ortho and meta substituents, were investigated. Finally, an ether derivative has been synthesized in order to understand if the -CF<sub>3</sub> can be further modified. (Table 10).

As showed in data, the trifluoromethyl group must be kept unaltered, otherwise the compound loses its inhibition properties, as in the case of MM-54 bearing a trifluoromethoxy. Anyway, from

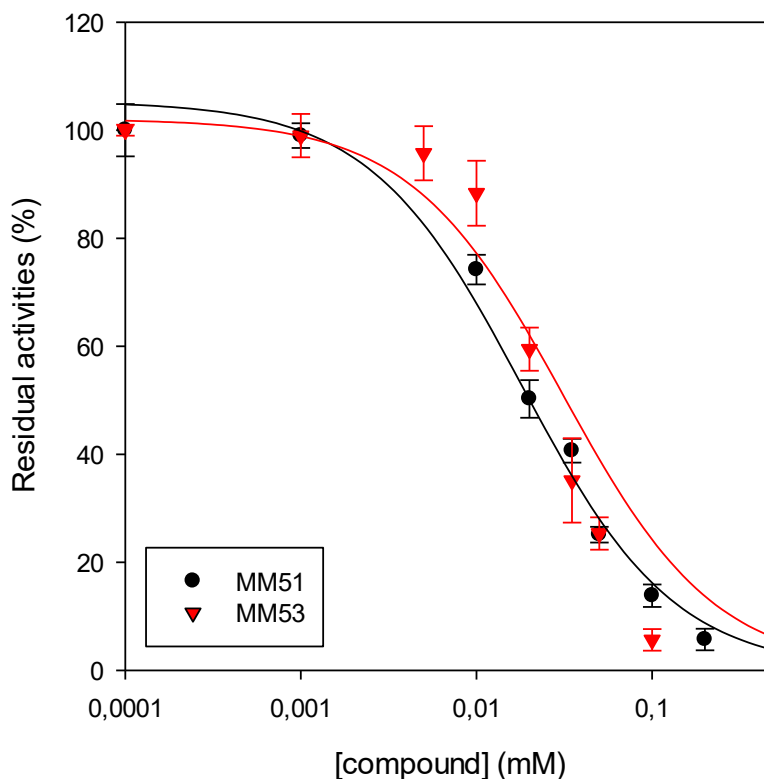
this series, MM-19 compound with the  $-CF_3$  in meta is interesting because it shows a comparable inhibition to MM-38. By contrast, the same group in ortho causes a significant loss of activity.

Molecule	Structure	MbtI residual activity %
MM-38		$56.3 \pm 9.7$
MM-19		$42.0 \pm 6.3$
MM-39		$98.0 \pm 16.6$
MM-51		$7.0 \pm 3.8$
MM-52		$66.1 \pm 5.6$
MM-53		$6.3 \pm 1.1$
MM-54		$71.2 \pm 5.6$

**Table 10.** Structures of derivatives of MM-38 compound.

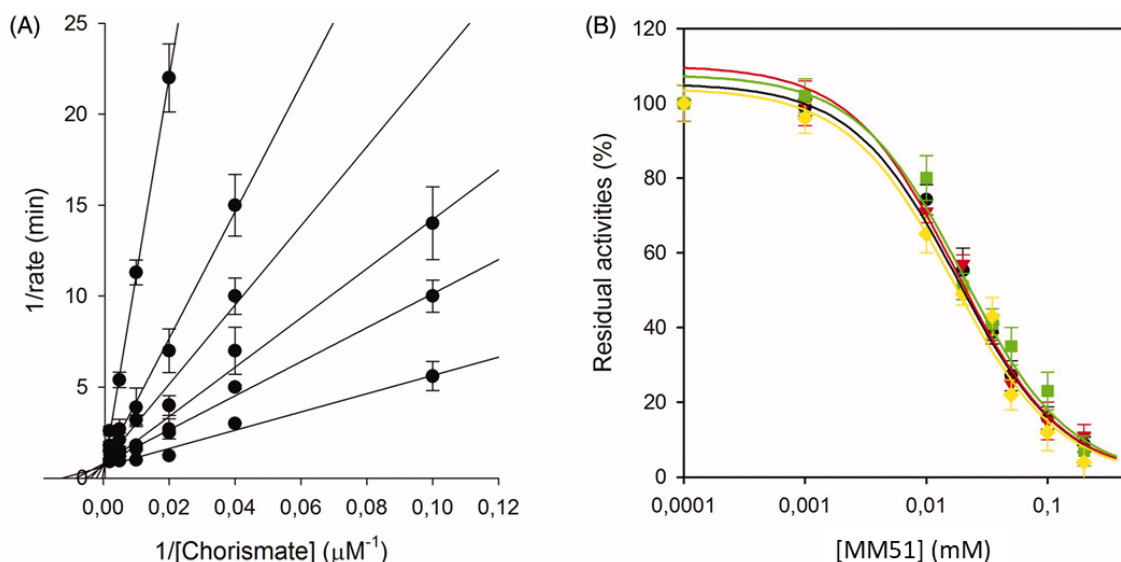
Starting from this consideration, two  $-CF_3$  groups have been added in ortho and meta positions giving rise to two compounds that possess a remarkable inhibition property: MM-51 and MM-53. In their presence, indeed, MbtI residual activity is less than 10%. Intriguingly, the addition of an electron attractor group in ortho to MM-38 significantly increased the potency of this compound. By contrast no improvements were found if the group is added in meta position.

According to the  $IC_{50}$  values of MM-51 and MM-53 ( $18.0 \pm 1.8 \mu\text{M}$  and  $31.0 \pm 8.0 \mu\text{M}$ , respectively) (Figure 22) the two compounds can be considered good inhibitors of MbtI, although no great improvements are obtained with respect to MM-40. Anyway, these compounds are potentially less cytotoxic compared to MM-40, and for this reason they are interesting from a pharmacological point of view. Also, the obtained data are a further proof of the essentiality of an electron attractor group on the phenyl ring in the construction of a strong inhibitor against MbtI.



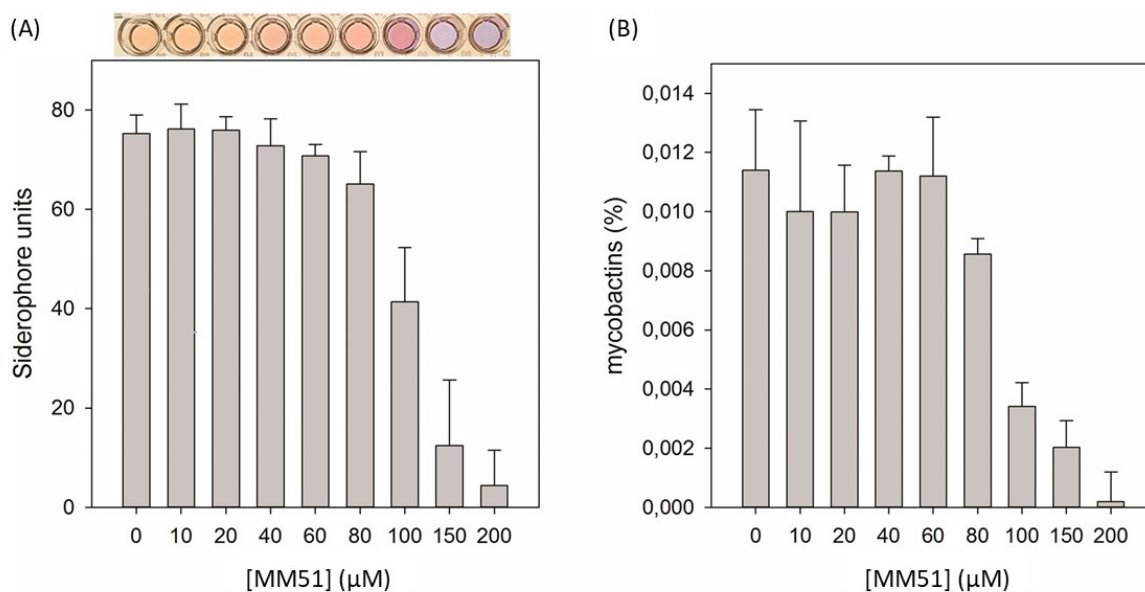
**Figure 22.**  $IC_{50}$  of MM-51 (black) and MM-53 (red) compounds.

MM-51 was confirmed to not behave as a PAIN compound, and to be an effective MbtI competitive inhibitor, with a  $K_i$  value of  $8.8 \pm 0.7 \mu\text{M}$  (Figure 23).



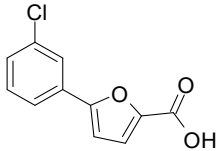
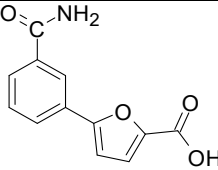
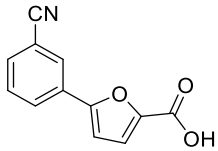
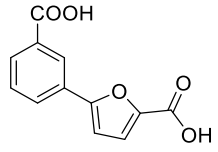
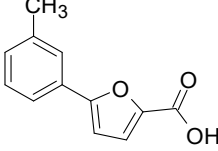
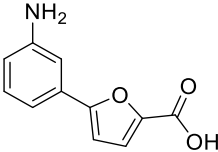
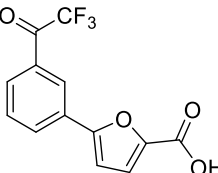
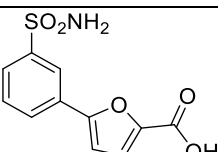
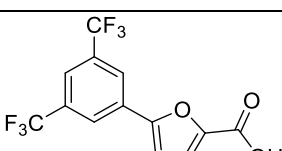
**Figure 23.** A) Global reciprocal plot of data from MbtI steady-state kinetics analysis towards chorismic acid, in the presence of different concentrations of MM-51. B) IC<sub>50</sub> plots of MM-51 in the presence of BSA (green squares), Triton X-100 (red triangles) and DTT (yellow diamonds)

Unfortunately, when assayed against the mycobacterial cells, the compound was found to be significantly less effective than MM-40, showing an IC<sub>50</sub> value of 250 μM. In any case, the activity is linked to siderophore inhibition, as demonstrated by CAS assay and mycobactin determination (Figure 24).



**Figure 24.** A) Universal CAS assay performed on culture media of *M. bovis* BCG cells grown in the presence of MM-51. B) Determination of the mycobactins in the above-mentioned cells. All data are mean ± SD of three replicates.

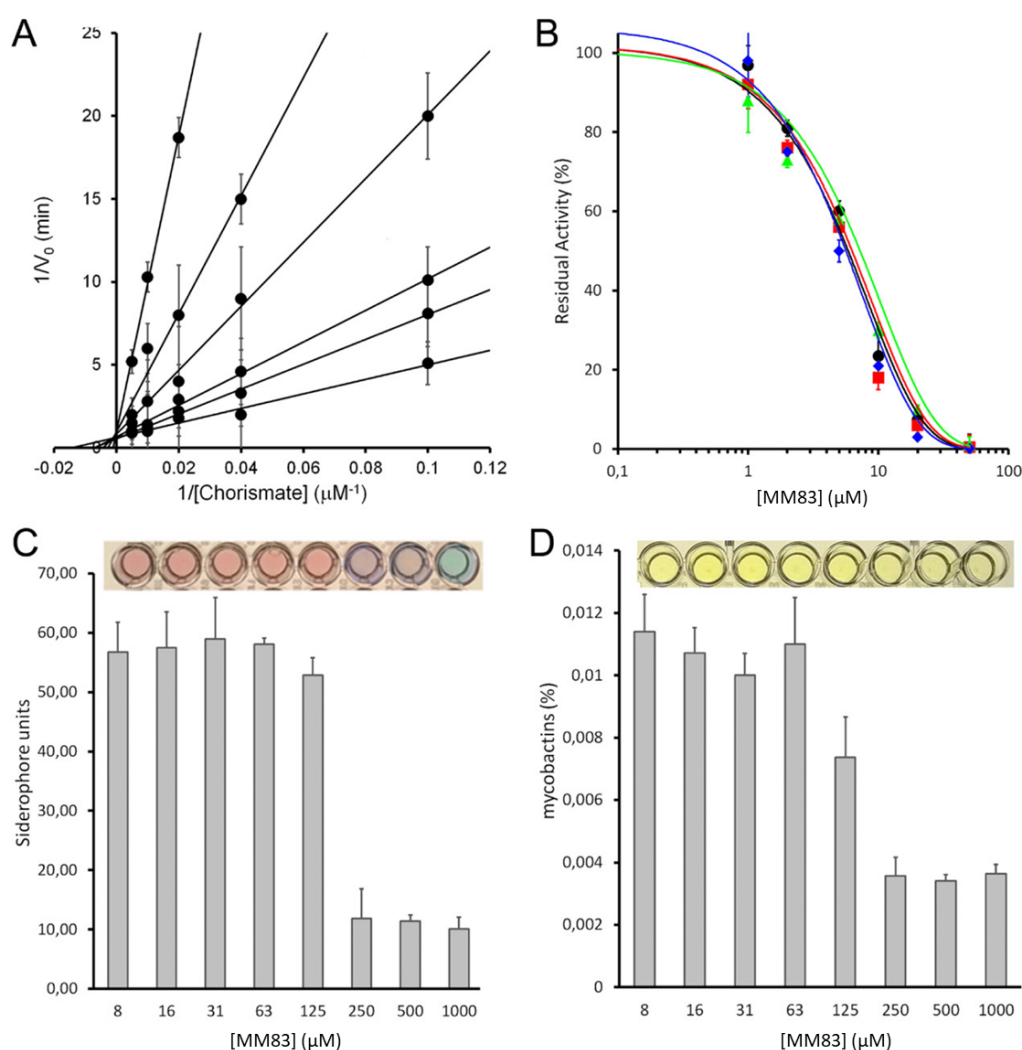
Due to the lack of improved antitubercular activity of MM-53, we further explored the meta position of the benzenic ring that was not investigated in previous trials, leading to a new series of compounds with interesting results.

Molecule	Structure	MbtI residual activity %
MM-55		101.6 ± 7.8
MM-74		23.3 ± 3.0
MM-83		3.1 ± 1.0
MM-84		78.2 ± 7.6
MM85		101.6 ± 7.8
MM-86		64.6 ± 10.8
MM-87		10.0 ± 0.6
MM-88		28.6 ± 6.8
MM-90		8.9 ± 1.6

**Table 11.** Structures of meta substituents on the benzenic ring.

As reported in table 11, the compounds bearing an electron withdrawing group were new strong inhibitors of MbtI, with the exception of the one with a carboxylic group probably due to the negative charge of this moiety. Among these compounds, the 3-cyano derivative MM-83 was the best inhibitor, with an  $IC_{50}$  of  $10.5 \pm 2.3 \mu M$ , while the meta 3-trifluoroacetyl derivative MM-87 showed an  $IC_{50}$  of  $15.4 \pm 2.8 \mu M$  and the 3,5-bis-trifluoromethyl MM-90 of  $18.8 \pm 6.8 \mu M$ .

The inhibition of the MM-83 compound was in-depth evaluated confirming it as the best inhibitor of MbtI, with a  $K_i$  value of  $4.2 \pm 0.8 \mu M$ , and not a PAIN compound (Figure 27 A and B). The antimycobacterial activity of MM-83 against *M. bovis* BCG strain, in iron-limiting conditions, was similar to that of the MM-40 compounds with a  $MIC^{99}$  value of  $125 \mu M$ , concentration that inhibited the synthesis of mycobactins and siderophore (Figure 25 C and D).

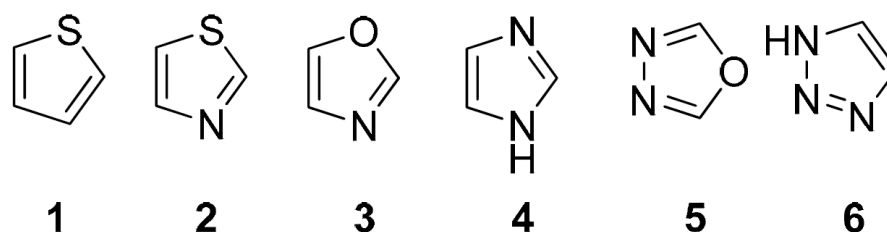


**Figure 25.** Biological characterization of MM-83. A) Global reciprocal plot of data from MbtI steady-state kinetics analysis toward chorismic acid at different concentrations of MM-83. B)  $IC_{50}$  plot of MM-83 in the presence of BSA (red), Triton X-100 (green), and DTT (blue). C) Universal CAS assay performed on *M. bovis* BCG, grown at different concentrations of MM-83. D) Determination of mycobactins in the abovementioned cells. Bars represent mean and standard deviations of three independent experiments.



## SAR of the furan moiety

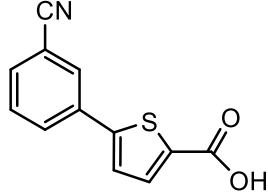
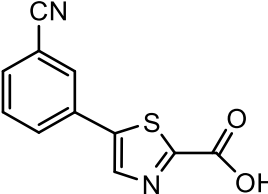
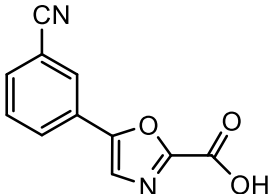
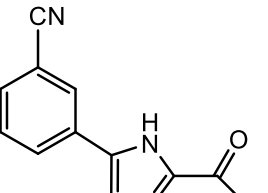
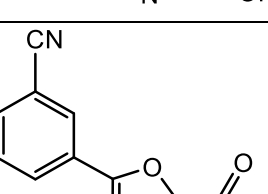
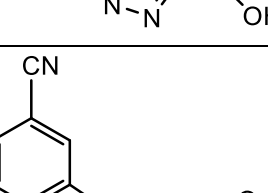
In literature it has been reported that in some cases the furan core was replaced by other heterocycles, improving the activity. In this context, we investigated whether the furan moiety of MM-40 and MM-83 could be replaced by different heterocycles (Figure 26).

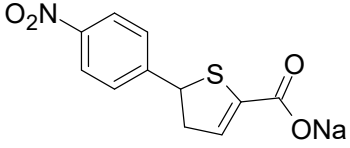
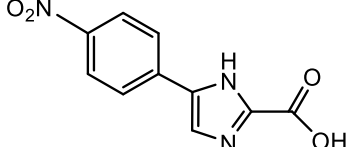
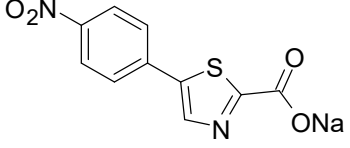
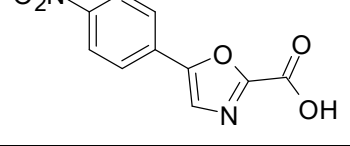
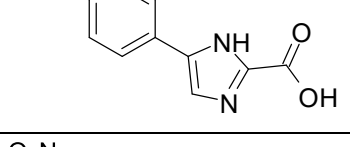
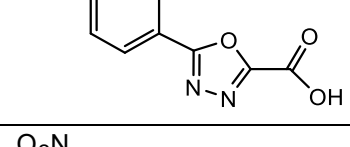
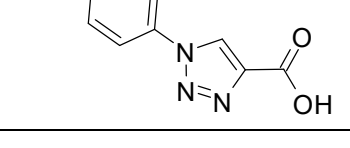


**Figure 26.** Chemical structure of the heterocyclic cores tested: 1 (thiophene), 2 (thiazole), 3 (oxazole), 4 (imidazole), 5 (1,3,4-oxadiazole), 6 (1,2,3-triazole).

In several articles, the use of a thiophene ring showed an improvement of antibacterial activity (Nayak and Gaonkar, 2019; Wilson *et al.*, 2013), thus the substitution of furan with this moiety was evaluated. The furan was then substituted by a thiazole (2) group, one of the most common heterocycles in drug design, which is part of the structure of several antitubercular compounds (Machado *et al.*, 2018). To expand our investigations, we evaluated the effects of the introduction of an oxazole (3), where the sulfur atom of the thiazole ring is substituted by an oxygen, and of the imidazole group, which is an attractive isostere of thiazole and oxazole. Finally, we explored the 1,3,4-oxadiazole (5), and the 1,2,3-triazole (6).

However, the related compounds reported in Table 12 and 13 showed no further improvements of the inhibitors, with  $IC_{50}$  higher than MM-40 and MM-83 compounds. The modest biological activity of the new derivatives prompted us to reconsider the furan as the best heterocyclic core, suggesting the critical nature of an appropriately substituted furan moiety to maintain a significant enzymatic inhibition thus to achieve antitubercular activity.

Molecule	Structure	MbtI IC <sub>50</sub> (μM)
GW-03		22.5 ± 10.8
MC-07		28.8 ± 1.8
MC-03		38.0 ± 7.6
GW-06		21.2 ± 1.0
GW-09		75.0 ± 9.8
FL-111		67.9 ± 6.6
<p><b>Table 12.</b> Structure of derivatives of MM-83 compounds with different heterocycles.</p>		

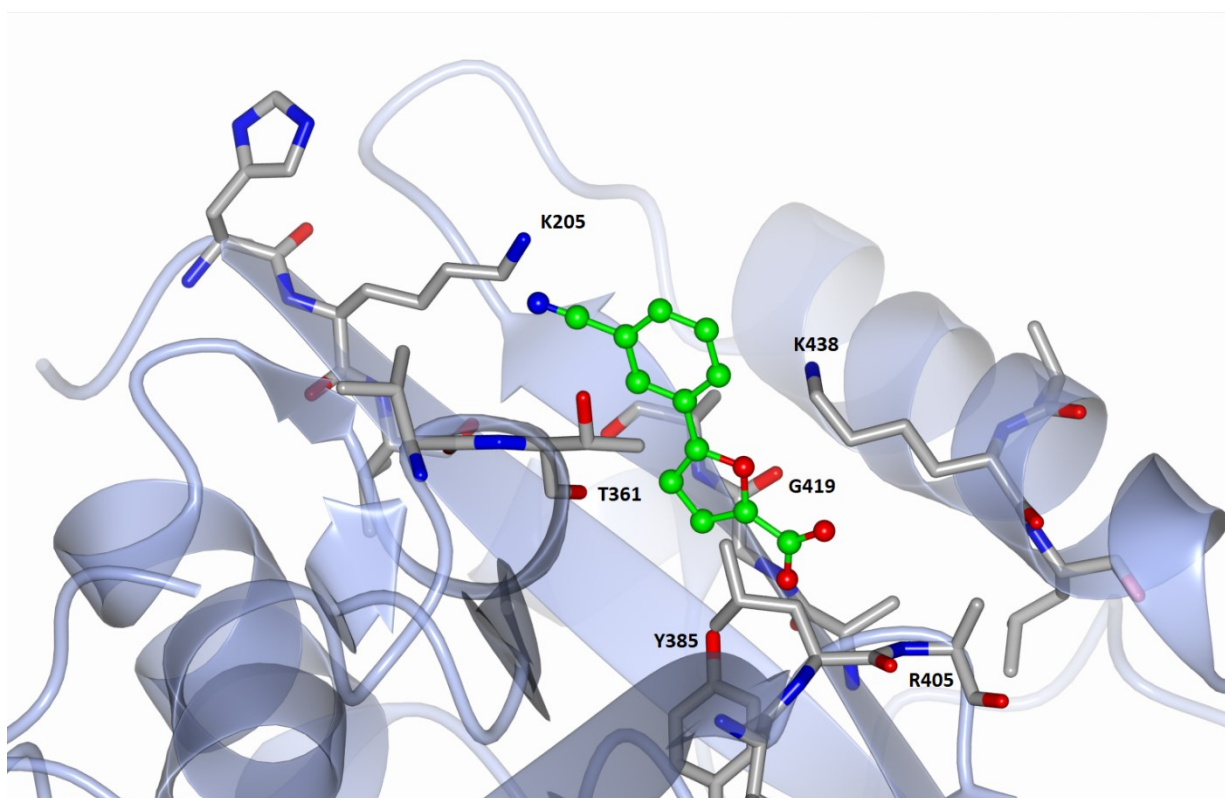
Molecule	Structure	MbtI IC <sub>50</sub> (μM)
GW-2		18.6 ± 1.7
GW-05		18.2 ± 4.9
MC-06		n.d
MC-02		21.1 ± 2.7
GW-05		27.5 ± 2.3
GW-08		59.0 ± 4.3
FL-102		32.7 ± 7.8
<p><b>Table 13.</b> Structures of derivatives of MM-40 compounds with different heterocycles of thiophene ring substituents.  <sup>a</sup> n.d. not determined as the residual activity at 100 μM was &gt; 30%</p>		

Except for GW-05 and GW-06, which have an imidazole ring replacing the furan moiety, none of our substitutions showed an improved inhibition. Anyway, GW-05 has a IC<sub>50</sub> of 27.5 ± 2.3 μM, while GW-06 of 39.3 ± 3.0 μM, both higher compared to MM-50 and MM-51. All the results of all the furan ring substitutions are summarized in figure 33 and 34.

## Optimization of the new MM-83 lead compound

To better definitively characterize the binding mode of our inhibitors, in collaboration with Dr. Marco Bellinzoni (Unité de Microbiologie Structurale, Institute Pasteur Paris), the crystal structure of MbtI in complex with MM-83 was solved.

The compound was found to interact with the MbtI active site through H bonds between its carboxylic group and Tyr385, Arg405, Gly419, and an ordered water molecule; moreover, the oxygen of the furan ring interacts with Arg405, and the phenyl ring forms a cation- $\pi$  interaction with Lys438 and a van der Waals contact with Thr361. Finally, the cyano group forms a H-bond with Lys205 (Figure 27). This residue is a key amino acid for the first step of the reaction, likely responsible for the activation of a water molecule for nucleophilic attack ( $SN_2''$ ) on C2 of chorismate, leading to the release of the hydroxyl group at position 4, after its protonation mediated by Glu252, thereby affording isochorismate (Zwahlen *et al.*, 2007).

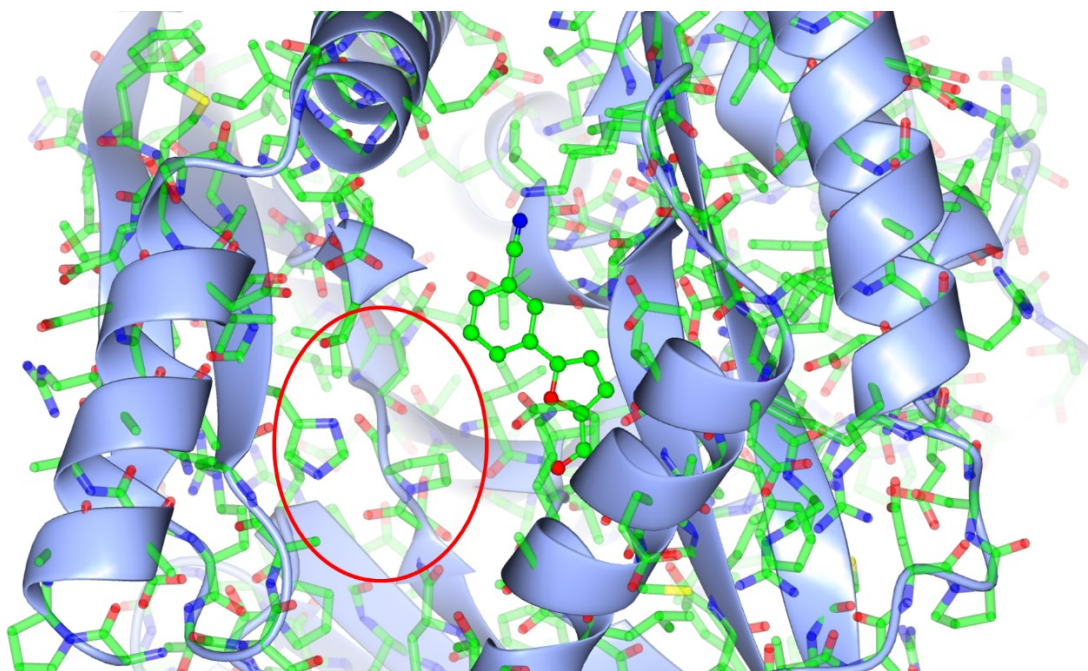


**Figure 27.** Ribbon diagram of the MbtI-MM-83 structure (PDB ID 6ZA4).

The structure of the enzyme in complex with the MM-83 inhibitor constitutes the basis for the development of a novel pharmacophore model for MbtI ligands, which could be profitably

employed in lead optimization focused on the development of more potent analogues of this compound.

In this context the crystal structure of the MbtI/MM-83 complex revealed the possibility to introduce a large moiety at position 5 of the phenyl ring of the compound. Indeed, as shown in figure 28, the structure presents a cavity around the phenyl ring of MM-83, that can accommodate bulky moieties.



**Figure 28.** Ribbon diagram of the MbtI-MM-83 structure from a different angle (PDB ID 6ZA4).

One of the reasons for which MM-83 has a low antimycobacterial activity (MIC 125  $\mu\text{M}$ ), despite the good activity against the enzyme (3  $\mu\text{M}$ ) could be the low lipophilicity of the compounds, which prevent membrane permeability. In this context, we focused on improving the hydrophobicity of our lead compound to help the drug delivery inside the cell through cell wall, taking the advantage of the fact that it is possible to insert a lipophilic substituent to the molecule in position 4 of the phenyl ring. We assayed different compounds, bearing saturated and unsaturated aliphatic chains, as well as different aromatic substituents, reported in Table 14.

Code	Structure	MbtI IC <sub>50</sub> (μM)	MIC BCG (μM)	Code	Structure	MbtI IC <sub>50</sub> (μM)	MIC BCG (μM)
CB-13		16.7 ± 1.3	>500	DA-5		19.1 ± 1.3	250
CB-14		16.6 ± 2.1	>500	DA-6		29.7 ± 1.6	250
CB-17		21.7 ± 1.3	62.5	DA-7		17.5 ± 1.5	125
CB-18		6.8 ± 2.4	>500	DA-8		37.5 ± 1.5	250
CB-20		40 ± 0.05	>500	DA-9		26.1 ± 1.4	125
CB-22		21.8 ± 0.2	62.5	DA-10		25.1 ± 1.3	125
CB-24		41.3 ± 0.7	125	SB-2		16.3 ± 1.2	125
CB-25		33.5 ± 3.4	>500	SB-3		12.1 ± 2.0	62.5
CB-27		21.7 ± 2.4	32	SB-4		19.2 ± 2.8	125
DA-1		18.0 ± 0.9	250	SB-5		51 ± 1.5	125
DA-2		11.0 ± 1.4	>500	SB-6		39 ± 0.9	>500
DA-3		20.9 ± 1.9	>500	SB-7		45.0 ± 2.5	125
DA-4		20.8 ± 2.0	125	SB-10		<sup>a</sup> n.d	250

**Table 14.** IC<sub>50</sub> and MIC of more lipophilic derivatives on *M. bovis* BCG.

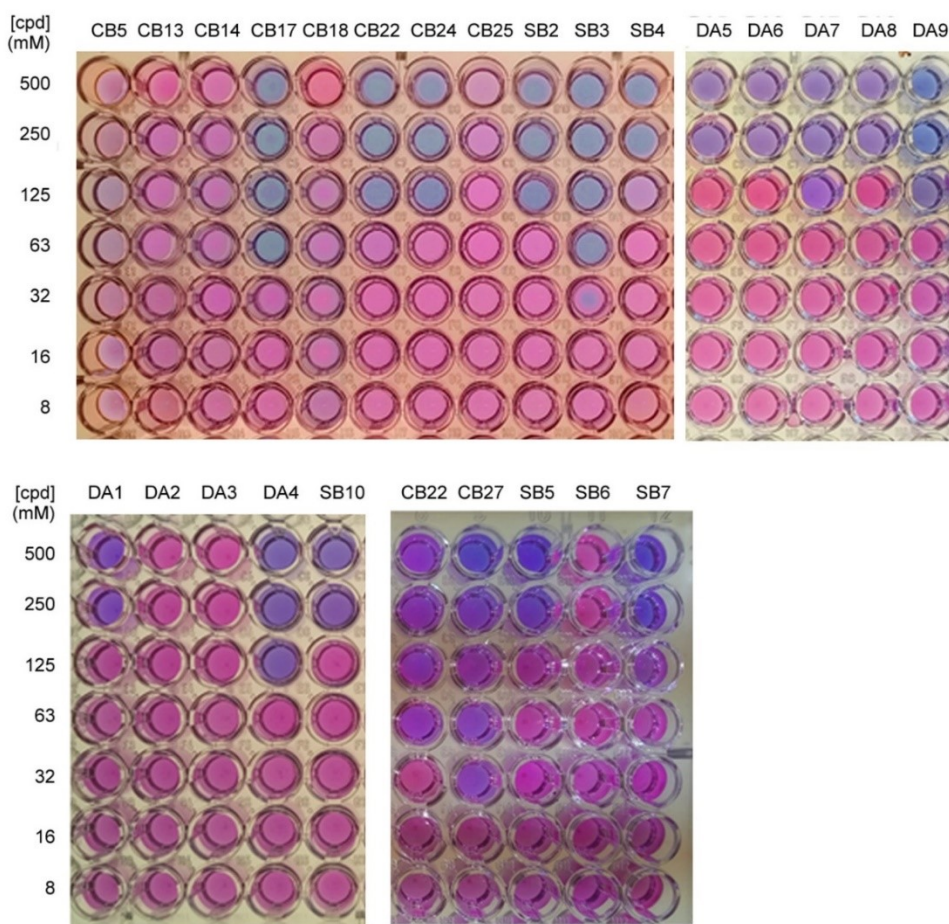
<sup>a</sup>n.d. not determined as the residual activity at 100 μM was > 25%



As reported in table 14, the addition of a short-medium aliphatic chains doesn't impair the inhibition capability of the molecule. However, the inhibition decreases with the extension of this tails, as shown by CB-20. Anyway, the IC<sub>50</sub> of the best derivatives, are higher than MM-83, suggesting that these moieties may slightly impair the binding of the inhibitors with the amino acids in the active site. For instance, the IC<sub>50</sub> of CB-22 is 21.8 ± 2.5 μM, while the one of CB-17 is 21.71 ± 2.4 μM, both about twice higher compared to MM-83.

Also, the presence of insaturations in the lipophilic tails have different effect on the compounds, improving or decreasing the inhibition, as shown by the IC<sub>50</sub> of CB-24 that is 41.3 ± 3.2 μM, CB-13 of 16.7 ± 1.3 μM, and CB-18 of 6.8 ± 0.4 μM.

Considering the previous data on lipophilic tails, a new series of compound have been developed, to further improve the membrane crossing capability of our hit compound. The DA derivative series, has been implemented with branched aliphatic or aromatic chains. The IC<sub>50</sub> values of these compounds, ranging from 10 to 30 μM underline how the new substituents showed a minor impact on the molecule inhibition effect compared to the previous long linear tails. Being all these compounds active against MbtI enzyme activity, their MIC against *M. bovis* BCG was determined (Table 14 and Figure 29).



**Figure 29.** MIC of the lipophilic derivatives on *M. bovis* BCG evaluated by REMA assay. The best compound CB27 showed a MIC of 32 μM, while CB-17, SB-3 and CB-22 were 63 μM.

The introduction of hydrophobic moieties effectively led to improvement of the cellular activity of the compound. In particular the medium saturated aliphatic chains (4-6 C atoms) led to a significant decrease in the MIC values, with the best compounds CB-22, bearing an isopropyl group showing a MIC of 32  $\mu\text{M}$ . By contrast, despite the introduction of unsaturation improved the inhibition against the enzyme activity, these compounds did not show increased antitubercular activity, with MIC generally higher than 500  $\mu\text{M}$ . A similar behavior was also found with the introduction of aromatic substituents.



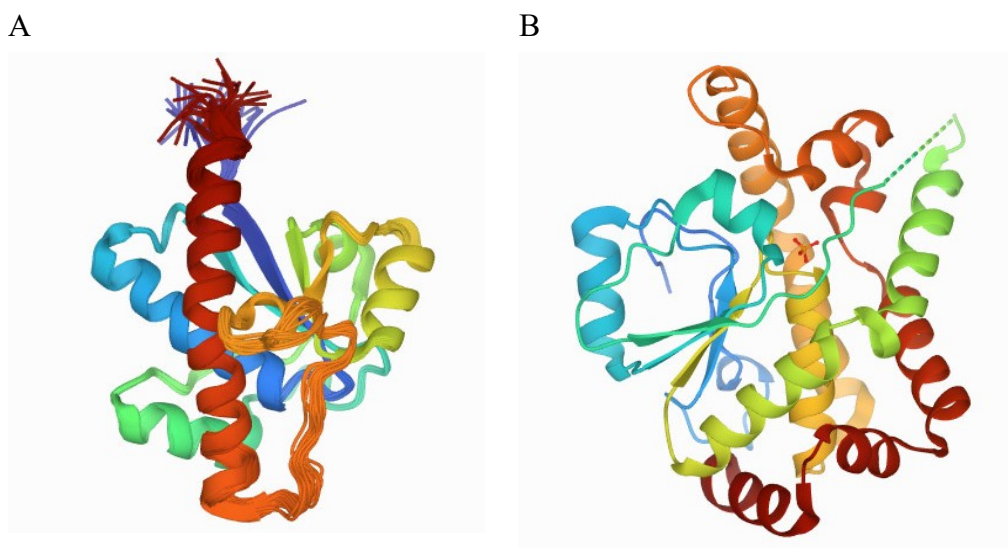
## Chapter 2. Virulence factor PtpB as potential therapeutic targets

### PtpA and PtpB general features

As mentioned above, MptpA and MptpB, also known more simply as PtpA and PtpB, are two of *M. tuberculosis* virulence factors, that is, two enzymes involved in mycobacterial pathogenesis. Both enzymes are protein tyrosine phosphatases (PTP), showing the typical classical features of this enzymes class: a P-loop within the active site that is strictly conserved and can be superimposed from different phosphatases, a Cys-X5-Arg motif with a high variation of the 5 central amino acids, and the presence of an Asp residue that plays role of acid during the catalysis (Barford *et al.*, 1998). PtpA is classify as a low molecular PTP (LMW), while PtpB is a dual specificity PTP (DSP).

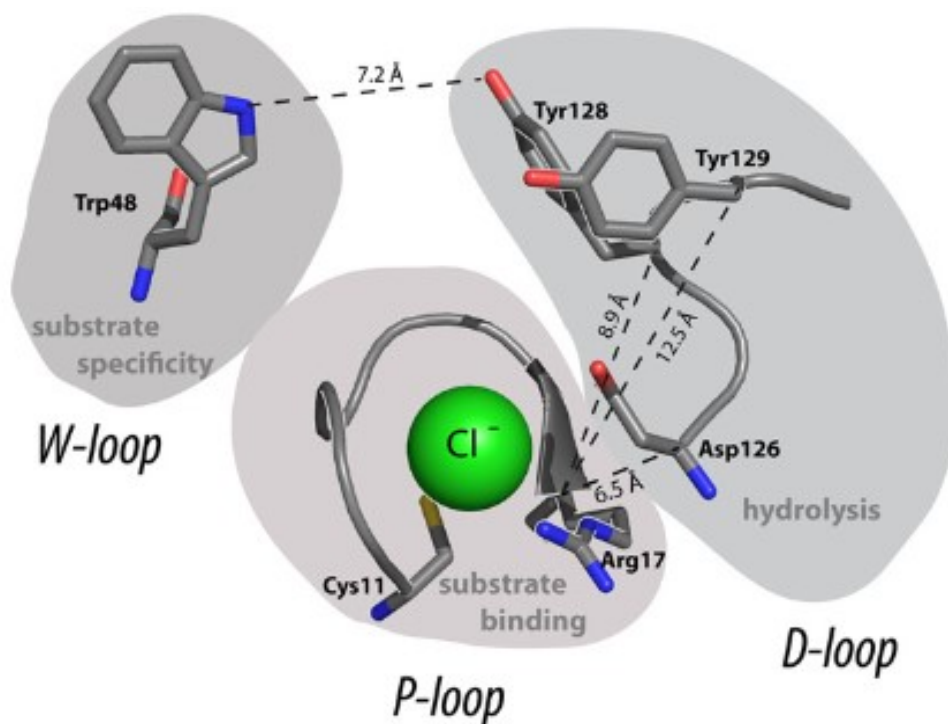
PtpA, more specifically, inhibits the lysosome V-ATPase by binding the H subunit, and dephosphorylate VSP33B, a component of the C-VPS complex involved in the phagosome-lysosome fusion (Bach *et al.*, 2008; Wong *et al.*, 2011). Whit its double action, PtpA prevents the phagolysosome maturation and allows *M. tuberculosis* to survive in the host cell.

PtpA is a monomeric protein of 164 amino acids (17 980 Da), that shows the typical four-stranded parallel beta-sheets connected via 5  $\alpha$ -helices structure of this family, as shown in figure 30-A.



**Figure 30.** Structures of PtpA (A. <https://www.rcsb.org/structure/2LUO>) and PtpB (B. <https://www.rcsb.org/structure/1YWF>).

PtpA active site motif ( $^{11}\text{CTGNICRS}^{18}$ ) is highly conserved among LMW-PTPs and its catalytic Cys<sup>11</sup> is located in a deep cleft surrounded by the hydrophobic residues of three loops. Of these, the W-loop exposes also the Trp<sup>48</sup> essential for substrate selectivity, and the D-loop the Asp<sup>126</sup> that is involved in catalysis (Stehle *et al.*, 2012).

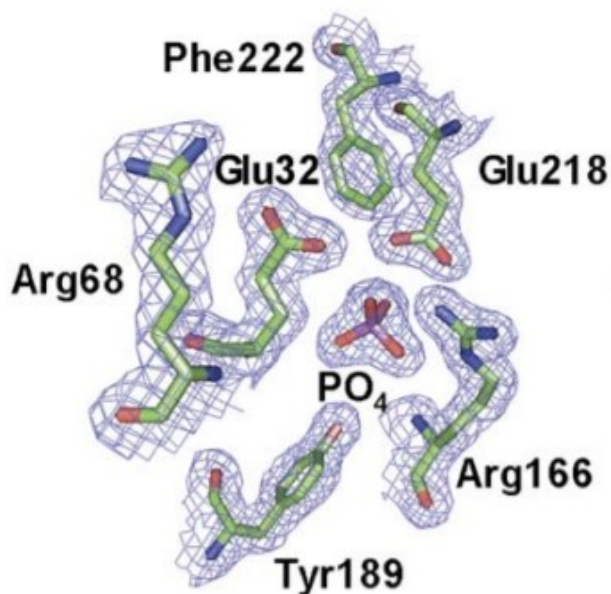


**Figure 31.** Structure of PtpA active site co-crystallized with a Cl<sup>-</sup> atom. The Trp<sup>48</sup> located on the W-loop is involved in substrate specificity, while the Cys<sup>11</sup> and Arg<sup>17</sup> on P-loop in the binding with the substrate. Finally, Tyr<sup>128</sup>, Tyr<sup>129</sup> and Asp<sup>126</sup> on D-loop are the catalytic amino acids.

PtpB inhibits the macrophages inflammatory processes by interfering with the expression of proinflammatory IL-6 and IL1- $\beta$  in addition to NF $\kappa$ B and MAPK signaling pathways. However, its natural targets are still not well known.

It is also a monomeric globular protein, of 272 amino acids (32 460 Da), characterized, just like PtpA, by the typical structure of this family, as described above.

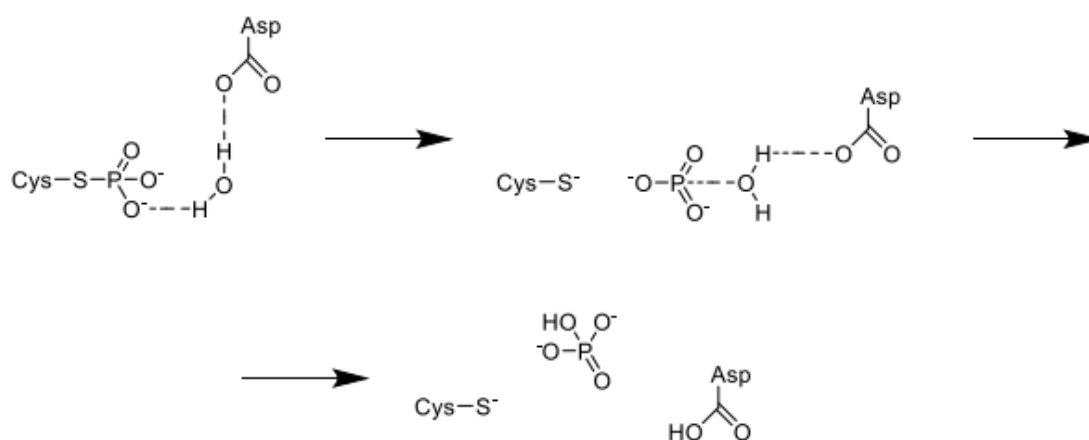
PtpB active site show the motif ( $^{159}\text{HCXAGXXR}^{166}$ ) located on the P-loop, with the catalytic Cys<sup>160</sup>. Asp<sup>82</sup> has been demonstrated to be the general acid Asp essential for catalysis (Grundner *et al.*, 2005).



**Figure 32.** Structure of PtpB active site co-crystallized with an inorganic  $\text{PO}_4$  molecule. The Phe<sup>222</sup> and Glu<sup>218</sup> located on a mobile lid block the substrate access (cause of the presence of the inorganic  $\text{PO}_4$ ), while the Arg<sup>166</sup> in the P-loop is involved in substrate binding (Grundner *et al.*, 2005).

The general catalytic mechanism of phosphatases has been identified through *in vitro* studies, using the 4-nitrophenylphosphate (4-NPP) as substrate.

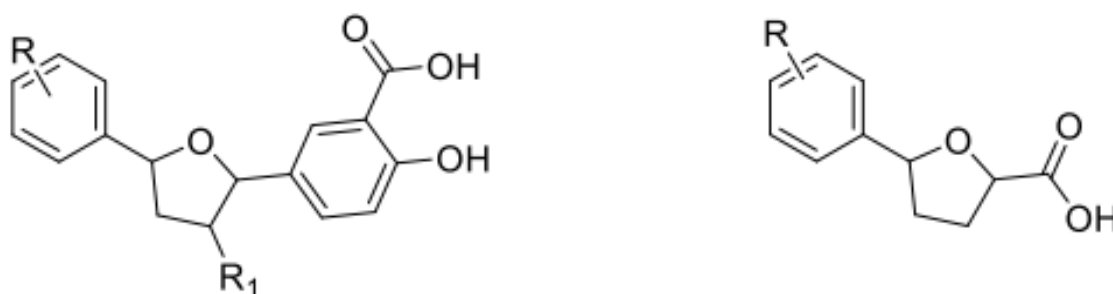
The catalysis starts with the transfer of the phosphate present on the substrate tyrosine to the lateral chain of a nucleophilic Cys located in the active site. This phosphate dissociation is mediated also by an acid Asp in proximity of the receiving Cys. The resulting intermediate phosphoenzyme is rapidly hydrolyzed with the release of a molecule of inorganic phosphate in the active site pocket (Asthagiri *et al.*, 2002; Fanzani *et al.*, 2015).



**Scheme 4.** General catalytic mechanism of phosphatases enzymes (Fanzani *et al.*, 2015).

## Aim of the work

Different inhibitors for both PtpA and PtpB are already described in literature. Our attention, anyway, was caught by the structures of benzo-furan derivatives described by Zhou and colleagues against PtpB (Zhou *et al.*, 2010).

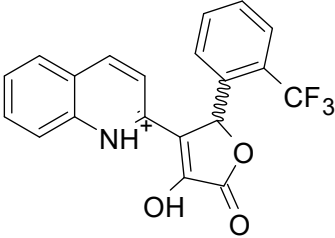
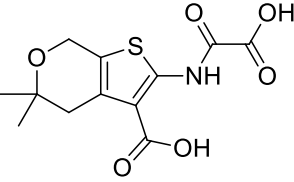
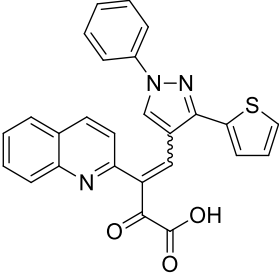
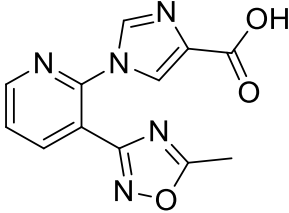
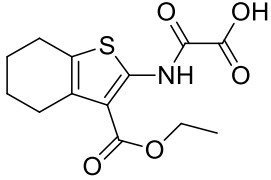
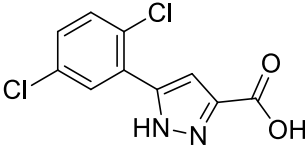
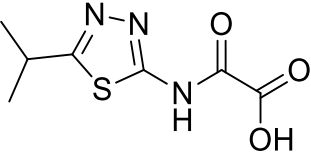
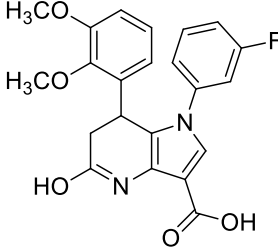


**Figure 33.** Backbone of PtpB salicylic-benzofuran inhibitors on the left (Zhou *et al.*, 2010) and backbone of MbtI benzofuran inhibitors on the right (Chiarelli *et al.*, 2018).

Considering our previous work on MbtI and the literature about mycobacterial phosphatases inhibitors, we attempted to develop multitarget compounds that can block simultaneously the mycobactins biosynthesis and the above-mentioned virulence factor PtpB. To do that, we followed in parallel two different paths. The first, was to assay all the previous most interesting inhibitors of MbtI against PtpB. The second was to develop novel inhibitors against PtpB that will be cross-evaluated against MbtI.

Moreover, to prove the selectivity of the multitarget molecules obtained, PtpA has been used as negative control, since this enzyme was demonstrated to be similar to human phosphatase LMW-PtpA (Koul *et al.*, 2000).

About the second path, the pharmaceutical chemists group led by Prof. Stefania Villa (Dipartimento di Scienze Farmaceutiche DISFARM, Università degli Studi di Milano) evaluated against PtpB, through *in silico* docking analysis, 4 million commercial compounds belonging to the Vitas-M, ChemBridge, Enamine, and Pharmeks commercial databases, using the software iCon implemented in LigandScout. Maintaining the benzofuran backbone feature, 8 possible candidates were proposed as potential PtpB candidates. Those compounds are reported in table 15.

Code	Chemical structure	Code	Chemical Structure
1		5	
2		6	
3		7	
4		8	

**Table 15.** PtpB inhibitors identified by virtual screening.

Just likely for MbtI, to assess if the identified compounds are indeed effective PtpB inhibitors, the *ptpb* gene from *M. tuberculosis* was cloned in an expression vector. The recombinant enzyme was produced in *E. coli* and subjected to purification through chromatography. Finally, to evaluate the effects of the new compounds, the appropriate inhibition enzymatic assay was set up.

All the candidates were also tested on MbtI to evaluate any possible inhibitory effect and against PtpA to evaluate the selectivity.

## Materials and methods

### Materials

#### *Chemicals, bacterial strain and media growth*

Most of the chemical, the LB media growth and the bacterial strain BL21(DE3) *E. coli* have already been described in MbtI “materials” section.

Beyond that, the 4-nitrophenylphosphate (4NPP) was from Sigma-Aldrich and the In-Fusion HD cloning kit was from Takara Bio USA.

*E. coli* Stellar™ competent cells HST08 strain by Takara, lack the gene cluster for cutting foreign methylated DNA (*mrr-hsdRMS-mcrBC* and *mcrA*). They were used for cloning both the new enzymes.

#### *MPtpB and MPtpA expression and purification.*

The Rv0153c gene, encoding *M. tuberculosis* PtpB, was amplified by PCR, using the following primers.

forward: (5'ATGGGTCGCGGATCCGAGAATCTTTATTTTCAGGGCATGGCTGTCCGTGAACTGC3')

reverse: (5'TGCGGCCGCAAGCTTTCATCCGAGCAGCACCCC3').

The primers were designed according to the In-fusion HD Cloning Kit protocol; the forward primer carried the Tobacco etch virus (TEV) protease cleavage site (underlined) to remove the 6-histidine tag from the protein. The purified PCR fragment was recombined into the *Bam*HI-*Hind*III digested pET-28b according to the In-fusion HD Cloning Kit's instructions, to give the pET28b-MPtpB vector. The recombinant products were transformed into *E. coli* Stellar™ competent cells, and the resulting colonies were checked for the presence of the insert by colony PCR and sequencing.

For the protein expression, *E. coli* BL21(DE3) cells were transformed with pET28b-PtpB and grown in LB medium, containing 50 µg/ml kanamycin, at 37 °C until OD600 = 0.6; then, the culture was induced with 0.5 mM IPTG at 25 °C for 15 h.

Cells were harvested by centrifugation, resuspended in 50 mM potassium phosphate buffer pH 8.0, 500 mM KCl, (Buffer A) supplemented with 1 mM phenylmethylsulfonyl fluoride, disrupted by sonication, and centrifuged at 50 000 g for 20 min at 4 °C. Cell free extract was loaded on a His-Trap (1 ml; GE Healthcare, Chicago, IL, USA), equilibrated in buffer A; the column was washed with 50 mM imidazole in buffer A, and PtpB eluted with 250 mM imidazole in buffer A.

The purified enzyme was dialyzed in 50 mM potassium phosphate pH 8.0, 150 mM KCl (Buffer B), in the presence of 2 mg TEV protease. The digested protein was further purified by a second affinity chromatography, followed by a size exclusion chromatography on a HiLoad Superdex 75 column (GE Healthcare), equilibrated in buffer B. Samples purity was checked by SDS-PAGE and protein concentration evaluated according to Lowry (Lowry *et al.*, 1951).

To clone the protein tyrosine phosphatase A (PtpA), the Rv2234 gene was amplified by PCR, using the following primers:

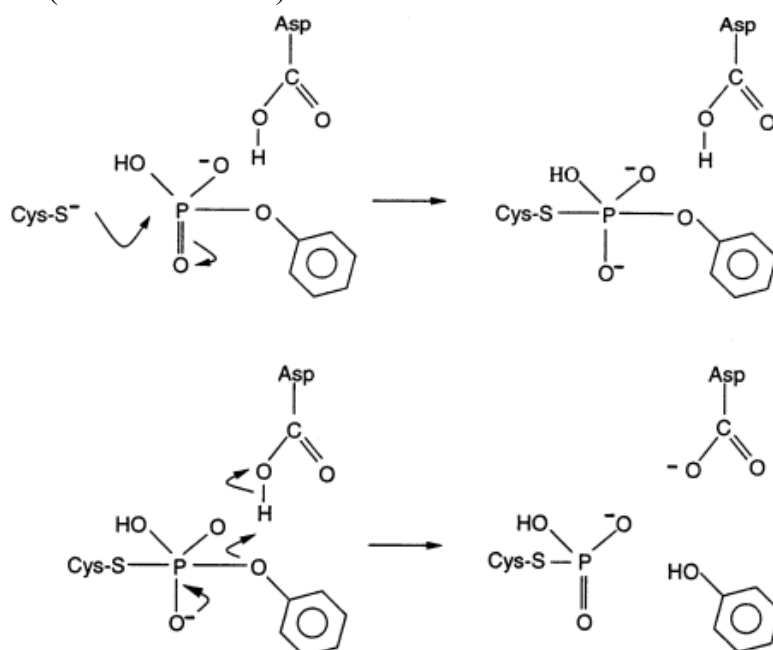
forward (5' ATGGGTCGCGGATCCGAAAACCTGTATTTTCAGGGCGTGTCTGATC  
CGCTGCAC 3')

reverse (5' GTGCGGCCGCAAGCTTTCAACTCGGTCCGTT 3').

The purified PCR fragment was recombined into the *Bam*HI-*Hind*III digested pET-28b as above to give the pET28b-PtpA vector. PtpA was then expressed and purified following the same protocol adopted for PtpB.

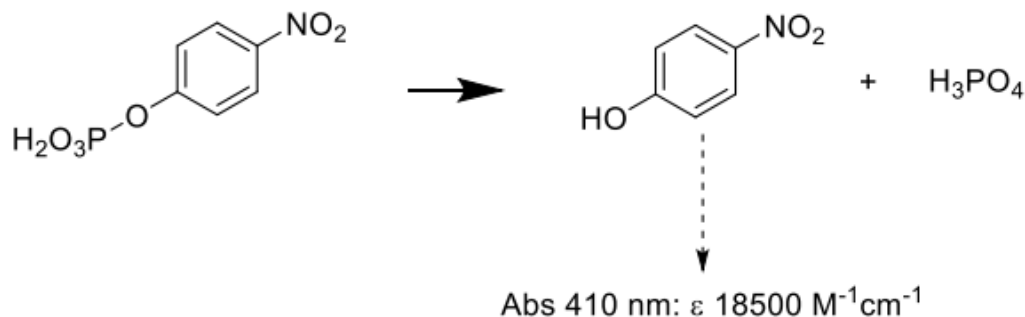
#### Enzyme activity assay

PtpA and PtpB enzyme activity were determined by measuring the production of 4-nitrophenol, by a continuous spectrophotometric assay already described in literature (Asthagiri *et al.*, 2002; Fanzani *et al.*, 2015) (scheme 5). Nitrophenol, indeed absorb specifically and can be quantified at 410 nm ( $\epsilon=18\ 500\ \text{M}^{-1}\text{cm}^{-1}$ ).



**Scheme 5.** General mechanism of action of phosphatases. A molecule of phenyl-phosphate is converted into a molecule of phenol and inorganic phosphate is released.

The assays (figure 34) were performed at 37°C in a final volume of 100 µl, using the Denovix DS-C spectrophotometer. Typically, the reaction mixture contained 50 mM potassium phosphate pH 8.0 and 1-2 µM PtpA or PtpB.



**Figure 34.** PtpA/PtpB spectrophotometer assay

Steady-state kinetic parameters were determined by assaying the enzyme activity at 6 or more different substrate concentrations and fitting the data to the Michaelis-Menten equation. All assays were performed in triplicate, and results analyzed using the GraphPad Prism 8.0 software.

*Inhibition assays and Pan Assay Interference Compounds (PAINS) analysis.*

The evaluation of the inhibition activity of different compounds was evaluated using the above reported spectrophotometric assay.

For a first screen, the assays were performed at subsaturating concentrations of 4-NPP (5 mM for PtpB and 4 mM for PtpA), in presence of putative inhibitors (stock dissolved 20 mM in DMSO) analyzed at final concentration of 100 µM. Blank control was performed by adding DMSO. The assays were performed in triplicate, and the percentage of inhibition was evaluated in triple as “enzymatic activity in presence of inhibitor” just as already done for MbtI.

PAIN analysis was performed in presence of 0.1 mg/ml of bovine serum albumin (BSA) or in the presence of 0.01% (v/v) Triton X-100 as detergent or 100 µM of 1,4-dithio-DL-threitol (DTT), as described for MbtI.



## Results and discussion

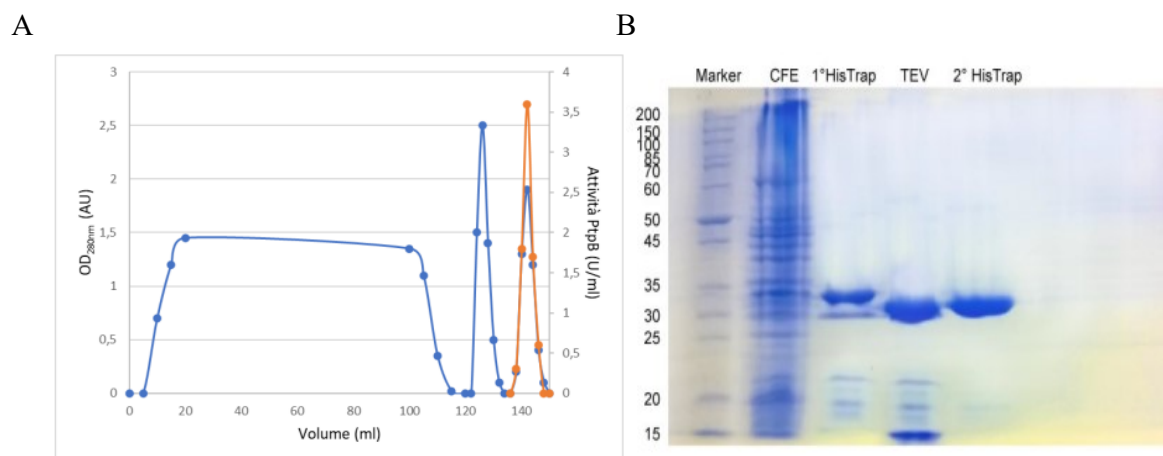
In parallel with MbtI study and according to literature (Zhou *et al.*, 2010), this study aims to identify novel potent PtpB inhibitors, but also multitarget inhibitors that may be simultaneously active against MbtI and the same PtpB.

In collaboration with the pharmaceutical chemists group lead by Prof. Villa, by virtual screening of four different databases (Vitas-M, ChemBridge, Enamine, and Pharmeks), eight molecules have been identified as putative ligands of PtpB with a potential affinity also for MbtI. These compounds have been evaluated for their activity against both enzymes, and for this reason the recombinant enzymes have been produced and purified.

Finally, the same compounds have been evaluated also on PtpA, to verify their selectivity.

### Expression, purification and characterization of the recombinant PtpB

PtpB was expressed and purified as reported in Material and Methods section (Figure 35).

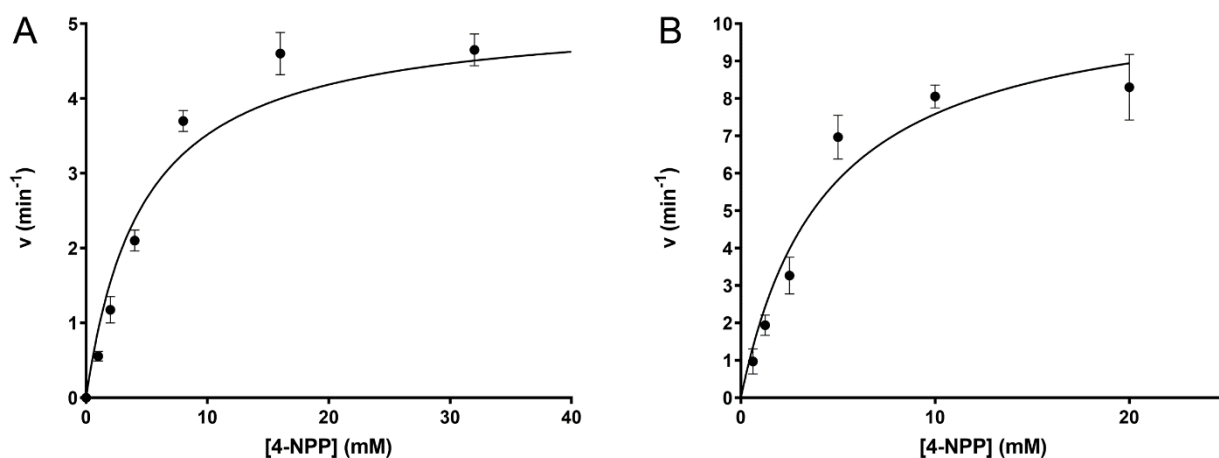


**Figure 35.** Purification PtpB: A) Elution profile of PtpB from the HisTrap chromatography. Blue line represents the absorbance at 280 nm. Red squares indicate the enzyme activity. B) SDS-Page of different purification steps of PtpB. Marker on first line; CFE: free cell extract; 1° HisTrap: elution with 25 mM of Imidazole in Buffer A; TEV: analysis after digestion; 2° HisTrap: PtpB after second IMAC.

A typical PtpB purification, showing that the adopted procedure allowed to obtain about 6 mg of purified PtpB, with a specific activity of 4.5 U/mg, comparable to published results (Zhou *et al.*, 2010).

The main PtpB kinetic parameters have been evaluated to check the catalytic properties of the obtained recombinant protein. To this purpose, activity assays were set up at 37°C on a final volume

of 400  $\mu\text{l}$ , using a final PtpB concentration of 1-2  $\mu\text{M}$ , in the presence of different 4-NPP concentrations.



**Figure 36.** Steady state kinetic analysis of PtpB (panel A) and PtpA (panel B) as a function of 4-NPP concentration. Data are mean  $\pm$  SD of three different replicates.

As shown in figure 36A, the enzyme showed a hyperbolic response to the substrate, with a  $V_{\text{max}}$  of  $5.2 \pm 0.2 \text{ min}^{-1}$  and a  $K_{\text{m}}$  of  $4.8 \pm 0.5 \text{ mM}$ . These values are in agreement with the data previously reported in literature, confirm the validity of the enzyme preparation, now suitable for our purposes (Zhou *et al.*, 2010).

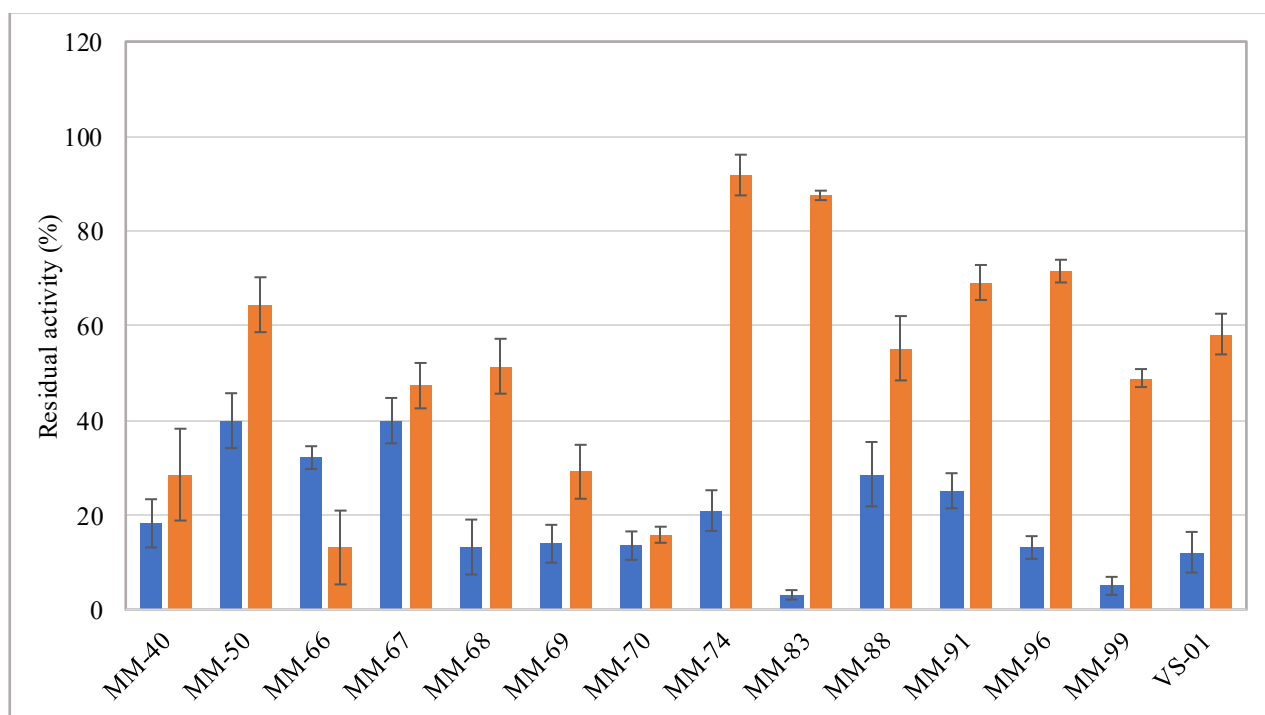
PtpA was similarly expressed, purified and kinetic constants determined: the resulting  $V_{\text{max}}$  is  $8.3 \pm 1.2$  and its  $K_{\text{m}}$  is of  $4.1 \pm 0.1 \text{ mM}$

## Inhibition assays of a selection of MbtI compounds on PtpB activity

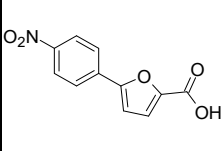
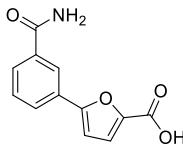
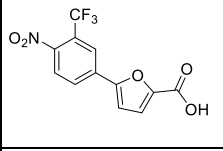
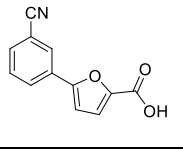
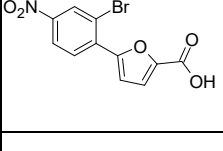
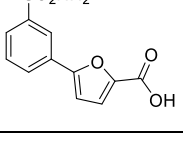
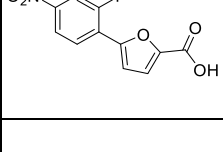
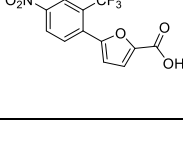
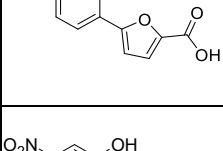
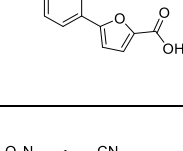
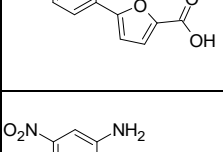
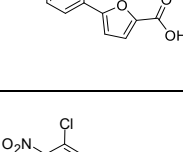
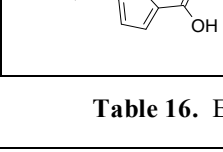
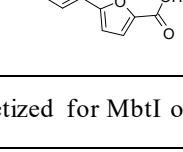
The obtained recombinant PtpB was used to verify the effect of a selection of MbtI inhibiting compounds. This analysis has a double aim: firstly, it can prove the possibility to develop dual compounds that may be active on both enzymes and secondly, it could be a starting point to identify few selected compounds that can be improved following the multi-targeting path.

As for MbtI, the first inhibition assay evaluates the percentage of inhibition at fixed concentration of each compound. The molecules are stored at a concentration of 20 mM in DMSO and evaluated in triplicate at a final concentration of 100  $\mu$ M. All assays were performed at a final concentration of 5 mM 4-NPP. This concentration is selected to keep the protein in non-saturating conditions in order to identify also competitive inhibitors, just likely MbtI.

Moreover, PtpB activity was assayed in presence of 2  $\mu$ l of pure DMSO to evaluate if the solvent has any inhibiting interaction with the enzyme. This test confirmed that the PtpB is not inhibited by the presence of this solvent.



**Figure 37.** Comparison between the inhibition effects of selected MbtI inhibitors (in blue) on PtpB activity (in orange).

Code	Structure	MbtI RA %	PtpB RA %	Code	Structure	MbtI RA %	PtpB RA %
MM-40		18.2 ± 5.1	28.5 ± 9.7	MM-74		20.9 ± 4.3	91.8 ± 4.5
MM-50		39.9 ± 5.8	64.4 ± 7.0	MM-83		3.1 ± 1.0	87.5 ± 6.8
MM-66		32.1 ± 2.4	13.1 ± 7.8	MM-88		28.6 ± 6.8	55.2 ± 2.4
MM-67		39.9 ± 4.8	47.3 ± 7.5	MM-91		25.1 ± 3.7	69.1 ± 7.2
MM-68		13.2 ± 5.8	51.4 ± 6.3	MM-96		13.1 ± 2.4	71.5 ± 9.7
MM-69		13.9 ± 4.0	29.0 ± 5.7	MM-99		5.0 ± 1.9	48.9 ± 10.3
MM-70		13.5 ± 3.8	15.8 ± 1.7	VS-01		12.1 ± 4.3	58.2 ± 5.7

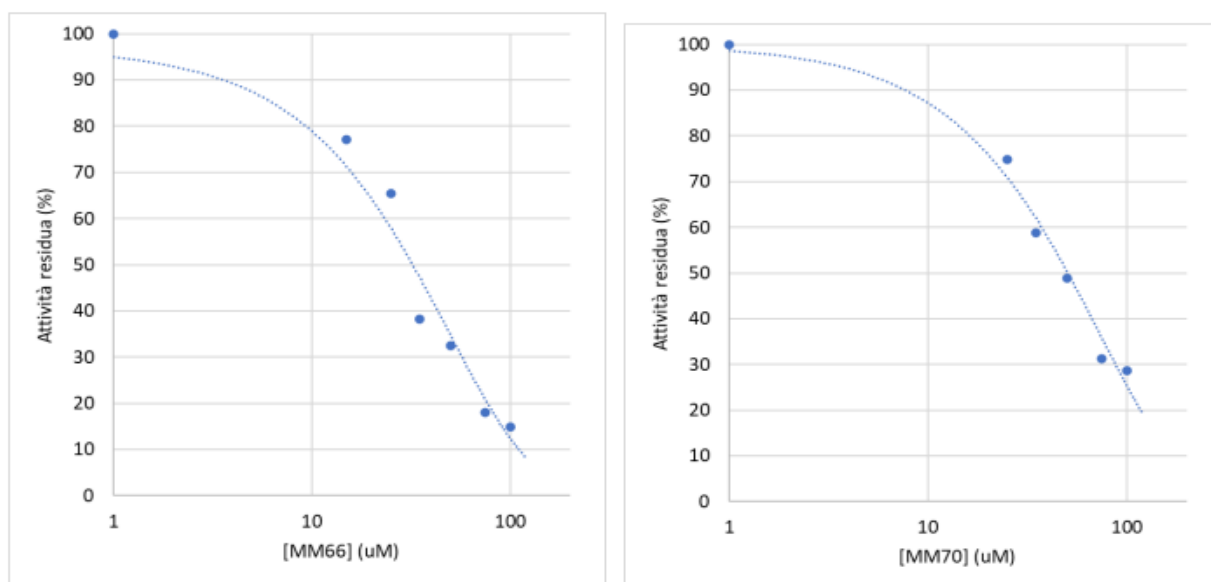
**Table 16.** Effects of a compounds selection synthesized for MbtI on PtpB.

Since the final aim of this work was to identify multitarget compounds, 14 molecules that showed an interesting inhibitory effect on MbtI have been tested also on PtpB. Among all of them, only 2 showed a significant inhibition on this enzyme, too. MM-66, indeed, inhibited PtpB of around 90% and more than 70% MbtI, while MM-70 inhibits PtpB of 80% while MbtI of 70%.

Furthermore, MM-40 and MM-69 also inhibits PtpB but only of around 70%. All others compounds resulted ineffective on this enzyme. All the active compounds are characterized by the presence of the 4-NO<sub>2</sub> group, with different substituent in 2-position. Interestingly substituent in 3-position have been found detrimental for the activity against PtpB (MM-50 and VS-01); similarly,

the compounds bearing a substituent in 3-position highly active against MbtI (MM-74, MM-83 and MM-88) were practically inactive against the phosphatase.

For the two best compounds MM-66 and MM-70 the determined  $IC_{50}$  was  $31.8 \pm 6.9 \mu\text{M}$  and  $30.5 \pm 6.8 \mu\text{M}$ , respectively (figure 38).



**Figure 38.**  $IC_{50}$  of MM-66 (on the right) and MM-70 (on the left) evaluated against PtpB.

Data of the 12 other molecules are reported in table 18.

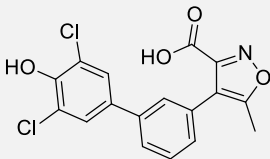
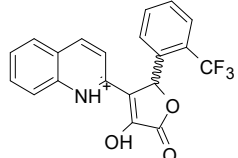
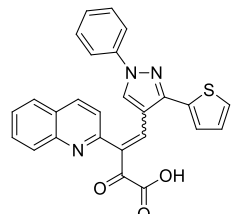
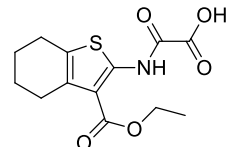
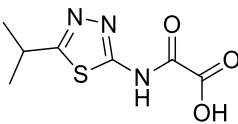
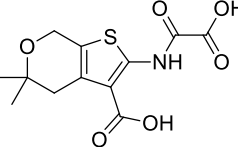
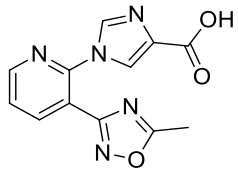
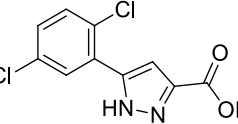
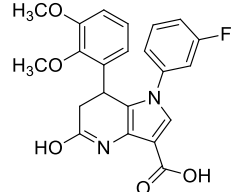
The fact that some molecules belonging to the previously built MbtI inhibitors library resulted to be active on PtpB, although only a mild inhibition was found, indicates the possibility to develop common PtpB and MbtI inhibitors.

## Inhibition assays of the compounds from virtual screening on PtpB activity

The virtual screening of four different databases (Vitas-M, ChemBridge, Enamine, and Pharmeks) run by Prof. Villa's medicinal chemist group, disclosed eight molecules as putative PtpB ligands with a potential affinity for MbtI.

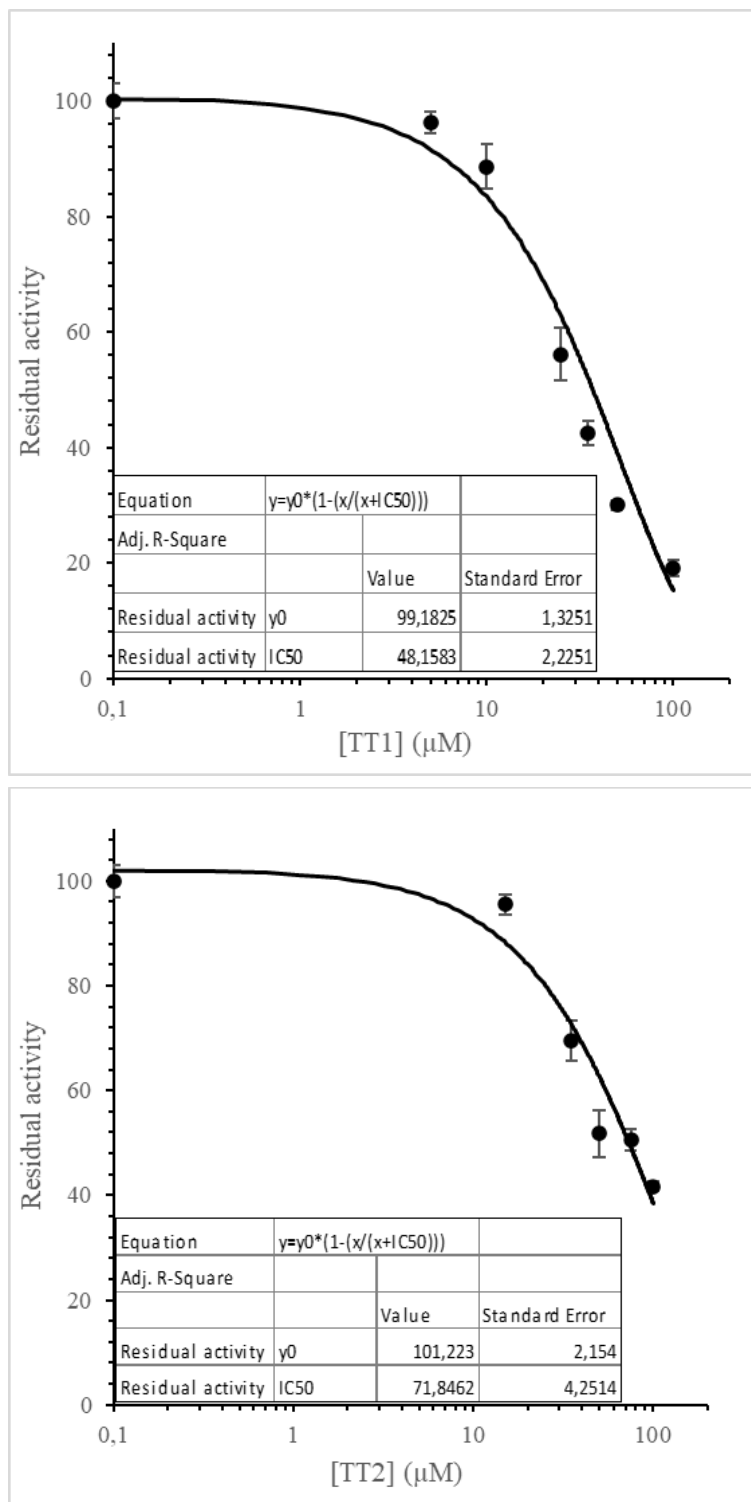
The 8 compounds have been purchased at the highest purity grade available (90%) from Enamine (1-3; SIA Enamine, Riga, Latvia) and Vitas M (4-8; Vitas M Chemical Ltd., Causeway bay, Hong Kong), and evaluated on recombinant PtpB activity to verify their *in vitro* effect.

As shown in table 17, compound I was found to highly affect PtpB activity, being able to inhibit the enzyme of 75% at the tested concentration. Compound 2 displayed a lower activity (PtpB residual activity about 70%) while the other compounds resulted low active (compounds 3, 4 and 6) or completely inactive (compounds 5, 7 and 8).

Code	Structure	%RA at 100 $\mu$ M	IC <sub>50</sub> ( $\mu$ M)
I (ref.)		10.9 $\pm$ 0.7	25.8 $\pm$ 4.5
1		24.3 $\pm$ 1.1	48.1 $\pm$ 2.2
2		29.8 $\pm$ 4.4	71.8 $\pm$ 4.2
3		69.5 $\pm$ 12.1	-
4		87.2 $\pm$ 18.7	-
5		103.7 $\pm$ 12.8	-
6		83.2 $\pm$ 3.6	-
7		108.9 $\pm$ 5.1	-
8		100.9 $\pm$ 9.4	-

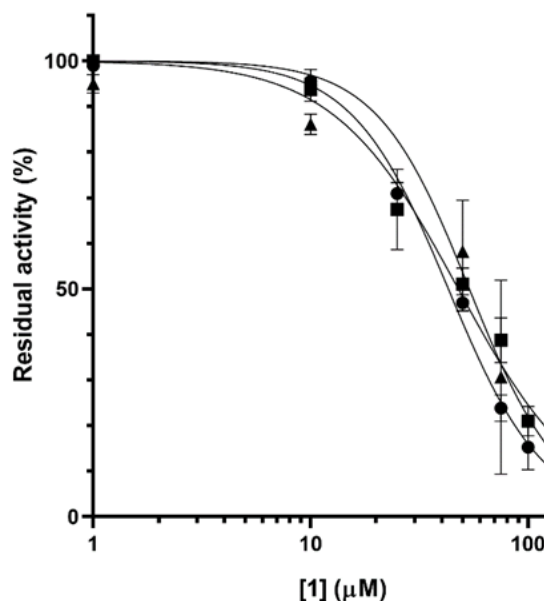
**Table 17.** Effect of compounds 1-8 on PtpB activity.

To confirm these results, the IC<sub>50</sub> of compound 1 and 2 have been determined. The two active compounds were able to inhibit PtpB activity in a concentration depending manner, showing IC<sub>50</sub> values of 48.1 ± 2.2 μM for 1 and of 71.8 ± 4.2 μM for 2 (table 17). These results confirm the validity of the approach and of the virtual screening used for the identification of these new hit compounds.



**Figure 39.** IC<sub>50</sub> of compounds 1 (top) and 2 (bottom) on PtpB evaluated with Origin software.

To exclude nonspecific promotion of PtpB aggregation, or inhibition caused by covalent reactions with its cysteine residues, TT-01 underwent PAINS evaluation. Similarly to MbtI, TT-01 IC<sub>50</sub> was evaluated again in presence of 0.1 mg/ml of BSA or with 0.01% (v/v) of Triton X-100 detergent to verify the possible formation of aggregates, and in presence of DTT, to exclude a promiscuous inhibition caused by a covalent reaction of the compound with PtpB cysteine residues (Figure 40).

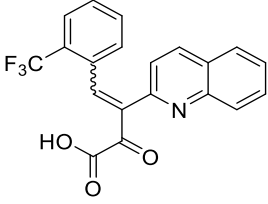
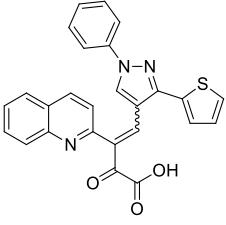
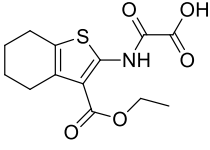
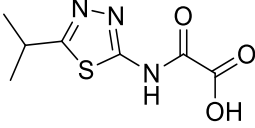
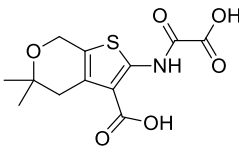
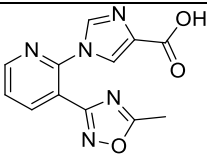
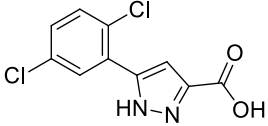
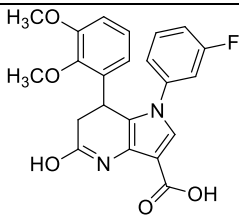


**Figure 40.** IC<sub>50</sub> plot of TT-01 on PtpB in the presence of BSA, Triton X-100 and DTT.

The IC<sub>50</sub> of TT-01 is unaltered in the presence of 0.1 mg/ml of BSA, 0.01% Triton X-100 or 100 µM DTT, confirming that the inhibitory activity of the compound was due to its binding to the active site of the enzyme.

The eight compounds have been tested also on MbtI for a cross-evaluation, confirming the possibility to develop multitarget inhibitors following both the discussed paths.



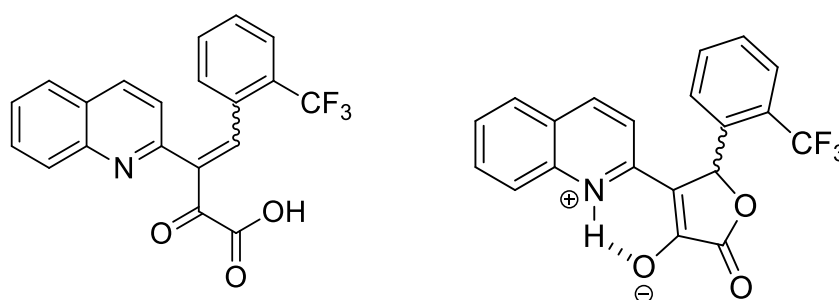
Molecule	Structure	PtpB residual activity %	MbtI residual activity %
1		24.3 ± 1.1	43.2 ± 1.4
2		29.8 ± 4.4	13.5 ± 3.0
3		69.5 ± 12.1	52.3 ± 1.5
4		87.2 ± 18.7	92.9 ± 1.0
5		103.7 ± 12.8	26.2 ± 0.5
6		83.2 ± 3.6	90.5 ± 1.1
7		108.9 ± 5.1	102.7 ± 1.5
8		100.9 ± 9.4	51.4 ± 0.5

**Table 18.** Cross-evaluation of compounds 1-8 on MbtI

The compound 1, indeed, showed an inhibition of 66% on MbtI while compound 2 of 86.3%. By these results, compound 1, that was the best hit against PtpB, was selected for the following SAR studies against both the enzymes of interest.

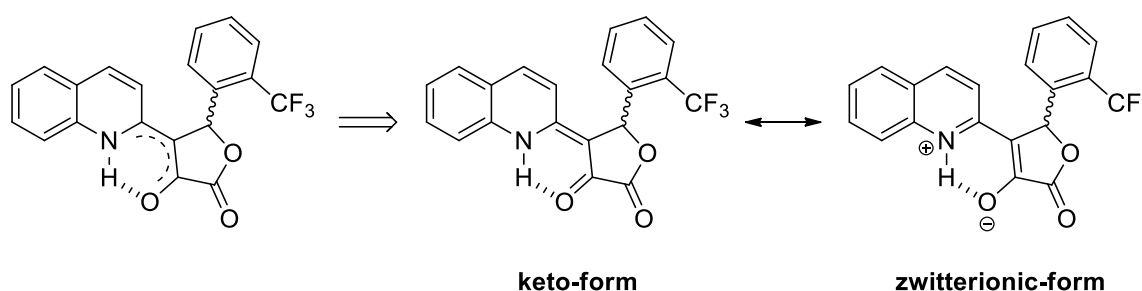
## Structure-activity relationship (SAR) studies.

The focus of this preliminary study was compound 1, the best PtpB inhibitor among the 8 molecules identified by the *in silico* approach. An NMR deeper molecular characterization of this compound revealed that it was slightly different than reported by the company. Indeed, the  $\alpha$ -keto acid moiety was absent, while replaced by a  $\gamma$ -lactone that connected the quinoline ring to an *o*-substituted phenyl group. Moreover, the  $\pi$ -bond was delocalized, determining the formation of a peculiar system between the quinoline and the enol group of the lactone. This structure can be considered a chiral center, with the consequently presence of a racemic mixture.



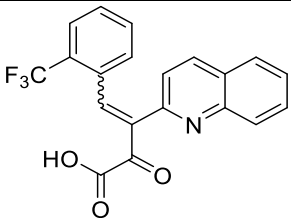
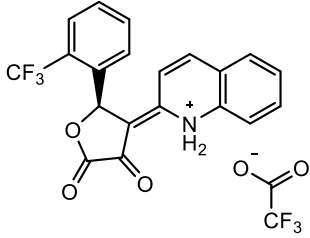
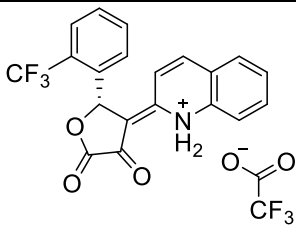
**Figure 41.** Compound 1 structure declared by the supplier (left) and experimental data by NMR (right).

Moreover, a further evaluation of compound 1 by crystallization revealed two resonance limit forms in equilibrium, one characterized by an exocyclic double bond (keto-form) and the other by a zwitterion (figure 42), similarly to what described in literature (Dobosz *et al.*, 2007; Sayapin *et al.*, 2010).



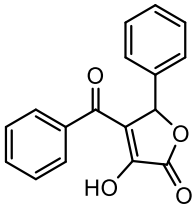
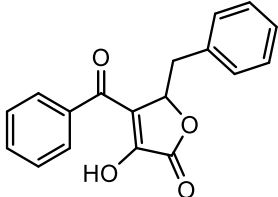
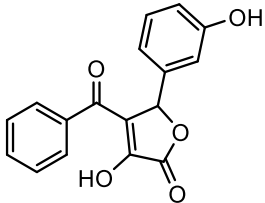
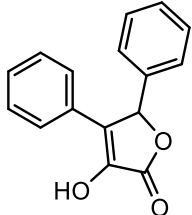
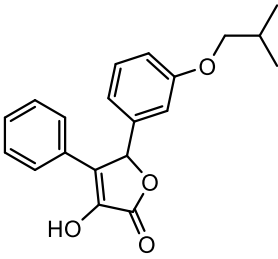
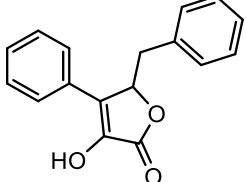
**Figure 42.** Tautomeric limit forms of compound 1.

According to the new data, the two enantiomers have been separated and evaluated *in vivo* revealing a different effect on PtpB activity. The enantiomer 1, indeed has a higher inhibition compared to 2, and their mix as an average effect on PtpB, as shown in table 19. Conversely, the two enantiomers showed a similar activity against MbtI.

Molecule	Structure	PtpB residual activity %	PtpB IC <sub>50</sub> μM	MbtI residual activity %
<b>TT-01</b>		24.3 ± 1.1	48.1 ± 2.2	43.2 ± 1.4
<b>TT-01 E1</b>		17.4 ± 0.2	31.2 ± 2.7	30.8 ± 1.4
<b>TT-01 E2</b>		29.6 ± 0.01	72.2 ± 3.4	33.3 ± 0.7

**Table 19.** Effect of the two enantiomers on PtpB and MbtI.

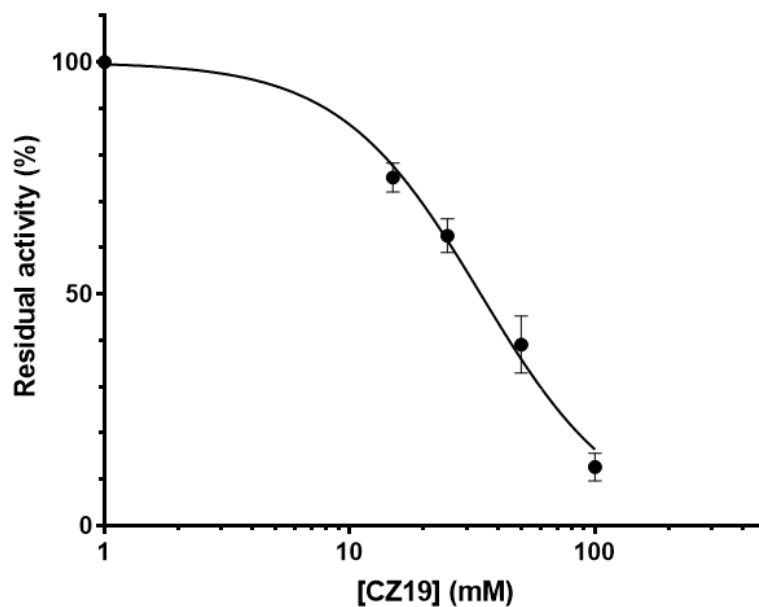
A series of TT-01 derivative were then designed, modifying the 4-quinoline and/or the 5-trifluoromethylphenyl moieties (Table 20).

Molecule	Structure	PtpB residual activity %	MbtI residual activity %
CZ-11b		101.9 ± 0.3	51.2 ± 1.4
CZ-13		81.7 ± 0.1	48.1 ± 0.5
CZ-16b		78.6 ± 0.01	53.7 ± 1.1
CZ-18		87.1 ± 0.1	22.2 ± 6.8
CZ-19		76 ± 0.1	11.1 ± 0.1
CZ-21		104.7 ± 0.5	40.7 ± 0.5

**Table 20.** Effect of TT-01 derivatives on PtpB and MbtI.

Among the 6 derivatives synthesized, none of them showed improved activity against PtpB, being all the CZ-18 compounds and the CZ-19 were significantly active against MbtI

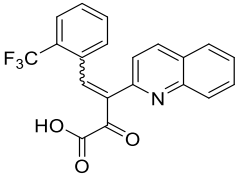
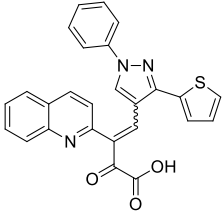
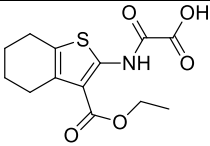
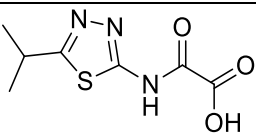
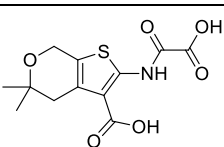
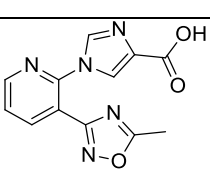
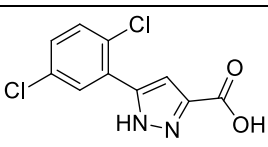
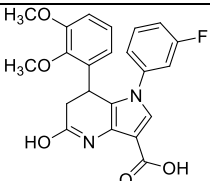
As shown in table 22, the 6 TT-01 derivatives were practically inactive on PtpB. By contrast, CZ-18, showing a 4-5 diphenyl substituent, and CZ-19, with a 4-phenyl-5(methylpropoxy)phenyl moiety, had an increased inhibitory effect against MbtI. Moreover, CZ-19 showed an  $IC_{50}$  of  $35.4 \pm 2.4 \mu\text{M}$  on MbtI (figure 43).



**Figure 43.** CZ-19 derivative against MbtI showed an  $IC_{50}$  of  $35.4 \pm 2.4 \mu\text{M}$ .

## PtpB selectivity study

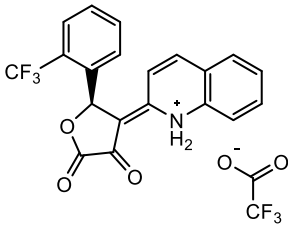
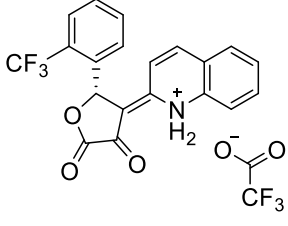
The compounds synthesized for PtpB have been evaluated also on PtpA, to verify their selectivity, since PtpA is mostly similar to human LMW-PtpA (Koul *et al.*, 2000).

Molecule	Structure	PtpB residual activity %	PtpA residual activity %
1		24.3 ± 1.1	53.4 ± 0.06
2		29.8 ± 4.4	N/A
3		69.5 ± 12.1	72.5 ± 0.2
4		87.2 ± 18.7	64.1 ± 0.3
5		103.7 ± 12.8	73.7 ± 0.05
6		83.2 ± 3.6	62.7 ± 0.2
7		108.9 ± 5.1	64 ± 0.1
8		100.9 ± 9.4	68.7 ± 0.6

**Table 21.** Evaluation of effects of compounds 1-8 on PtpA.

As shown in table 21, none of the previous inhibitors has a remarkable effect on PtpA. Also, our best hit TT-01 has only a mild effect on this enzyme, proving that it is indeed selective for PtpB.

To further confirm the selectivity of TT-01, the two enantiomers have been tested on PtpA. Their behavior against this enzyme is comparable to what has been observed for PtpB, but their inhibition effect results milder on this enzyme (table 22).

Molecule	Structure	PtpB residual activity %	PtpA residual activity %
<b>TT-01 E1</b>		17.4 ± 0.2	54.4 ± 0.06
<b>TT-01 E2</b>		29.6 ± 0.01	51.5 ± 0.05

**Table 22.** Effect of the two enantiomers on PtpA.

This study confirms not only that is possible to develop multitarget inhibitors for MbtI and PtpB, but they may also be selective only for the desired targets. Selectivity is indeed an important feature for drug candidates, since avoiding nonspecific interactions, for example with host's proteins, implicates the consequential decreasing toxicity for human cells.

## Conclusion

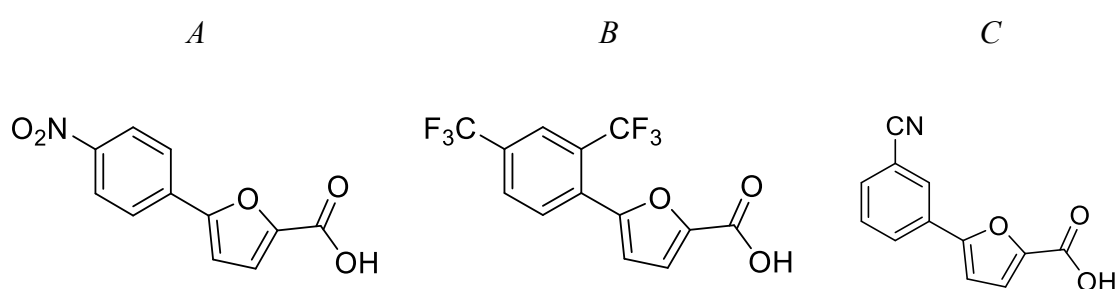
MbtI and PtpB are validated and attractive antitubercular targets, and their inhibition could lead to a reduced mycobacterial pathogenicity without toxicity issues, due to the absence of these targets in the host.

### *About MbtI*

In a previous study, a virtual screening of Enamine database against MbtI using Ligandscout software, identified five molecules as putative enzyme inhibitors.

A first *in vitro* evaluation revealed that two of them were effective against MbtI. In the attempt to design a powerful inhibitor, the most effective molecule I was chemically tailored by the chemists group lead by Prof. Villa (Dipartimento di Scienze Farmaceutiche DISFARM, Università degli Studi di Milano), to explore the different moieties of the compound and to improve its inhibition properties.

The compounds, synthesized by modification of different functional groups in various position of the considered scaffold, were tested against the recombinant MbtI, identifying three new potent competitive inhibitors of this enzyme (MM-40, MM-51 and MM-83, Figure 44).



**Figure 44.** MM-40 (A), MM-51 (B) and MM-83 (C) structures.

From the structure activity relationship studies the following moieties have been found responsible of the activity of the compound: 1) the carboxylic group bound to the furan ring, necessary for the interaction between the inhibitor and the amino acids of MbtI active site, as if replaced or modified the compound loses its activity; 2) a functional group in para or meta position of the phenyl ring with a specific electronegativity; 3) a certain distance between the phenyl ring and the carboxylic group. This information is used to explore different substituents, in order to reduce the potential



mutagenic effects of the nitro group identified in MM-40, affording two novel compounds, with potent activity, bearing the potential less toxic trifluoromethyl substituent (MM-51) and cyanide group (MM-83). The crystal structure of MbtI in complex with the latter compounds revealed the possibility to add a hydrophobic moiety to the phenyl ring. These results expand the SAR study among the benzofuran class of derivatives, exploiting unconsidered pharmacophoric features and improving the lipophilicity of the compounds, and by consequence its antimycobacterial activity.

Anyway, further implementations of the molecule are still possible, such as fusion with other small molecular fragments and substituents, to realize a functional and effective multitarget drug that may act also on PtpB enzyme.

### *About PtpB*

To develop multitarget drug candidates against *M. tuberculosis*, a novel study has started covering two paths.

The first is based on the inhibitors previously developed against MbtI. A selection of the most interesting inhibitors was evaluated on PtpB to verify the effect of those molecules on enzymatic activity. Among all, MM-66 and MM-70 showed an inhibitory effect of more than 80%, proving that is possible to develop multitarget drugs against the two selected enzymes.

The second path is based on the *ex novo* development of PtpB inhibitors. A virtual study of four different databases (Vitas-M, ChemBridge, Enamine, and Pharmeks) against PtpB using the Ligandscout software highlighted eight possible inhibitor candidates, with a potential activity also on MbtI. Only one compound, TT-01, resulted to be effective, and showed a significant inhibition against both enzymes (75.5% for PtpB and 57.8% for MbtI). TT-01 is a racemic mixture, of which the enantiomer 1 has a slightly higher effect on both enzymes (83.6% on PtpB, 69.2% MbtI). Interestingly, the separated enantiomers seem to be more active on MbtI than the racemic mixture.

From the structure activity relationship study of the analyzed TT-01 derivatives, none of them showed an effect on the enzymes, suggesting that other routes need to be covered to implement TT-01 inhibitory effect.

Finally, all the compounds that impaired MbtI and PtpB activity showed no effect on PtpA, confirming that the evaluated molecules are selective for their targets. This feature is important to avoid unwanted possible toxic effect on host.

These results, although very preliminary are encouraging and pave the way for further studies to achieve potent multitargeting compounds with significant antitubercular activity.

## Bibliography

- Alderwick L.J., Birch H.L., Mishra A.K., Eggeling L., Besra G.S. (2007) Structure, function and biosynthesis of the *Mycobacterium tuberculosis* cell wall: arabinogalactan and lipoarabinomannan assembly with a view to discovering new drug targets. *Biochem Soc Trans* 35:1325-1328. doi: 10.1042/BST0351325
- Andries K., Verhasselt P., Guillemont J., Gohlmann H.W., Neefs J.M., Winkler H., Van Gestel J., Timmerman P., Zhu M., Lee E., Williams P., de Chaffoy D., Huitric E., Hoffner S., Cambau E., Truffot-Pernot C., Lounis N., Jarlier V. (2005) A diarylquinoline drug active on the ATP synthase of *Mycobacterium tuberculosis*. *Science* 307:223-227. doi: 10.1126/science.1106753
- Asthagiri D., Dillet V., Liu T., Noodleman L., Van Etten R.L., Bashford D. (2002) Density functional study of the mechanism of a tyrosine phosphatase: I. Intermediate formation. *J Am Chem Soc* 124:10225-10235. doi: 10.1021/ja020046n
- Ates L.S., Ummels R., Commandeur S., van de Weerd R., Sparrius M., Weerdenburg E., Alber M., Kalscheuer R., Piersma S.R., Abdallah A.M., Abd El Ghany M., Abdel-Haleem A.M., Pain A., Jimenez C.R., Bitter W., Houben E.N. (2015) Essential Role of the ESX-5 Secretion System in Outer Membrane Permeability of Pathogenic Mycobacteria. *PLoS Genet* 11:e1005190. doi: 10.1371/journal.pgen.1005190
- Augenstreich J., Arbues A., Simeone R., Haanappel E., Wegener A., Sayes F., Le Chevalier F., Chalut C., Malaga W., Guillhot C., Brosch R., Astarie-Dequeker C. (2017) ESX-1 and phthiocerol dimycocerosates of *Mycobacterium tuberculosis* act in concert to cause phagosomal rupture and host cell apoptosis. *Cell Microbiol* 19. doi: 10.1111/cmi.12726
- Bach H., Papavinasasundaram K.G., Wong D., Hmama Z., Av-Gay Y. (2008) *Mycobacterium tuberculosis* virulence is mediated by PtpA dephosphorylation of human vacuolar protein sorting 33B. *Cell Host Microbe* 3:316-322. doi: 10.1016/j.chom.2008.03.008
- Balganesh M., Dinesh N., Sharma S., Kuruppath S., Nair A.V., Sharma U. (2012) Efflux pumps of *Mycobacterium tuberculosis* play a significant role in antituberculosis activity of potential drug candidates. *Antimicrob Agents Chemother* 56:2643-2651. doi: 10.1128/AAC.06003-11

- Barberis I., Bragazzi N.L., Galluzzo L., Martini M. (2017) The history of tuberculosis: from the first historical records to the isolation of Koch's bacillus. *J Prev Med Hyg* 58:E9-E12.
- Barford D., Das A.K., Egloff M.P. (1998) The structure and mechanism of protein phosphatases: insights into catalysis and regulation. *Annu Rev Biophys Biomol Struct* 27:133-164. doi: 10.1146/annurev.biophys.27.1.133
- Baulard A.R., Betts J.C., Engohang-Ndong J., Quan S., McAdam R.A., Brennan P.J., Locht C., Besra G.S. (2000) Activation of the pro-drug ethionamide is regulated in mycobacteria. *J Biol Chem* 275:28326-28331. doi: 10.1074/jbc.M003744200
- Bhardwaj A.K., Kumar D., Raina S.K., Sharma S., Chander V. (2015) Assessment of extra pulmonary tuberculosis (EPTB) cases from selected tuberculosis units (TUs) of Himachal Pradesh, India. *International Journal of Health* 3:29-33. doi: 10.14419/ijh.v3i2.4567
- Bloom B.R., Murray C.J. (1992) Tuberculosis: commentary on a reemergent killer. *Science* 257:1055-1064. doi: 10.1126/science.257.5073.1055
- Braun V., Killmann H. (1999) Bacterial solutions to the iron-supply problem. *Trends in Biochemical Sciences* 24:104-109. doi: 10.1016/s0968-0004(99)01359-6
- Campbell E.A., Korzheva N., Mustaev A., Murakami K., Nair S., Goldfarb A., Darst S.A. (2001) Structural Mechanism for Rifampicin Inhibition of Bacterial RNA Polymerase. *Cell* 104:901-912. doi: 10.1016/s0092-8674(01)00286-0
- Chiarelli L.R., Mori G., Esposito M., Orena B.S., Pasca M.R. (2016) New and Old Hot Drug Targets in Tuberculosis. *Curr Med Chem* 23:3813-3846. doi: 10.2174/1389557516666160831164925
- Chiarelli L.R., Mori M., Barlocco D., Beretta G., Gelain A., Pini E., Porcino M., Mori G., Stelitano G., Costantino L., Lapillo M., Bonanni D., Poli G., Tuccinardi T., Villa S., Meneghetti F. (2018) Discovery and development of novel salicylate synthase (MbtI) furanic inhibitors as antitubercular agents. *Eur J Med Chem* 155:754-763. doi: 10.1016/j.ejmech.2018.06.033
- Cole S.T., Brosch R., Parkhill J., Garnier T., Churcher C., Harris D., Gordon S.V., Eiglmeier K., Gas S., Barry C.E., 3rd, Tekaia F., Badcock K., Basham D., Brown D., Chillingworth T., Connor R., Davies R., Devlin K., Feltwell T., Gentles S., Hamlin N., Holroyd S., Hornsby T., Jagels K., Krogh A., McLean J., Moule S., Murphy L., Oliver K., Osborne J., Quail M.A.,

- Rajandream M.A., Rogers J., Rutter S., Seeger K., Skelton J., Squares R., Squares S., Sulston J.E., Taylor K., Whitehead S., Barrell B.G. (1998) Deciphering the biology of *Mycobacterium tuberculosis* from the complete genome sequence. *Nature* 393:537-544. doi: 10.1038/31159
- Comas I., Coscolla M., Luo T., Borrell S., Holt K.E., Kato-Maeda M., Parkhill J., Malla B., Berg S., Thwaites G., Yeboah-Manu D., Bothamley G., Mei J., Wei L., Bentley S., Harris S.R., Niemann S., Diel R., Aseffa A., Gao Q., Young D., Gagneux S. (2013) Out-of-Africa migration and Neolithic coexpansion of *Mycobacterium tuberculosis* with modern humans. *Nat Genet* 45:1176-1182. doi: 10.1038/ng.2744
  - Crofton J., Mitchison D.A. (1948) Streptomycin resistance in pulmonary tuberculosis. *Br Med J* 2:1009-1015. doi: 10.1136/bmj.2.4588.1009
  - Daffé M., Crick D.C., Jackson M. (2014) Genetics of Capsular Polysaccharides and Cell Envelope (Glyco)lipids. *Microbiology Spectrum* 2. doi: 10.1128/microbiolspec.MGM2-0021-2013
  - Dahlin J.L., Nissink J.W., Strasser J.M., Francis S., Higgins L., Zhou H., Zhang Z., Walters M.A. (2015) PAINS in the assay: chemical mechanisms of assay interference and promiscuous enzymatic inhibition observed during a sulfhydryl-scavenging HTS. *J Med Chem* 58:2091-2113. doi: 10.1021/jm5019093
  - Dahlin J.L., Walters M.A. (2016) How to Triage PAINS-Full Research. *Assay Drug Dev Technol* 14:168-174. doi: 10.1089/adt.2015.674
  - Daniel T.M. (2006) The history of tuberculosis. *Respiratory Medicine* 100:1862-1870. doi: 10.1016/j.rmed.2006.08.006
  - Davies J., Gorini L., Davis B.D. (1965) Misreading of RNA codewords induced by aminoglycoside antibiotics. *Mol Pharmacol* 1:93-106.
  - de Carvalho L.P., Fischer S.M., Marrero J., Nathan C., Ehrh S., Rhee K.Y. (2010) Metabolomics of *Mycobacterium tuberculosis* reveals compartmentalized co-catabolism of carbon substrates. *Chem Biol* 17:1122-1131. doi: 10.1016/j.chembiol.2010.08.009
  - De Voss J.J., Rutter K., Schroeder B.G., Su H., Zhu Y., Barry C.E., 3rd. (2000) The salicylate-derived mycobactin siderophores of *Mycobacterium tuberculosis* are essential for growth in macrophages. *Proc Natl Acad Sci U S A* 97:1252-1257. doi: 10.1073/pnas.97.3.1252

- DeBarber A.E., Mdluli K., Bosman M., Bekker L.G., Barry C.E., 3rd. (2000) Ethionamide activation and sensitivity in multidrug-resistant *Mycobacterium tuberculosis*. Proc Natl Acad Sci U S A 97:9677-9682. doi: 10.1073/pnas.97.17.9677
- Dobosz R., Kolehmainen E., Valkonen A., Ośmiałowski B., Gawinecki R. (2007) Tautomeric preferences of phthalones and related compounds. Tetrahedron 63:9172-9178. doi: 10.1016/j.tet.2007.06.064
- Ducati R.G., Ruffino-Netto A., Basso L.A., Santos D.S. (2006) The resumption of consumption -- a review on tuberculosis. Mem Inst Oswaldo Cruz 101:697-714. doi: 10.1590/s0074-02762006000700001
- Eoh H., Wang Z., Layre E., Rath P., Morris R., Branch Moody D., Rhee K.Y. (2017) Metabolic anticipation in *Mycobacterium tuberculosis*. Nat Microbiol 2:17084. doi: 10.1038/nmicrobiol.2017.84
- Fan L., Wu X., Jin C., Li F., Xiong S., Dong Y. (2018) MptpB Promotes mycobacteria survival by inhibiting the expression of inflammatory mediators and cell apoptosis in macrophages. Front Cell Infect Microbiol 8:171. doi: 10.3389/fcimb.2018.00171
- Fanzani L., Porta F., Meneghetti F., Villa S., Gelain A., Lucarelli A.P., Parisini E. (2015) *Mycobacterium tuberculosis* low molecular weight phosphatases (MPtpA and MPtpB): from biological insight to inhibitors. Curr Med Chem 22:3110-3132. doi: 10.2174/0929867322666150812150036
- Fu L.M., Fu-Liu C.S. (2022) Is *Mycobacterium tuberculosis* a closer relative to Gram-positive or Gram-negative bacterial pathogens? Tuberculosis (Edinb) 82:85-90. doi: 10.1054/tube.2002.0328
- Galagan J.E., Minch K., Peterson M., Lyubetskaya A., Azizi E., Sweet L., Gomes A., Rustad T., Dolganov G., Glotova I., Abeel T., Mahwinney C., Kennedy A.D., Allard R., Brabant W., Krueger A., Jaini S., Honda B., Yu W.H., Hickey M.J., Zucker J., Garay C., Weiner B., Sisk P., Stolte C., Winkler J.K., Van de Peer Y., Iazzetti P., Camacho D., Dreyfuss J., Liu Y., Dorhoi A., Mollenkopf H.J., Drogaris P., Lamontagne J., Zhou Y., Piquenot J., Park S.T., Raman S., Kaufmann S.H., Mohny R.P., Chelsky D., Moody D.B., Sherman D.R., Schoolnik G.K. (2013) The *Mycobacterium tuberculosis* regulatory network and hypoxia. Nature 499:178-183. doi: 10.1038/nature12337

- Gandhi N.R., Moll A., Sturm A.W., Pawinski R., Govender T., Lalloo U., Zeller K., Andrews J., Friedland G. (2006) Extensively drug-resistant tuberculosis as a cause of death in patients co-infected with tuberculosis and HIV in a rural area of South Africa. *The Lancet* 368:1575-1580. doi: 10.1016/s0140-6736(06)69573-1
- Gengenbacher M., Kaufmann S.H.E. (2012) *Mycobacterium tuberculosis*: success through dormancy. *Fems Microbiol Rev* 36:514-532. doi: 10.1111/j.1574-6976.2012.00331.x
- Gobin J., Horwitz M.A. (1996) Exochelins of *Mycobacterium tuberculosis* remove iron from human iron-binding proteins and donate iron to mycobactins in the *M. tuberculosis* cell wall. *J Exp Med* 183:1527-1532. doi: 10.1084/jem.183.4.1527
- Görke B., Stülke J. (2008) Carbon catabolite repression in bacteria: many ways to make the most out of nutrients. *Nat Rev Microbiol* 6:613-624. doi: 10.1038/nrmicro1932
- Gröschel M.I., Sayes F., Simeone R., Majlessi L., Brosch R. (2016) ESX secretion systems: mycobacterial evolution to counter host immunity. *Nat Rev Microbiol* 14:677-691. doi: 10.1038/nrmicro.2016.131
- Grundner C., Ng H.L., Alber T. (2005) *Mycobacterium tuberculosis* protein tyrosine phosphatase PtpB structure reveals a diverged fold and a buried active site. *Structure* 13:1625-1634. doi: 10.1016/j.str.2005.07.017
- Harrison A.J., Yu M., Gardenborg T., Middleditch M., Ramsay R.J., Baker E.N., Lott J.S. (2006) The structure of MbtI from *Mycobacterium tuberculosis*, the first enzyme in the biosynthesis of the siderophore mycobactin, reveals it to be a salicylate synthase. *J Bacteriol* 188:6081-6091. doi: 10.1128/JB.00338-06
- Hershkovitz I., Donoghue H.D., Minnikin D.E., Besra G.S., Lee O.Y., Gernaey A.M., Galili E., Eshed V., Greenblatt C.L., Lemma E., Bar-Gal G.K., Spigelman M. (2008) Detection and molecular characterization of 9,000-year-old *Mycobacterium tuberculosis* from a Neolithic settlement in the Eastern Mediterranean. *PLoS One* 3:e3426. doi: 10.1371/journal.pone.0003426
- Homolka S., Koser C., Archer J., Rusch-Gerdes S., Niemann S. (2009) Single-nucleotide polymorphisms in Rv2629 are specific for *Mycobacterium tuberculosis* genotypes Beijing and Ghana but not associated with rifampin resistance. *J Clin Microbiol* 47:223-226. doi: 10.1128/JCM.01237-08

- Horita Y., Maeda S., Kazumi Y., Doi N. (2014) In vitro susceptibility of *Mycobacterium tuberculosis* isolates to an oral carbapenem alone or in combination with beta-lactamase inhibitors. *Antimicrob Agents Chemother* 58:7010-7014. doi: 10.1128/AAC.03539-14
- Imlay J.A., Chin S.M., Linn S. (1988) Toxic DNA damage by hydrogen peroxide through the Fenton reaction in vivo and in vitro. *Science* 240:640-642. doi: 10.1126/science.2834821
- Ishikawa E., Ishikawa T., Morita Y.S., Toyonaga K., Yamada H., Takeuchi O., Kinoshita T., Akira S., Yoshikai Y., Yamasaki S. (2009) Direct recognition of the mycobacterial glycolipid, trehalose dimycolate, by C-type lectin Mincle. *J Exp Med* 206:2879-2888. doi: 10.1084/jem.20091750
- Jarlier V., Nikaido H. (1994) Mycobacterial cell wall: structure and role in natural resistance to antibiotics. *FEMS Microbiol Lett* 123:11-18. doi: 10.1111/j.1574-6968.1994.tb07194.x
- Jones C.M., Wells R.M., Madduri A.V., Renfrow M.B., Ratledge C., Moody D.B., Niederweis M. (2014) Self-poisoning of *Mycobacterium tuberculosis* by interrupting siderophore recycling. *Proc Natl Acad Sci U S A* 111:1945-1950. doi: 10.1073/pnas.1311402111
- Kalscheuer R., Weinrick B., Veeraraghavan U., Besra G.S., Jacobs W.R., Jr. (2010) Trehalose-recycling ABC transporter LpqY-SugA-SugB-SugC is essential for virulence of *Mycobacterium tuberculosis*. *Proc Natl Acad Sci U S A* 107:21761-21766. doi: 10.1073/pnas.1014642108
- Kapur V., Whittam T.S., Musser J.M. (1994) Is *Mycobacterium tuberculosis* 15,000 years old? *J Infect Dis* 170:1348-1349. doi: 10.1093/infdis/170.5.1348
- Koch R. (1882) Die Aetiologie der Tuberkulose. *Berliner klinische Wochenschrift* 19:221-230.
- Koul A., Choidas A., Treder M., Tyagi A.K., Drlica K., Singh Y., Ullrich A. (2000) Cloning and characterization of secretory tyrosine phosphatases of *Mycobacterium tuberculosis*. *J Bacteriol* 182:5425-5432. doi: 10.1128/JB.182.19.5425-5432.2000
- Litwin C.M., Calderwood S.B. (1993) Role of iron in regulation of virulence genes. *Clin Microbiol Rev* 6:137-149. doi: 10.1128/CMR.6.2.137

- Liu Z., Liu F., Aldrich C.C. (2015) Stereocontrolled Synthesis of a Potential Transition-State Inhibitor of the Salicylate Synthase MbtI from *Mycobacterium tuberculosis*. *J Org Chem* 80:6545-6552. doi: 10.1021/acs.joc.5b00455
- Machado D., Azzali E., Couto I., Costantino G., Pieroni M., Viveiros M. (2018) Adjuvant therapies against tuberculosis: discovery of a 2-aminothiazole targeting *Mycobacterium tuberculosis* energetics. *Future Microbiol* 13:1383-1402. doi: 10.2217/fmb-2018-0110
- Mahairas G.G., Sabo P.J., Hickey M.J., Singh D.C., Stover C.K. (1996) Molecular analysis of genetic differences between *Mycobacterium bovis* BCG and virulent *M. bovis*. *J Bacteriol* 178:1274-1282. doi: 10.1128/jb.178.5.1274-1282.1996
- Manos-Turvey A., Bulloch E.M., Rutledge P.J., Baker E.N., Lott J.S., Payne R.J. (2010) Inhibition studies of *Mycobacterium tuberculosis* salicylate synthase (MbtI). *ChemMedChem* 5:1067-1079. doi: 10.1002/cmdc.201000137
- Manos-Turvey A., Cergol K.M., Salam N.K., Bulloch E.M., Chi G., Pang A., Britton W.J., West N.P., Baker E.N., Lott J.S., Payne R.J. (2012) Synthesis and evaluation of *M. tuberculosis* salicylate synthase (MbtI) inhibitors designed to probe plasticity in the active site. *Org Biomol Chem* 10:9223-9236. doi: 10.1039/c2ob26736e
- Meneghetti F., Villa S., Gelain A., Barlocco D., Chiarelli L.R., Pasca M.R., Costantino L. (2016) Iron Acquisition Pathways as Targets for Antitubercular Drugs. *Curr Med Chem* 23:4009-4026. doi: 10.2174/0929867323666160607223747
- Murray J.F., Rieder H.L., Finley-Croswhite A. (2016) The King's Evil and the Royal Touch: the medical history of scrofula. *Int J Tuberc Lung Dis* 20:713-716. doi: 10.5588/ijtld.16.0229
- Nayak S., Gaonkar S.L. (2019) A Review on Recent Synthetic Strategies and Pharmacological Importance of 1,3-Thiazole Derivatives. *Mini Rev Med Chem* 19:215-238. doi: 10.2174/1389557518666180816112151
- Nicklisch N., Maixner F., Ganslmeier R., Friederich S., Dresely V., Meller H., Zink A., Alt K.W. (2012) Rib lesions in skeletons from early neolithic sites in Central Germany: on the trail of tuberculosis at the onset of agriculture. *Am J Phys Anthropol* 149:391-404. doi: 10.1002/ajpa.22137
- Palomino J.C., Martin A., Camacho M., Guerra H., Swings J., Portaels F. (2002) Resazurin microtiter assay plate: simple and inexpensive method for detection of drug resistance in



- Mycobacterium tuberculosis*. Antimicrob Agents Chemother 46:2720-2722. doi: 10.1128/AAC.46.8.2720-2722.2002
- Raffetseder J. Interplay of human macrophages and *Mycobacterium tuberculosis* phenotypes. 2016.
  - Ratledge C. Mycobacteria: Molecular Biology and Virulence. C. Ratledge, J.W. Dale, (eds). Blackwell Science, 1999, Chapter Iron Metabolism, pp. pp. 260–286.
  - Ratledge C. (2004) Iron, mycobacteria and tuberculosis. Tuberculosis (Edinb) 84:110-130. doi: 10.1016/j.tube.2003.08.012
  - Riccardi G., Pasca M.R. (2014) Trends in discovery of new drugs for tuberculosis therapy. J Antibiot (Tokyo) 67:655-659. doi: 10.1038/ja.2014.109
  - Rivers E.C., Mancera R.L. (2008) New anti-tuberculosis drugs in clinical trials with novel mechanisms of action. Drug Discov Today 13:1090-1098. doi: 10.1016/j.drudis.2008.09.004
  - Rodriguez G.M. (2006) Control of iron metabolism in *Mycobacterium tuberculosis*. Trends Microbiol 14:320-327. doi: 10.1016/j.tim.2006.05.006
  - Rodriguez G.M., Smith I. (2006) Identification of an ABC transporter required for iron acquisition and virulence in *Mycobacterium tuberculosis*. J Bacteriol 188:424-430. doi: 10.1128/JB.188.2.424-430.2006
  - Rodriguez G.M., Voskuil M.I., Gold B., Schoolnik G.K., Smith I. (2002) IdeR, an Essential Gene in *Mycobacterium tuberculosis*: Role of IdeR in Iron-Dependent Gene Expression, Iron Metabolism, and Oxidative Stress Response. Infection and Immunity 70:3371-3381. doi: 10.1128/iai.70.7.3371-3381.2002
  - Saeed B.W. (2006) Malignant tuberculosis. J Ayub Med Coll Abbottabad 18:1-2.
  - Saleh M.T., Belisle J.T. (2000) Secretion of an acid phosphatase (SapM) by *Mycobacterium tuberculosis* that is similar to eukaryotic acid phosphatases. J Bacteriol 182:6850-6853. doi: 10.1128/jb.182.23.6850-6853.2000
  - Sayapin Y.A., Duong B.N., Komissarov V.N., Dorogan I.V., Makarova N.I., Bondareva I.O., Tkachev V.V., Shilov G.V., Aldoshin S.M., Minkin V.I. (2010) Synthesis, structure, and photoisomerization of derivatives of 2-(2-quinolyl)-1,3-tropolones prepared by the

condensation of 2-methylquinolines with 3,4,5,6-tetrachloro-1,2-benzoquinone. *Tetrahedron* 66:8763-8771. doi: 10.1016/j.tet.2010.08.077

- Schmitt M.P., Predich M., Doukhan L., Smith I., Holmes R.K. (1995) Characterization of an iron-dependent regulatory protein (IdeR) of *Mycobacterium tuberculosis* as a functional homolog of the diphtheria toxin repressor (DtxR) from *Corynebacterium diphtheriae*. *Infect Immun* 63:4284-4289. doi: 10.1128/iai.63.11.4284-4289.1995
- Schwyn B., Neilands J.B. (1987) Universal chemical assay for the detection and determination of siderophores. *Analytical Biochemistry* 160:47-56. doi: 10.1016/0003-2697(87)90612-9
- Serafini A., Pisu D., Palu G., Rodriguez G.M., Manganelli R. (2013) The ESX-3 secretion system is necessary for iron and zinc homeostasis in *Mycobacterium tuberculosis*. *PLoS One* 8:e78351. doi: 10.1371/journal.pone.0078351
- Shyam M., Shilkar D., Verma H., Dev A., Sinha B.N., Brucoli F., Bhakta S., Jayaprakash V. (2021) The Mycobactin Biosynthesis Pathway: A Prospective Therapeutic Target in the Battle against Tuberculosis. *J Med Chem* 64:71-100. doi: 10.1021/acs.jmedchem.0c01176
- Siegrist M.S., Unnikrishnan M., McConnell M.J., Borowsky M., Cheng T.Y., Siddiqi N., Fortune S.M., Moody D.B., Rubin E.J. (2009) Mycobacterial Esx-3 is required for mycobactin-mediated iron acquisition. *Proc Natl Acad Sci U S A* 106:18792-18797. doi: 10.1073/pnas.0900589106
- Skepper O., Pálfi G., Kozocsay G., Pósa A., Bereczki Z., Molnár E. (2012) New cases of probable skeletal tuberculosis from the Neolithic period in Hungary, a morphological study *Act Biol Szeged* 56:115-123.
- Smith J., Manoranjan J., Pan M., Bohsali A., Xu J., Liu J., McDonald K.L., Szyk A., LaRonde-LeBlanc N., Gao L.Y. (2008) Evidence for pore formation in host cell membranes by ESX-1-secreted ESAT-6 and its role in *Mycobacterium marinum* escape from the vacuole. *Infect Immun* 76:5478-5487. doi: 10.1128/IAI.00614-08
- Stamm C.E., Collins A.C., Shiloh M.U. (2015) Sensing of *Mycobacterium tuberculosis* and consequences to both host and bacillus. *Immunol Rev* 264:204-219. doi: 10.1111/imr.12263
- Stehle T., Sreeramulu S., Lohr F., Richter C., Saxena K., Jonker H.R., Schwalbe H. (2012) The apo-structure of the low molecular weight protein-tyrosine phosphatase A (MptpA) from

*Mycobacterium tuberculosis* allows for better target-specific drug development. J Biol Chem 287:34569-34582. doi: 10.1074/jbc.M112.399261

- Takayama K., Armstrong E.L., Kunugi K.A., Kilburn J.O. (1979) Inhibition by ethambutol of mycolic acid transfer into the cell wall of *Mycobacterium smegmatis*. Antimicrob Agents Chemother 16:240-242. doi: 10.1128/aac.16.2.240
- Tiberi S., du Plessis N., Walzl G., Vjecha M.J., Rao M., Ntouni F., Mfinanga S., Kapata N., Mwaba P., McHugh T.D., Ippolito G., Migliori G.B., Maeurer M.J., Zumla A. (2018) Tuberculosis: progress and advances in development of new drugs, treatment regimens, and host-directed therapies. The Lancet Infectious Diseases 18:e183-e198. doi: 10.1016/s1473-3099(18)30110-5
- Vasan M., Neres J., Williams J., Wilson D.J., Teitelbaum A.M., Remmel R.P., Aldrich C.C. (2010) Inhibitors of the salicylate synthase (MbtI) from *Mycobacterium tuberculosis* discovered by high-throughput screening. ChemMedChem 5:2079-2087. doi: 10.1002/cmdc.201000275
- Vergne I., Chua J., Lee H.H., Lucas M., Belisle J., Deretic V. (2005) Mechanism of phagolysosome biogenesis block by viable *Mycobacterium tuberculosis*. Proc Natl Acad Sci U S A 102:4033-4038. doi: 10.1073/pnas.0409716102
- Vilcheze C., Jacobs W.R., Jr. (2007) The mechanism of isoniazid killing: clarity through the scope of genetics. Annu Rev Microbiol 61:35-50. doi: 10.1146/annurev.micro.61.111606.122346
- Weinberg E.D. (1999) The role of iron in protozoan and fungal infectious diseases. J Eukaryot Microbiol 46:231-238. doi: 10.1111/j.1550-7408.1999.tb05119.x
- Wilson J.W., Tsukayama D.T. (2016) Extensively Drug-Resistant Tuberculosis: Principles of Resistance, Diagnosis, and Management. Mayo Clin Proc 91:482-495. doi: 10.1016/j.mayocp.2016.01.014
- Wilson R., Kumar P., Parashar V., Vilcheze C., Veyron-Churlet R., Freundlich J.S., Barnes S.W., Walker J.R., Szymonifka M.J., Marchiano E., Shenai S., Colangeli R., Jacobs W.R., Jr., Neiditch M.B., Kremer L., Alland D. (2013) Antituberculosis thiophenes define a requirement for Pks13 in mycolic acid biosynthesis. Nat Chem Biol 9:499-506. doi: 10.1038/nchembio.1277

- Wong D., Bach H., Sun J., Hmama Z., Av-Gay Y. (2011) *Mycobacterium tuberculosis* protein tyrosine phosphatase (PtpA) excludes host vacuolar-H<sup>+</sup>-ATPase to inhibit phagosome acidification. *Proc Natl Acad Sci U S A* 108:19371-19376. doi: 10.1073/pnas.1109201108
- Zhou B., He Y., Zhang X., Xu J., Luo Y., Wang Y., Franzblau S.G., Yang Z., Chan R.J., Liu Y., Zheng J., Zhang Z.Y. (2010) Targeting mycobacterium protein tyrosine phosphatase B for antituberculosis agents. *Proc Natl Acad Sci U S A* 107:4573-4578. doi: 10.1073/pnas.0909133107
- Zumla A., Nahid P., Cole S.T. (2013) Advances in the development of new tuberculosis drugs and treatment regimens. *Nat Rev Drug Discov* 12:388-404. doi: 10.1038/nrd4001
- Zwahlen J., Kolappan S., Zhou R., Kisker C., Tonge P.J. (2007) Structure and mechanism of MbtI, the salicylate synthase from *Mycobacterium tuberculosis*. *Biochemistry* 46:954-964. doi: 10.1021/bi060852x

#### Uncategorized references

- Working Group on New TB Drugs. Available at <https://www.newtbdrugs.org/>
- World Health Organization (WHO). 2017 Global TB Report. <https://apps.who.int/iris/bitstream/handle/10665/259366/9789241565516-eng.pdf?sequence=1>
- World Health Organization (WHO). 2021 Global TB Report. <https://www.who.int/teams/global-tuberculosis-programme/tb-reports/global-tuberculosis-report-2021>.